Title
Exact tensor network ansatz for strongly interacting systems

Author
Zaletel, Michael P.

Publication Date
2014

Peer reviewed|Thesis/dissertation

Exact tensor network ansatz for strongly interacting systems

by

Michael P Zaletel

A dissertation submitted in partial satisfaction of the

requirements for the degree of

Doctor of Philosophy

in

Physics

in the

Graduate Division

of the

University of California, Berkeley

Committee in charge:

Professor Joel E. Moore, Chair
Professor Ashvin Vishwanath
Professor Maciej Zworski

Fall 2014

Exact tensor network ansatz for strongly interacting systems

Abstract

Exact tensor network ansatz for strongly interacting systems

by

Michael P Zaletel

Doctor of Philosophy in Physics

University of California, Berkeley

Professor Joel E. Moore, Chair

It appears that the *tensor network* ansatz, while not quite complete, is an efficient coordinate system for the tiny subset of a many-body Hilbert space which can be realized as a low energy state of a local Hamiltonian. However, we don't fully understand precisely which phases are captured by the tensor network ansatz, how to compute their physical observables (even numerically), or how to compute a tensor network representation for a ground state given a microscopic Hamiltonian. These questions are algorithmic in nature, but their resolution is intimately related to understanding the nature of quantum entanglement in many-body systems.

For this reason it is useful to compute the tensor network representation of various 'model' wavefunctions representative of different phases of matter; this allows us to understand how the entanglement properties of each phase are expressed in the tensor network ansatz, and can serve as test cases for algorithm development. Condensed matter physics has many illuminating model wavefunctions, such as Laughlin's celebrated wave function for the fractional quantum Hall effect, the Bardeen-Cooper-Schrieffer wave function for superconductivity, and Anderson's resonating valence bond ansatz for spin liquids. This thesis presents some results on exact tensor network representations of these model wavefunctions. In addition, a tensor network representation is given for the time evolution operator of a long-range one-dimensional Hamiltonian, which allows one to numerically simulate the time evolution of power-law interacting spin chains as well as two-dimensional strips and cylinders.

Contents

Acknowledgments

To my mother and father, $\mathcal{L}.\mathcal{E}.\mathcal{B}.$, and to Prof. Joel Moore, for being a generous, wise, patient, and indulgent (but not overly indulgent) advisor.

For the generosity of the National Science Foundation Graduate Research Fellowship Program and all of us that support it. For Prof. Rick Heller's undergraduate advising that brought that support.

For my time at Deep Springs, David Neidorf, the faculty, staff, and fellow students who inspired me towards this 'temperate and prudent sort of play.'

And for my Berkeley Physics comrades with whom daily conversation and strolls for lunch drew me away from my sunny backyard garden: Ashvin Vishwanath, Dung-Hai Lee, Frank Pollmann, Jens Bardarson, Tarun Grover, Sid Parameswaran, Yuan-Ming Lu, Dan Varjas, Jonas Kjall, Xie Chen, Drew Potter, Christoph Karrasch, Roni Ilan, Yasaman Bahri, Phillip Dumitrescu, and in particular Roger Mong, a great intellectual companion when you can get him to stop tap dancing.

Chapter 1

Introduction

It's a remarkable property of quantum mechanics that the lowest energy state of a system can be interesting. For example, consider particles whose coordinates are constrained to a square grid, with a density of one particle per two sites. Classically, the lowest energy state of the system must form a crystalline pattern (or perhaps, with sufficient frustration, there may be extensive degeneracy). Very little information is required to specify the state, just the location of the particles within a unit cell. In a quantum mechanical system, the space of states is vastly larger, as we can linearly superpose different density configurations with amplitudes and phases. By superposing enough states, the crystalline order may melt, resulting in a liquid. Since the state arises by superposing configurations that differ in space, the liquid is necessarily *entangled*, and neighboring regions of the system become correlated by the fluctuating density. These liquids are distinguished not by any crystalline pattern (there is none), but rather by structures in the quantum mechanical amplitudes and phases.

Since there are exponentially many density configurations, scaling as $\mathcal{O}(d^V)$ for a system of volume V (with $d = 2$ for the half-filled example above), allowing for superposition at first makes the space of quantum states seem prodigious. But taking into account locality, the relevant part of Hilbert space is much smaller (and less linear) than it first appears. This is because it is only energetically favorable to superpose states which are connected by an element of the Hamiltonian, and a *local* Hamiltonian is exponentially sparse. The interplay between the vastness of Hilbert space and the tight constraints of locality gives rise to the richness of quantum many-body theory.

We can heuristically calculate the amount of information required to parameterize the space of all possible eigenstates of all local Hamiltonians. To do so, we just parameterize the space of all Hamiltonians, followed by a number n specifying the

eigenstate. Restricting the range of each local term in $H = \sum_i H_i$ to a volume V_H, each H_i is specified by a matrix of dimension d^{V_H}, with V such terms in the Hamiltonian. Hence the space of local Hamiltonians is parameterized by an amount of information $S_H \propto V d^{2V_H}$. Since there are d^V eigenstates, specifying which eigenstate requires an additional amount $S_\psi = V \log(d)$ of information. In total, we require $S_H + S_\psi = V(d^{2V_H} + \log(d))$ numbers to specify the space of all local eigenstates. In contrast to the d^V numbers required to specify an arbitrary state, this is only an *extensive* amount of information, so the space of such states is a vanishing fraction of the full many-body Hilbert space.

Since the manifold of relevant states is so small, it must not be linear. Indeed, the superposition of two macroscopically different states is a 'cat state' like $a|\uparrow\uparrow\cdots\rangle + b|\downarrow\downarrow\cdots\rangle$. Any two states which are uniform (for example, translation invariant) are macroscopically distinct, as their overlap must decrease exponentially as $(1-\epsilon)^V$ in the system size V. While such a state is formally allowed, *no observer can ever detect they are in such a superposition.* The superposition of two states $|\uparrow\cdots\rangle, |\downarrow\cdots\rangle$ is only physically detectable if there are local operators $\mathcal{O}$ and local evolution $U(t)$ which can connect the two states, $\langle\downarrow\cdots|U(-t)\mathcal{O}U(t)|\uparrow\cdots\rangle \neq 0$, over a time scale t relevant to the observer. This overlap always vanishes if the states are macroscopically different, as any two states generically are in the thermodynamic limit.

To make the counting more precise, fix an initial state $|\uparrow\cdots\rangle$. In Ref. [85] it was proven that the set of states that can be generated by *arbitrary* local evolution $U(t)|\uparrow\cdots\rangle$ occupies a tiny fractional volume $\mathcal{O}(V^V \epsilon^{d^V})$ of the total Hilbert space for some $\epsilon < 1$. This realization was called the 'convenient illusion' of Hilbert space; while the evolution is linear, only a vanishing portion of Hilbert space can ever be reached.[85]

Specifying a local Hamiltonian is a rather useless coordinate system - finding its spectrum is the difficult problem we wish to solve, and the coordinate system is full of discontinuities (phase transitions). But since the space of relevant states is relatively small, there may be a more manageable way to coordinatize it, which would provide the most general possible variational ansatz for relevant quantum states. Recently there has been rapid progress towards finding such a coordinate system, called tensor networks, at least for the *low energy* part of Hilbert space. [31, 137, 75, 123, 30, 78] These ansatz obey an 'area law:' the amount of quantum entanglement between a region A and its environment must scale no faster than the area of the boundary ∂A. Most low energy states indeed obey an area law, [109] with some exceptions for critical systems.[51] [1] For now this rules out capturing highly excited states at

[1] Progress has also been made in towards capturing logarithmic violations of the area law oc-

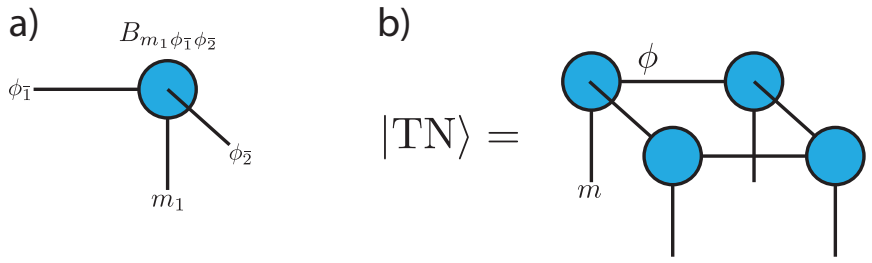

Figure 1.1: Depiction of a tensor network for a 2x2 lattice. a) Each tensor is a node with a 'leg' for each index. b) Contraction over indices is graphically represented by connecting legs; the dangling legs are the indices m_i of the 4-site wave function.

finite energy density, which generically obey a volume law. In one-dimension, tensor networks fully parameterize the ground states of all gapped, short-ranged interacting lattice models, [48] though it is not known what states are captured in two-dimensions and higher.

For lattice systems, the tensor network ansatz is specified on a graph, with vertices at each site i of the lattice and edges $\bar{i}$ with an approximately isotropic density. The onsite Hilbert spaces are indexed by $1 \leq m_i \leq d_i$, and on each edge $\bar{i}$ of the lattice we associated an 'auxiliary' Hilbert space indexed by $1 \leq \phi_{\bar{i}} \leq \chi_{\bar{i}}$. The variational space is parameterized by a tensors $B^{[i]}_{m_i,\{\phi\}_i}$ on each site, with a 'physical index' m_i and a set of auxiliary indices $\{\phi\}_i$ for each edge attached to the site. As illustrated in Fig. 1.1 , the ansatz wave function is given by

$$\Psi_{\{m\}} = \sum_{\phi=1}^{\chi} \prod_i B^{[i]}_{m_i,\{\phi\}_i}. \tag{1.1}$$

The $\chi_{\bar{i}}$ are the 'bond dimensions' of the ansatz; increasing χ increases the variational space, along with the difficulty of computing observables.

For completeness, in Chapter 1 I review some of the algorithmic aspects of 1-dimensional tensor networks, though the focus of this work is not an algorithms (for a recent review, see Ref. [74]). Instead I consider the relation between tensor networks and several famous variational ansatz in condensed matter, including the Bardeen-Cooper-Schrieffer wavefunction for superconductivity [6], Anderson's resonating valence bond state for spin systems [3], and Laughlin's state for the quantum Hall effect. [64] In this thesis I show why all three of these ansatz fall nicely within the framework of tensor networks.

curring for critical systems and Fermi surfaces, [30] but such violations are far weaker than the volume-law behavior generically expected at finite energy density.

Before proceeding to the rigorous results of the subsequent Chapters, I'll paint an idiosyncratic sketch (in water colors) of recent developments combining tensor networks, their entanglement properties, and topological order.

1.1 Tensor networks and generating functions

An important feature of a gapped ground state is that the wave function $\Psi[m]$ is a local functional of the configuration m. To see why the tensor network ansatz incorporates this result, we rewrite the tensor network ansatz as

$$\Psi[m] = \sum_{\phi=1}^{\chi} \prod_i B^{[i]}_{m_i,\{\phi\}_i} = \sum_{\{\phi\}} e^{-\sum_i S_i[\{\phi\}_i]+V[m_i,\{\phi\}_i]} \propto \langle e^{V[m,\phi]} \rangle_\phi. \tag{1.2}$$

where $\langle\rangle_\phi$ is an average with respect to the 'action' S. The sum over the D-dimensional lattice of auxiliary degrees of freedom ϕ looks like the path integral or statistical sum over a *local* D-dimensional system. The $V[m_i, \{\phi\}_i]$ are source fields for the path integral: the wave function $\Psi[m]$ is the *generating* functional of the auxiliary system. Recall that for standard continuum field theories we define the generating functional

$$\mathcal{Z}[J] = \int \mathcal{D}[\phi] e^{-S[\phi]+J\phi} = \mathcal{Z}\langle e^{J\phi}\rangle_\phi. \tag{1.3}$$

For the tensor networks, we generalize slightly the interaction between the 'source field' m, which is the physical degree of freedom, and the auxiliary fields ϕ. The cluster decomposition principle asserts that such generating functions depend locally on m.

The wave function $\Psi[m]$ of a $D+1$ dimensional tensor network is conceptually equivalent to the generating functional of the D-dimensional auxiliary system. This rewriting is purely a matter of notation. What can we learn about the physical state from the 'auxiliary' theory?

The bulk-boundary mapping

An important concept in tensor networks is the existence of a 'bulk boundary' mapping between configurations of the auxiliary ϕ and the physical states. Consider a region A with boundary ∂A cutting through auxiliary bonds $\{\phi_1, \phi_2 \cdots\} \in \partial A$, as shown in Fig. 1.2. Summing over the auxiliary bonds interior to A, while holding the boundary $\phi \in \partial A$ fixed defines a state $|\phi\rangle_A$. The mapping $\Gamma : \phi \in \partial A \to |\phi\rangle_A$ is

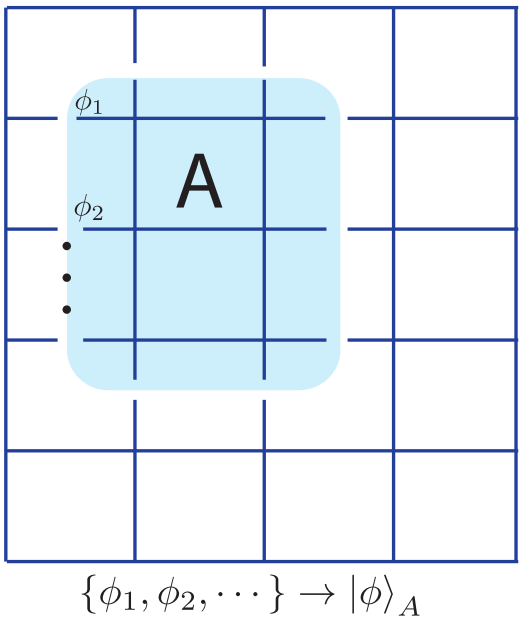

Figure 1.2: The bulk boundary mapping. Each region A with boundary ∂A defines a set of 'dangling bonds' $\{\phi_1, \phi_2 \cdots\} \in \partial A$ which cross the boundary. Fixing the value of these dangling bonds, but summing over the bonds in the interior of A generates a state which we call $|\phi\rangle_A$, where ϕ indicates the dependence on the state of the boundary value. This map $\{\phi_1, \phi_2 \cdots\} \to |\phi\rangle_A$ is the bulk-boundary mapping.

the bulk boundary map. It is natural to treat the boundary configurations ϕ as the basis states of a boundary Hilbert space, so Γ can then be extended to a *linear* map from the boundary Hilbert space to the bulk Hilbert space. Because of the area-law, for large enough regions the map is not surjective (onto), since the number of bulk state grows with the volume of A while the number of boundary states grows with the area ∂A. Γ is 'injective' if $\Gamma|\phi\rangle = 0$ if and only if $|\phi\rangle = 0$, or equivalently, no to boundary states map to the same bulk state. A tensor network is called 'injective' if there is a sufficiently large size such that *all* the bulk-boundary mappings for regions above that size are injective.

A generic tensor network (such as those drawn from random entries) is injective, and such networks are quite well understood.[77] An injective tensor network is always the unique ground state of some local 'parent' Hamiltonian made from a sum of projectors, but may or may not be gapless.[79, 98] It turns out that states with both symmetry protected [17] and intrinsic topological order cannot be injective, a theme we will return to.

Entanglement properties

The Hilbert space $\mathcal{H}$ of a system is a tensor product of its subregions L, R, $\mathcal{H} = \mathcal{H}_L \otimes \mathcal{H}_R$. The Schmidt decomposition

$$|\Psi\rangle = \sum_i e^{-E_i/2} |i\rangle_L \otimes |i\rangle_R, \quad \rho_{L/R} = \sum_i e^{-E_i} |i\rangle\langle i|_{L/R} \tag{1.4}$$

encodes how the degrees of freedom in L are entangled with those in R. The Schmidt decomposition requires that $|i\rangle_{L/R}$ be orthonormal vectors. Those with lower 'entanglement energy' E_i receive higher weight in the decomposition. While studied in other contexts for some time, a prescient paper of Kitaev and Preskill [58] noted that for certain 2D topological phases the spectrum E_i should be related to the energy spectrum of a physical edge; subsequently Li and Haldane called E_i the 'entanglement spectrum, and first explored this relation for quantum Hall systems.[66]

In a gapped system, the degrees of freedom in L which are entangled with R should only reside in the vicinity of the cut. If we fix a 'entanglement cutoff' $E_i < \Lambda$, then far from the boundary the $|i\rangle_R$ under the cutoff must look identical. To be precise, for any local operator $\mathcal{O}$ a distance x from the boundary,

$$\lim_{x\to\infty} \langle i|\mathcal{O}(x)|j\rangle_R \sim \delta_{ij}\langle\Psi|O(x)|\Psi\rangle + O_{ij} e^{-|x|/\ell(\Lambda)} \tag{1.5}$$

for all i, j under the cutoff. Since the allowed fluctuations in the low lying Schmidt states are localized near the cut, the density of entanglement energies must be proportional to the length of the cut, not the volume of L, R: this is the area law. [109]

Calculating the entanglement spectrum of a tensor network can be reduced to certain properties of the auxiliary theory. Using the bulk boundary mapping, a tensor network has a natural 'bipartition,' $|\Psi\rangle = \sum_{\phi\in\partial L} |\phi\rangle_L |\phi\rangle_R$, where $|\phi\rangle_{L/R}$ is a *non-orthogonal* basis. As shown in Fig. 1.3, we can contract all auxiliary indices $\phi \in L$, leaving 'dangling' indices on ∂L. Fixing the value of the dangling indices $\phi \in \partial L$ defines a state in the left $\Psi_L[m_L, \phi] \leftrightarrow |\phi\rangle_L$, and likewise on the right. In the notation of the previous section,

$$\Psi[m_L, m_R] = \sum_{\{\phi\}\in L\otimes R} e^{-S[\phi]+V[m,\phi]} \tag{1.6}$$

$$= \sum_{\{\phi\}\in\partial L} \Psi_L[m_L, \phi]\Psi_R[m_R, \phi] \tag{1.7}$$

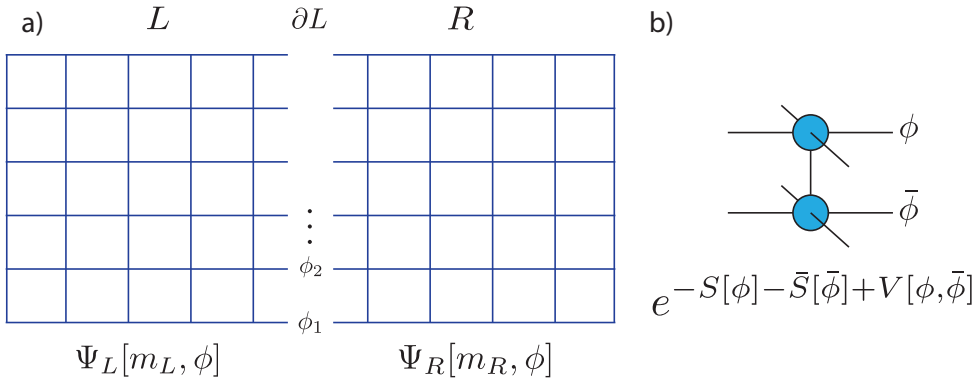

Figure 1.3: Partial contraction of the network to obtain a bipartition $\Psi[m_L, m_R] = \sum_{\{\phi\}\in\partial L} \Psi_L[m_L, \phi]\Psi_R[m_R, \phi]$. By tracing out all auxiliary indices apart for those along the boundary between L, R, we isolate the degrees of freedom entangling the two regions.

This is not generally a Schmidt decomposition, as the basis is not orthogonal. If the reader will indulge just one further change of notation,

$$\langle m|\Psi\rangle = \langle e^{V[m,\phi]}\rangle_\phi = \sum_\alpha \langle e^{V[m_L,\phi_L]}|\alpha\rangle\langle\alpha|e^{V[m_R,\phi_R]}\rangle. \tag{1.8}$$

The bipartition can be understood as inserting a resolution of the identity $\sum_\alpha |\alpha\rangle\langle\alpha|$ in the auxiliary space - this is just the some over the auxiliary indices α crossing the cut.

From Overlaps to Schmidt States

The bipartition of the state discussed above bounds the rank of the entanglement spectrum, as well as the number of Schmidt states of a specified charge, but doesn't provide the spectrum itself. To find E_i, suppose we have a bipartition of a state, but in a non-orthogonal basis:

$$|\Psi\rangle = \sum_i |i; L\rangle \otimes |i; R\rangle, \quad G_{ii';L/R} = \langle i; L/R|i'; L/R\rangle \tag{1.9}$$

Using the positive-semidefinite, hermitian, Gram matrix G, we can find an orthonormal basis 'a', via $\langle a| = G^{-1/2}_{ai}\langle i|$ (interpreted as a pseudo-inverse if G is not full rank).

Now consider the reduced density matrix for the left, as expressed in this new basis:

$$|\Psi\rangle = |a; L\rangle \left[G_L^{1/2} G^{1/2^T}_R\right]_{aa'} |a'; R\rangle \tag{1.10}$$

$$\rho_L = |a; L\rangle \left[G_L^{1/2} G_R^T G_L^{1/2}\right]_{aa'} \langle a'; L| \tag{1.11}$$

Hence the combination $G_L^{1/2} G_R^T G_L^{1/2}$ is unitarily-equivalent to the reduced density matrix. If a reflection symmetry guarantees the left and right are equivalent according to $G_R^T = G_L$, then $G_L^2 \sim \rho_L$ is itself unitarily equivalent to the reduced density matrix.

Calculating the Gram matrices

To calculate the overlap matrix $\langle\bar{\phi}|\phi\rangle_R = G_R$ of a tensor network, we first calculate the overlap of the tensor network for a single site, which leaves behind auxiliary indices ϕ from the ket-$|\Psi\rangle$ and $\bar{\phi}$ from the bra-$\langle\Psi|$. As shown in Fig. 1.3b, this defines a 'doubled' tensor T,

$$T^{[i]}[\{\phi\}_i, \{\bar{\phi}\}_i] = \sum_{m_i} B^{[i]}_{m_i,\{\phi\}_i} \bar{B}^{[i]}_{m_i,\{\bar{\phi}\}_i} = e^{-S_i[\{\phi\}_i] - \bar{S}_i[\{\bar{\phi}\}_i] + V_i[\{\phi\}_i, \{\bar{\phi}\}_i]} \tag{1.12}$$

$$\langle\Psi|\Psi\rangle \propto \langle e^{V[\phi,\bar{\phi}]}\rangle_{\phi,\bar{\phi}}. \tag{1.13}$$

By taking the overlap the physical index m disappears, but the summation over m couples the copies $\phi, \bar{\phi}$. Remarkably, the doubled tensor T *uniquely determines* $|\Psi\rangle$ up to a 1-site local unitary. It is fitting and proper to call the doubled auxiliary theory the 'plasma' theory for system, by analogy Laughlin's observation that the norm of the Laughlin state is the classical partition function of a one-component plasma. We will see this analogy is exact!

The Gram matrix G_R can be computed by summing over the $\phi, \bar{\phi}$ restricted to the right of the cut R; this again leaves 'dangling indices' on the cut ∂R which I denote by $\phi(0), \bar{\phi}(0)$. The dangling legs are a boundary condition on the trace,

$$G_{R,\bar{\phi}\phi} = \langle\bar{\phi}|\phi\rangle_R = \sum_{\phi\in R} \prod_{i\in R} T^{[i]}[\{\phi\}_i, \{\bar{\phi}\}_i] \tag{1.14}$$

$$\sim \int_{\phi(0)=\phi, \bar{\phi}(0)=\bar{\phi}}^{\infty} \mathcal{D}[\phi, \bar{\phi}] e^{-S[\phi] - S[\bar{\phi}] + V[\phi,\bar{\phi}]} \tag{1.15}$$

This is the same trick we use to calculate the ground state in a field theory: perform the path integral subject to boundary conditions on some time slice $\tau = 0$.

Choosing coordinates for the lattice such that τ runs perpendicular to the entanglement cut, we can pass to a 'Hamiltonian' picture by treating the integration over one column of the tensor network as a transfer operator taking $\tau \to \tau + 1$. There is no reason the transfer operator must arise from a Hermitian generator, so the spectrum of the transfer matrix may be complex. Nevertheless, the dominant eigenvalue (the eigenvalue of largest magnitude) must be 1 if Ψ is normalized and not a cat-state. The corresponding right eigenvector is precisely G_R; in this sense G_R is the 'ground state' of the doubled auxiliary theory. Furthermore, one can show that along the direction τ all correlations in the physical system decay with a correlation length set by the gap of the transfer matrix. So for short-range correlated states, the transfer matrix is gapped. This suggests G_R will have the same locality properties as a gapped ground state, but currently nothing rigorous can be said since it is difficult to characterize non-Hermitian transfer matrices.

Before proceeding further, I will introduce a concrete test case - the fractional quantum Hall effect.

1.2 The fractional quantum Hall effect: conformal block wavefunctions as continuum tensor networks

When a strong magnetic field is applied perpendicular to a very clean two-dimensional electron gas, a zoo of distinct incompressible phases is observed depending on the density of electrons ρ relative to the density of magnetic flux quanta, $\nu = \rho/2\pi\ell_B^2$, where ℓ_B is the magnetic length. [118] In their seminal paper, Moore and Read proposed that trial wave functions for the FQHE can be generated from the data of a conformal field theory (CFT), with a resulting topological order which can be read off from the CFT when certain conditions are met. [70] Recall Laughlin's ansatz for the first quantized wave function of electrons at a density $\nu = 1/3$, [64]

$$\Psi[\{z\}] = \prod_{i<j}(z_i - z_j)^3 e^{-\frac{1}{4}\sum_j |z_j|^2}, \tag{1.16}$$

where $z = x + iy$ are complex coordinates for the 2DEG. Moore and Read noted that the Laughlin wave function for N particles is the N-point function of a chiral conformal field theory (CFT),

$$\Psi[\{z_j\}] = \langle e^{\mathcal{O}_{bc}} \prod_{j=1}^{N} \mathcal{V}_e(z_j)\rangle_{\mathrm{CFT}}. \tag{1.17}$$

The operator $\mathcal{V}_e(z)$ is a suitably chosen local operator in the CFT called the 'electron operator,' which has either integral or half-integral conformal spin depending on whether the physical particles are bosonic or fermionic respectively. The insertion $\mathcal{O}_{bc}$ is a 'background charge' required to preserve $U(1)$. For the Laughlin state at $\nu = 1/q$, the CFT is a free chiral boson $\phi(z)$, with electron operator $\mathcal{V}_e(z) = e^{i\sqrt{q}\phi(z)}$ and background charge $\mathcal{O}_{bc} = -i\rho_e\sqrt{q}\phi$, with ρ_e the electron density. The two-point function of a free chiral boson is

$$\langle e^{i\sqrt{q}\phi(z_1)} e^{i\sqrt{q}\phi(z_2)} \rangle_{\text{CFT}} \sim (z_1 - z_2)^q, \tag{1.18}$$

and using Wick's theorem this result can repeated to generate the full $(z_i - z_j)^q$ Jastrow factor. The interactions with the pesky (but important) background charge produces the additional Gaussian.

In general, each choice of CFT and electron operator $\mathcal{V}_e$ gives a trial wave function for the quantum Hall effect, and there is a highly developed art to determine which wave functions are sensible and what topological order they possess. One aim of this thesis is to explain why the Moore-Read construction is a continuous version of a tensor network, and that this insight can be used to develop highly efficient numerical properties to study the resulting states. To make the relation clear, it is helpful to use the second-quantized formalism for the electron system. Recall that the coherent states are defined by $|\psi\rangle = e^{\int d^D x \psi(x)\hat{c}^\dagger(x)}|0\rangle$, where $|0\rangle$ is the Fock vacuum, $\hat{c}^\dagger$ is the creation operator, and $\psi(x)$ is a complex or Grassmann valued field. The coherent state wave functional for a state $|\Psi\rangle$ is $\Psi[\psi] = \langle\psi|\Psi\rangle$. Using coherent states, we can rewrite Eq. 1.17 as

$$\Psi[\psi] = \langle e^{\int d^2 z \mathcal{V}_e(z)\psi(z) + \mathcal{O}_{bc}} \rangle_{\text{CFT}}, \tag{1.19}$$

which is confirmed by Taylor expanding the exponential. Note that Eq. (1.19) is *precisely* the generating function of the CFT for the source $\mathcal{V}_e$. It is a continuum version of a tensor network as summarized in Eq. (1.2). Here the 'physical indices' which we earlier called m is the coherent state index ψ; the 'auxiliary' theory ϕ is a chiral boson; and the coupling $V[\psi, \phi] = \psi e^{i\phi\sqrt{q}}$.

Entanglement properties

Since the Moore-Read construction is a continuous tensor network, we can apply the same tricks to compute its entanglement spectrum. A detailed analysis is given in the work of Dubail and Read, [28] as well as my unpublished notes which were rendered duplicative by that work. Using the fundamental rule of coherent states, $\langle\bar{\psi}|\psi\rangle = e^{-\bar{\psi}\psi}$, we compute the doubled action T. The auxiliary field $\phi(z)$ is right

moving, while conjugated field $\bar{\phi}(\bar{z})$ is left moving, so the two copies can be combined into a single non-chiral boson, $\phi(z,\bar{z}) = \phi(z) + \bar{\phi}(\bar{z})$. The doubled theory is

$$\langle\Psi|\Psi\rangle \propto \int \mathcal{D}[\phi] e^{\int d^2z \left[\frac{1}{4\pi}(\nabla\phi)^2 + e^{i\phi\sqrt{q}} - i\sqrt{q}\rho_e\phi\right]} \tag{1.20}$$

where ϕ is a non-chiral boson. This is the sine-Gordon representation of a one-component plasma, the Lagrangian formulation of Laughlin's plasma. To compute the ground state $|G\rangle$, and hence the Gram matrix, we note that if the plasma screens, it behaves like a metal which imposes the Dirichlet constraint $\partial_x\phi = 0$ (an equipotential). So we expect that $|G\rangle$ behaves approximately like a Dirichlet boundary condition $|D\rangle$, which can be analyzed using the machinery of boundary conformal field theory. It can be argued that, up to certain irrelevant terms, the main correction to the Dirichlet state is to displace the Dirichlet boundary condition by the Debye length of the plasma, ℓ_{D}: $|G\rangle \sim e^{-\ell_{\mathrm{D}}H}|D\rangle$. [86] Note however that the Dirichlet condition $\partial_x\phi$ does not fully specify the state, due the the U(1) shift - we expect this ambiguity should be related to the topological degeneracy. We will return to this issue in more detail in the next section. Letting $|\alpha\rangle/|\bar{\alpha}\rangle$ denote states in the right / left moving CFTs, the resulting state $|G\rangle_a$ in topological sector a is

$$|G\rangle_a = \sum_{\alpha\in\mathcal{H}_a} e^{-\ell_{\mathrm{D}}H+\cdots}|\alpha\rangle|\bar{\alpha}\rangle \tag{1.21}$$

The same analysis holds for the left / right Gram matrices, so using Eqn.(1.11) we conclude the entanglement Hamiltonian is in fact H, up to some irrelevant corrections.

1.3 Topological order, minimally entangled states, and tensor networks

Minimally entangled states

A topologically ordered phase is characterized by a set of $\mathfrak{m}$ anyonic excitations which we label by a. [56] Each anyon corresponds to an emergent topological superselection sector: if a region contains an anyon a, there is no local operator which can remove the excitation. By definition, all excitations which arise by acting with local operators on the ground state, such as a spin flip or electron creation operator, are in the same superselection sector as the ground state, which we give the 'trivial' label $a = \mathbb{1}$. If two anyons a, b approach each other, by acting with local operators

that encompass both excitations they may 'fuse' together into an anyon c; if this process is allowed we write $N_{ab}^c > 0$. The theory is non-Abelian if there are anyons a, b with distinct possible outcomes, $\sum_c N_{ab}^c > 1$. These distinct outcomes can be used to robustly store quantum information, since no local operator can measure the actual result of fusing the anyons until they approach each other.

A theory with $\mathfrak{m}$-anyon types has a ground state degeneracy of $\mathfrak{m}$ when placed on a torus or infinitely long cylinder. [135] On an infinite cylinder, there is a canonical basis, which has been called the 'minimally entangled basis,' [143] and can be constructed in two equivalent ways.

In the first construction, let x denote the periodic direction of the cylinder, and y a coordinate along its length. Let $\hat{\gamma}_x^a(y)$ denote the adiabatic process of generating an $a - \bar{a}$ pair from the vacuum in the vicinity of y, dragging a around the cycle x (localized in a strip near y) and re-annihilating the pair to return to the vacuum. In general, this may have a non-trivial action on ground state manifold.[2] The minimally entangled basis is the *unique* basis in which $\hat{\gamma}_x^a(y)$ is diagonal for all anyon types a. A helpful picture for this basis is given in terms of 'topological flux,' as made precise in Abelian Chern-Simons theory. The operator $\hat{\gamma}_x^a(y) \sim e^{i\int dx A_x^a(x,y)}$ is a Wilson-loop in the theory; the path taken by the anyon pair defines an Amperian loop which detects the flux threading through the cylinder. Creating an anyon pair $b - \bar{b}$ and separating the pair out to $y = \pm\infty$, a process we denote $\hat{\gamma}_y^b(x)$, behaves like topological flux insertion through the cylinder. When the anyon b crosses the Amperian loop $\hat{\gamma}_x^a(y)$, it will detect that additional topological flux now threads the cylinder. The changed eigenvalue it determined by the mutual statistics S_{ab}:

$$\hat{\gamma}_x^a \hat{\gamma}_y^b = S_{ab} \hat{\gamma}_y^b \hat{\gamma}_x^a. \tag{1.22}$$

The minimally entangled basis has definite topological flux threading the cylinder, diagonalizing γ_x; dragging anyon pairs out to infinity with γ_y permutes the minimally entangled basis. Because of the non-degeneracy of braiding, each MES is uniquely labeled by it's set of eigenvalues under γ_x.

In the second construction, consider the Schmidt decomposition of one of the ground states, $|\psi\rangle = \sum_i s_i |i\rangle_L |i\rangle_R$. Let us define an equivalence relation on Schmidt states $|i\rangle_R \sim |j\rangle_R$, if there exists a local operator with non-trivial overlap between i, j. This equivalence relation allows us to decompose the Schmidt decomposition

[2] There are some exotic lattice theories in which dragging an anyon a around x permutes the anyon type, so it cannot be immediately re-annihilated - we ignore this case.

into equivalent sectors,

$$|\psi\rangle = \sum_{i\in a} s_i |i\rangle_L |i\rangle_R + \sum_{i\in b} s_i |i\rangle_L |i\rangle_R \cdots \tag{1.23}$$

$$= \sqrt{p_a}|a\rangle + \sqrt{p_b}|b\rangle + \cdots \tag{1.24}$$

where $i \in a$ denotes a particular equivalence class. It follows that if $|\psi\rangle$ is an eigenstate, the $|a\rangle, |b\rangle \cdots$ *must also be eigenstates*. This is because the Hamiltonian H is a local operator, so $\langle a|H|b\rangle = 0$ by the definition of the equivalence class. By construction, the states $|a\rangle$ cannot be further decomposed - they are the minimally entangles states. If the entanglement entropy of $|a\rangle$ is S_a, then

$$S_\psi = \sum_a p_a S_a - \sum_a p_a \log(p_a). \tag{1.25}$$

Superimposing the minimally entangled states generates an additional entropy $-\sum_a p_a \log(p_a)$, so the ME basis states are local minima of the entanglement entropy.

Let's see why these two definitions are equivalent. In the first definition, each MES a is an eigenstate of $\gamma_x^b(y)|a\rangle = S_{ba}(y)|a\rangle$. If we temporarily view the infinite cylinder as a 1D system, the operators γ behave like order parameters to detect the ground state. If we consider Schmidt state $|i\rangle_{Ra}, |j\rangle_{Rb}$ from different MES basis states a, b (according to definition 1), then we see that no local operator can connect them. This is because, for y very far from the cut,

$$\langle i|\gamma_x^b(y)|i\rangle_{Ra} = S_{ba}(y) \neq \langle j|\gamma_x^b(y)|j\rangle_{Rac} = S_{bc}(y) \tag{1.26}$$

Since the Schmidt states have a different expectation value for any y far from the cut, the two states must be macroscopically distinct, so cannot be connected by any local operator. Hence the 1st definition is equivalent to the 2nd definition.

In the MES basis for a cylinder of circumference L, the entanglement entropy of sector $|a\rangle$ scales as [58, 65]

$$S_a(L) = \alpha L - \log(\mathcal{D}/d_a) + \mathcal{O}(e^{-L/\xi}), \quad \mathcal{D} = \sqrt{\sum_a d_a^2}. \tag{1.27}$$

The subleasing correction $\gamma_a = \log(\mathcal{D}/d_a)$ is known as the 'topological entanglement entropy,' and measures the quantum dimensions d_a of the anyons.

MES in the conformal block picture

Like any tensor network, there is a bipartition of the quantum Hall states in correspondence with the states of the auxiliary CFT. Working on a cylinder, do *all*

states in the CFT appear in this bipartition? Let us suppose that the vacuum state $|\mathbb{1}\rangle$ appears in the bipartition. The rest of the states in the bipartition are built up from $|\mathbb{1}\rangle$ by acting with various powers of the electron operator $\mathcal{V}_e(z)$, as this is the *only* operator coupling to physical fluctuations. It follows that only states in the CFT which are generated from $\mathcal{V}_e(z)$ acting on $|\mathbb{1}\rangle$ need appear in the bipartition. This Hilbert space, $\mathcal{H}_{\mathbb{1}} \in \mathcal{H}_{CFT}$, is a representation of the 'chiral algebra' generated by $\mathcal{V}_e(z)$; it includes the action of the Virasora algebra and the current $\partial\phi$ as subalgebras. But $\mathcal{H}_{\mathbb{1}}$ is *not* the entire Hilbert space of the CFT. For example, the state $e^{i\phi/\sqrt{q}}|\mathbb{1}\rangle \notin \mathcal{H}_{\mathbb{1}}$. Under the action of the chiral algebra generated by $\mathcal{V}_e(z)$, the Hilbert space of the CFT decomposes into irreducible representations $\mathcal{H}_{CFT} = \sum_{a=1}^{\mathfrak{m}} \mathcal{H}_a$. If there are $\mathfrak{m}$ anyons, there will be $\mathfrak{m}$ sectors.

The restriction of the bipartition to states in a particular sector $\mathcal{H}_a$ gives precisely the minimally entangled basis.

Anyons

Given a region A with boundary ∂A, we have discussed why the tensor network generates a map from configurations of the auxiliary field $\phi \in \partial A$ on the boundary to a physical state in A, which we call $|\phi\rangle_A$. An interesting test for topological order is to test whether this map is injective, meaning that each distinct ϕ leads to a distinct $|\phi\rangle_A$. In the case of quantum Hall, where ϕ is the configuration of a chiral boson, consider states $|\phi\rangle_A, |\phi + 2\pi/\sqrt{q}\rangle_A$. The action of the chiral boson is invariant under this shift, as is the electron operator $\mathcal{V}_e = e^{i\phi(z)\sqrt{q}}$. Only the background charge $\mathcal{O}_b c = -i\sqrt{q}\rho_e\phi$ is sensitive to the shift, so we find

$$|\phi + 2\pi/\sqrt{q}\rangle_A = e^{-i2\pi\rho_e V_A}|\phi\rangle_A, \tag{1.28}$$

where V_A is the volume of region A. Hence the map is not injective, and implies a sort of 'gauge symmetry' of the tensor network, since we can insert *closed* string operators which shift $\phi \to 2\pi/\sqrt{q}$ with impunity anywhere in the auxiliary theory. This suggests that if we shift $\phi \to 2\pi/\sqrt{q}$ along a string that *terminates* as some z, there will be an excitation at z, since the string is invisible elsewhere.

In the Hamiltonian formalism, the operator $\mathcal{V}_{qh} = e^{i\phi(x)/\sqrt{q}}$ takes $\phi \to \phi + 2\pi/\sqrt{q}\theta(-x)$, so is exactly the desired non-local string operator. As pointed out by Moore and Read, Laughlin's ansatz for a quasi-hole position η is indeed generated by the insertion of $\mathcal{V}_{qh}$:

$$\Psi_{qp}[z;\eta] = \prod_i (z_i - \eta) \prod_{i<j} (z_i - z_j)^q e^{-\frac{1}{4}\sum_i |z_i|^2} \quad = \left\langle e^{i\phi(\eta)/\sqrt{q}} \prod_i \mathcal{V}_e(z) e^{\mathcal{O}_{bc}} \right\rangle_{\text{CFT}}. \tag{1.29}$$

This suggests the following general principle: if a tensor network has a gauge symmetry in the auxiliary degrees of freedom, meaning that there are closed string-like operators that can be inserted into the tensor network while leaving the physical state unchanged, then the insertion of an *open* string into the auxiliary theory generates an anyon at the endpoint of the string. To rule out trivial counterexamples (such as the CZX model of Ref. [17]) it is important to specify that the dimension of the bulk-boundary map's kernel should *saturate* with the length of the boundary, rather than growing extensively. Otherwise there will be extensively many short open auxiliary strings which do nothing, rather than produce anyons.

This picture is consistent with the Moore-Read construction, where these string operators are precisely the primary fields in one-to-one correspondence with the anyons, like $\mathcal{V}_{qh}$ for the Laughlin state. For a variety of tensor networks models, such as those for Levin-Wen string-net models and Dikgraaf-Witten theories, it has been indeed been shown the gauge symmetry of the auxiliary theory is a necessary and sufficient condition for topological order.[114, 98, 18, 12]

This concludes my sketch.

1.4 Organization

This thesis is organized as follows.

In Chapter 1, I review 1D tensor networks (matrix product states), the algorithms used to work with them, and their behavior near quantum critical points.

In Chapter 2, I elaborate on the exact tensor network representation of the FQHE, work done in collaboration with Roger Mong. To make the tensor network practically useful, the physical Hilbert space is mapped to a 1D fermion chain by using the Landau gauge on a cylinder. Using the resulting 1D tensor network, a variety of properties can be efficiently computed, such as the entanglement spectrum and statistical Berry phases of the anyons.

In Chapter 3, I consider a different class of model wavefunctions, the parton ansatz for spin-systems. In the construction studied here, a spinful fermionic BCS superconductor is projected onto an occupation of one fermion per site, leaving behind a spin-1/2 wavefunction. I show that for an arbitrary BCS superconductor, we can obtain an exact tensor network representation of the ground state, which can trivially be projected to get a spin wave function. This will be useful for various studies of potential quantum spin-liquids, such as the Kagome Heisenberg anti-ferromagnet.

Finally, in Chapter 4, I show how to approximate a time evolution operator e^{-itH} using a tensor-network representation. The inspiration for this result is an exact representation for Hamiltonians which can be decomposed into commuting or anti-

commuting terms. In the more general case, this reduces to an approximate scheme which can be used to efficiently simulate time evolution for arbitrary Hamiltonians.

Chapter 2

Matrix Product States and Algorithms

In this section I review the matrix product state (MPS) ansatz as well as algorithms for finding ground states and simulating time evolution. The infinite time evolving block decimation (iTEBD) [126] and the infinite density matrix renormalization group (iDMRG) [69] algorithms are both based on the infinite matrix-product state (iMPS) representation. [126] As we explain shortly, MPSs can efficiently represent many-body wave functions with the accuracy controlled by the *bond dimension* χ (the error decreases rapidly with increasing χ). Methods which work with infinite systems have a number of advantages: no extrapolation to the thermodynamic limit is needed; there are no edge modes which can complicate the convergence of the algorithm; and, as shown later on in this section, finite entanglement scaling can be used to extract quantities such as the central charge. We begin by reviewing some details of this infinite system representation focusing on translationally invariant systems, and then contrast and compare the two numerical methods using a consistent notation. We do not aim to provide a complete discussion of the techniques but rather a clear and compact introduction to the methods used. [1]

2.1 Matrix product states

The concept of entanglement is central to the MPS representation and the algorithms based on it. The so-called *entanglement spectrum* [66] is obtained from the Schmidt decomposition (singular value decomposition): Given a bipartition $\mathcal{H} = \mathcal{H}_L \otimes \mathcal{H}_R$ of the Hilbert space (below $\mathcal{H}_L$ and $\mathcal{H}_R$, respectively, represent the

[1] Portions of this work appear in Phys. Rev. B 87, 235106

states on sites to the left and right of a bond), any state $|\Psi\rangle \in \mathcal{H}$ can be decomposed as

$$|\Psi\rangle = \sum_{\alpha} \Lambda_\alpha |\alpha\rangle_L \otimes |\alpha\rangle_R, \quad |\alpha\rangle_{R/L} \in \mathcal{H}_{R/L}. \tag{2.1}$$

The Schmidt coefficients (singular values) Λ_α can always be chosen positive. The states $\{|\alpha\rangle_L\}$ and $\{|\alpha\rangle_R\}$ form orthonormal sets in $\mathcal{H}_L$ and $\mathcal{H}_R$ respectively, i.e., $\langle\alpha|\beta\rangle_L = \langle\alpha|\beta\rangle_R = \delta_{\alpha\beta}$, and by normalization $\sum_\alpha \Lambda_\alpha^2 = \langle\Psi|\Psi\rangle = 1$. The Schmidt decomposition is related to the reduced density matrix for one half of the system, $\rho^R = \mathrm{Tr}_{\mathcal{H}_L}(|\psi\rangle\langle\psi|)$. In particular, the Schmidt states $|\alpha\rangle_R$ are the eigenstates of ρ^R and the Schmidt coefficients are the square roots of the corresponding eigenvalues, i.e., $\rho^R = \sum_\alpha \Lambda_\alpha^2 |\alpha\rangle\langle\alpha|_R$ (and analogously for ρ^L). This directly gives the entanglement entropy through

$$S_E = -\sum_{\alpha} \Lambda_\alpha^2 \log \Lambda_\alpha^2. \tag{2.2}$$

Finally, the entanglement spectrum $\{\epsilon_\alpha\}$ is related to the spectrum $\{\Lambda_\alpha^2\}$ of the bipartition by $\Lambda_\alpha^2 = \exp(-\epsilon_\alpha)$ for each α.

Matrix-product states

A general quantum state $|\Psi\rangle$ on a chain with N sites can be written in the following MPS form: [31, 75, 94]

$$|\Psi\rangle = \sum_{j_1,\ldots,j_N} A^{[1]j_1} A^{[2]j_2} \ldots A^{[N]j_N} |j_1, \ldots, j_N\rangle. \tag{2.3}$$

Here, $A^{[n]j_n}$ is a $\chi_{n-1} \times \chi_n$ matrix and $|j_n\rangle$ with $j_n = 1, \ldots, d$ is a basis of local states at site n. We call the indices of the matrices "bond" indices. The matrices at the boundary, i.e., $n = 1$ and $n = N$, are vectors, that is $\chi_0 = \chi_N = 1$, such that the matrix product in (2.3) produces a scalar coefficient. The superscript $[n]$ denotes the fact that for a generic state, each site is represented by a different set of matrices. Ground states of one dimensional gapped systems can be efficiently approximated by an MPS,[38, 100] in the sense that the value of the χ's needed to approximate the ground state wave function to an arbitrary precision is finite as $N \to \infty$. The physical insight that allows us to make this statement is the area law, which holds for this class of systems. [122, 48, 122]

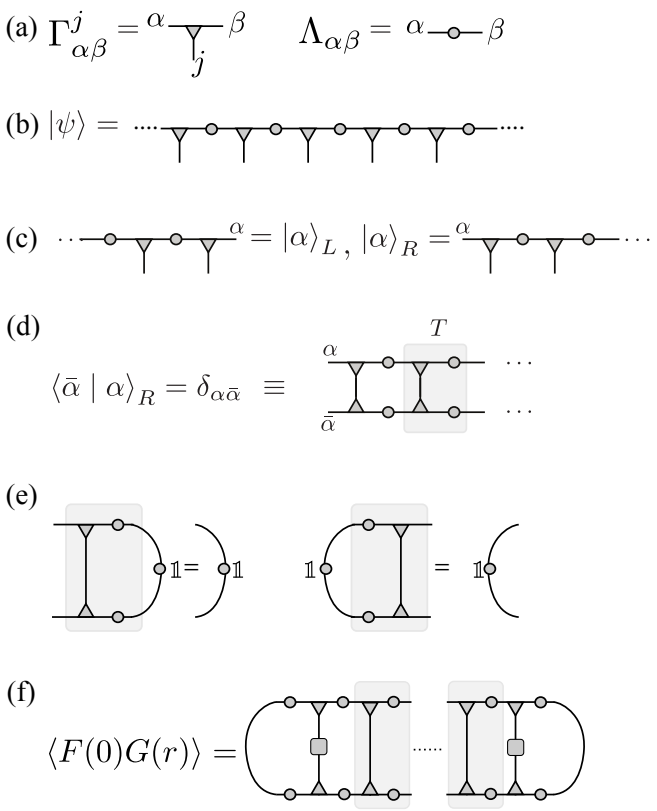

Figure 2.1: Diagrammatic representation of (a) the tensors Γ and Λ. The horizontal lines represent the bond indices $\alpha \in \{1, \ldots, \chi\}$ and the vertical lines the physical indices $j \in \{1, \ldots, d\}$. (b) An MPS formed by the tensors Γ and Λ. Connected lines between tensors (or within a single tensor) denote summation over the corresponding indices. (c) Definition of the right and left (Schmidt) basis states with respect to a partition on a bond with index α. (d) Condition for the MPS to be in the canonical form. The transfer matrix T of Eq. (2.6) has been shaded. The upside-down triangles are the complex conjugate of the Γ tensors. (e) If the state is in canonical form, then the dominant right eigenvector of T is the 'identity matrix' with eigenvalue equal to 1. A similar condition applies for the left transfer matrix $\tilde{T}$. (f) The correlation function defined in Eq. (2.9). The squares correspond to the operators $F(0)$ and $G(r)$.

Canonical form. Without a loss of generality, we write the matrices A^j as a product of $\chi_{j-1} \times \chi_j$ complex matrices Γ^j and positive, real, square diagonal matrices

Λ,

$$|\Psi\rangle = \sum_{j_1,\ldots,j_N} \Gamma^{[1]j_1}\Lambda^{[1]}\Gamma^{[2]j_2}\Lambda^{[2]}\cdots\Lambda^{[N-1]}\Gamma^{[N]j_N} \times |j_1,\ldots,j_N\rangle \ , \tag{2.4}$$

which is pictorially illustrated in Figs. 2.1(a) and 2.1(b). A rank-n tensor is represented by a symbol with n protruding lines. (For example, Γ, a rank-3 tensor, has three indices and is represented by a triangle with three lines protruding from it.) Connecting the lines among tensors symbolizes a tensor contraction, i.e., summing over the relevant indices. In the following we will motivate the choice (2.4) for the MPS form.

Equation (2.4) allows for many possible representation of the same wave function, as we can insert a resolution of the identity $\mathbb{1} = XX^{-1}$ into any bond. This freedom can be used to define a 'canonical form' of the MPS.[128, 126]. Any bond n defines a bipartition of the system into sites $L = \{1,\ldots,n\}$ and $R = \{n+1,\ldots,N\}$ to the left and right of the bond. From the form of the MPS, we can define a set of χ_n wave functions $|\alpha\rangle^{[n]}_{L/R}$ to the left/right of the bond [see Fig. 2.1(c)] such that state takes the form

$$|\psi\rangle = \sum_{\alpha=1}^{\chi} \Lambda^{[n]}_\alpha |\alpha\rangle^{[n]}_L \otimes |\alpha\rangle^{[n]}_R, \quad |\alpha\rangle^{[n]}_{R/L} \in \mathcal{H}_{R/L}. \tag{2.5}$$

The MPS representation $\{\Gamma^{[1]},\Lambda^{[1]},\ldots,\Gamma^{[N]}\}$ is in canonical form if: *For every bond, the set of wave functions* $|\alpha\rangle^{[n]}_{L/R}$ *along with* $\Lambda^{[n]}$ *form a Schmidt decomposition of* Ψ. In other words we must have $\langle\bar\alpha|\alpha\rangle^{[n]}_L = \delta_{\bar\alpha\alpha}$ and $\langle\bar\alpha|\alpha\rangle^{[n]}_R = \delta_{\bar\alpha\alpha}$, along with $\sum(\Lambda^{[n]}_\alpha)^2 = 1$ on every bond. For finite systems, a generic MPS can be transformed into canonical form by successively orthogonalizing the bonds starting from either the left or right end of the chain. [97]

Infinite matrix product states. In this paper we are most interested in infinite chains, $N \to \infty$. In this case, translational invariance is restored and the set of matrices on any given site becomes the same, that is $\Gamma^{[n]j} = \Gamma^j$ and $\Lambda^{[n]} = \Lambda$ for all integers n. To check if the iMPS is in canonical form, we need to compute the overlaps $\langle\bar\alpha|\alpha\rangle_R$, which would appear to require an infinite tensor contraction. Alternatively, we can use the translation invariance to proceed inductively. For an infinite MPS, the orthogonality condition (i.e., canonical form) is conveniently expressed in terms of the *transfer matrix* T [illustrated in Fig. 2.1(d)] defined as

$$T_{\alpha\bar\alpha;\beta\bar\beta} = \sum_j \Gamma^j_{\alpha\beta}\left(\Gamma^j_{\bar\alpha\bar\beta}\right)^*\Lambda_\beta\Lambda_{\bar\beta}, \tag{2.6}$$

where '*' denotes complex conjugation (pictorially represented by an upside-down triangle). The transfer matrix T relates the overlaps defined on bond n with overlaps defined on bond $n+1$. Given that the right basis states $|\beta\rangle_R^{[n+1]}$ on bond $n+1$ are orthonormal, the states $|\alpha\rangle_R^{[n]}$ on bond n will also be orthonormal if T has a *right* eigenvector $\delta_{\beta\bar{\beta}}(=\mathbb{1})$ with eigenvalue $\eta = 1$, as illustrated in Fig. 2.1(e). For the left set of states we define an analogous transfer matrix $\tilde{T}$,

$$\tilde{T}_{\alpha\bar{\alpha};\beta\bar{\beta}} = \sum_j \Lambda_\alpha \Lambda_{\bar{\alpha}} \, \Gamma^j_{\alpha\beta} \left(\Gamma^j_{\bar{\alpha}\bar{\beta}}\right)^* \tag{2.7}$$

which must have a *left* eigenvector $\delta_{\alpha\bar{\alpha}}$ with $\eta = 1$. These eigenvector criteria are clearly necessary conditions for all bonds to be canonical; in fact, assuming in addition that $\eta = 1$ is the dominant eigenvalue, they are sufficient. There is an algorithm to explicitly transform an arbitrary infinite MPS to the canonical form.[73].

If the infinite MPS is not translational invariant with respect to a one-site unit cell, all the above can be simply generalized by considering a unit-cell of L sites which repeats itself, e.g., in the case of $L = 2$ the tensors are given by

$$\begin{aligned} \Gamma^{[2n]} &= \Gamma^A, \qquad \Lambda^{[2n]j} = \Lambda^A, \\ \Gamma^{[2n+1]} &= \Gamma^B, \qquad \Lambda^{[2n+1]} = \Lambda^B, \end{aligned} \tag{2.8}$$

for $n \in \mathbb{Z}$. Reviews of MPSs as well as the canonical form can be found in Refs. [78, 73, 126].

Calculations of observables from an iMPS. If the MPS is given in canonical form, we can use the orthogonality of the Schmidt states to evaluate local expectation values by contracting the tensors locally.[126] Correlation functions can be obtain using the transfer matrix Eq. (2.6). For this we evaluate $\langle P(0)Q(r)\rangle$ of an iMPS. Let $r > 0$, then

$$\begin{aligned} \langle P(0)Q(r)\rangle &= \Upsilon_L(P) T^{r-1} \Upsilon_R(Q), \\ \Upsilon_L(P)_{\alpha\bar{\alpha}} &= \sum_\gamma \Lambda^2_\gamma \big(\Gamma^i_{\gamma\bar{\alpha}}\big)^* P^{ij} \Gamma^j_{\gamma\alpha} \Lambda_\alpha \Lambda_{\bar{\alpha}}, \\ \Upsilon_R(Q)_{\beta\bar{\beta}} &= \sum_\gamma \Lambda^2_\gamma \big(\Gamma^i_{\bar{\beta}\gamma}\big)^* Q^{ij} \Gamma^j_{\beta\gamma}. \end{aligned} \tag{2.9}$$

$\Upsilon_{L/R}$ are the "stubs" which measures the operators P and Q locally, in between which we put $r-1$ copies of the transfer matrix T, see Fig. 2.1(f) for a pictorial representation. Local observables $\langle P(0)\rangle$ can be obtained from the same expression,

replacing $\Upsilon_R(Q)_{\beta\bar{\beta}}$ with the identity operator $\delta_{\beta\bar{\beta}}$. By generalizing the transfer matrix to include one-site operators

$$T_{\alpha\alpha';\beta\beta'}[R] = \sum_{jj'} R_{jj'} \Gamma^{j'}_{\alpha\beta} \left(\Gamma^{j}_{\alpha'\beta'}\right)^* \Lambda_\beta \Lambda_{\beta'}, \tag{2.10}$$

non-local order parameters can be obtained with the same approach. For example, calculating the correlation function with $P = Q = S_z$ and $R = e^{i\pi S^z}$, we obtain a "string order" parameter. The resulting correlation functions generically take the form of a sum of exponentials, with the slowest decaying exponential determined by the second largest (in terms of absolute value) eigenvalue ϵ_2 of the transfer matrix. We define the correlation length of the MPS as

$$\xi = -\frac{1}{\log|\epsilon_2|}, \tag{2.11}$$

which is readily obtained using a sparse algorithm to find the eigenvalues of the transfer matrix. A degenerate largest eigenvalue indicates that the state is in a 'cat state,' i.e., in a superposition of different superselection sectors, which can occur when there is spontaneous symmetry breaking.[80]

In systems with a conserved quantum number (e.g., the total S_z), one can calculate the correlation length for operators (P, Q) corresponding to different sectors from the corresponding eigenvalues of the transfer matrix. In this paper we denote the two correlation lengths corresponding to operators which change the quantum numbers by $S_z = 0$ (e.g. $\langle S^z S^z \rangle$) as ξ_0 and $S_z = \pm 1$ (e.g. $\langle S^+ S^- \rangle$) as ξ_1. The correlation length ξ is given by the largest one, i.e., $\xi = \max(\xi_0, \xi_1, ...)$.

2.2 Infinite Time Evolving Block Decimation (iTEBD)

In the iTEBD algorithm, we are interested in evaluating the time evolution of a quantum state:

$$|\psi(t)\rangle = U(t)|\psi(0)\rangle. \tag{2.12}$$

The time evolution operator U can either be $U(t) = \exp(-iHt)$ yielding a real time evolution, or an imaginary time evolution $U(\tau) = \exp(-H\tau)$. The latter is used to find ground states of the Hamiltonian H through the relation

$$|\psi_{\mathrm{GS}}\rangle = \lim_{\tau\to\infty} e^{-\tau H}|\psi_0\rangle. \tag{2.13}$$

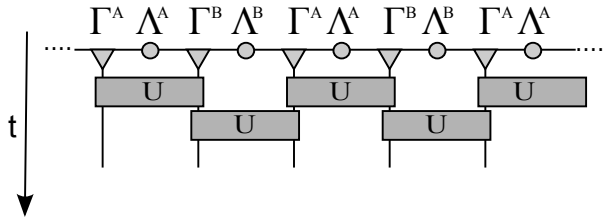

Figure 2.2: In iTEBD each time step δt of a time evolution is approximated using a Trotter-Suzuki decomposition, i.e., the time evolution operator is expressed as a product of unitary two-site operators.

To achieve this, one makes use of the Trotter-Suzuki decomposition, which approximates the exponent of a sum of operators, with a product of exponents of the same operators. For example, the first order expansion reads

$$e^{(V+W)\delta} = e^{V\delta}e^{W\delta} + \mathcal{O}(\delta^2). \tag{2.14}$$

Here V and W are operators, and δ is a small parameter. The second order expansion similarly reads

$$e^{(V+W)\delta} = e^{V\delta/2}e^{W\delta}e^{V\delta/2} + \mathcal{O}(\delta^3). \tag{2.15}$$

To make use of these expressions, we assume that the Hamiltonian is a sum of two-site operators of the form $H = \sum_n h^{[n,n+1]}$ and decompose it as a sum

$$\begin{aligned} H &= H_{\text{odd}} + H_{\text{even}} \\ &= \sum_{n \text{ odd}} h^{[n,n+1]} + \sum_{n \text{ even}} h^{[n,n+1]}. \end{aligned} \tag{2.16}$$

Each term H_{odd} and H_{even} consists of a sum of commuting operators.

We now divide the time into small time slices $\delta t \ll 1$ (the relevant time scale is in fact the inverse gap) and consider a time evolution operator $U(\delta t)$. Using, as an example, the first order decomposition (2.14), the operator $U(\delta t)$ can be expanded into products of two-site unitary operators

$$U(\delta t) \approx \left[\prod_{n \text{ odd}} U^{[n,n+1]}(\delta t)\right]\left[\prod_{n \text{ even}} U^{[n,n+1]}(\delta t)\right], \tag{2.17}$$

where

$$U^{[n,n+1]}(\delta t) = e^{-i\,\delta t\, h^{[n,n+1]}} \tag{2.18}$$

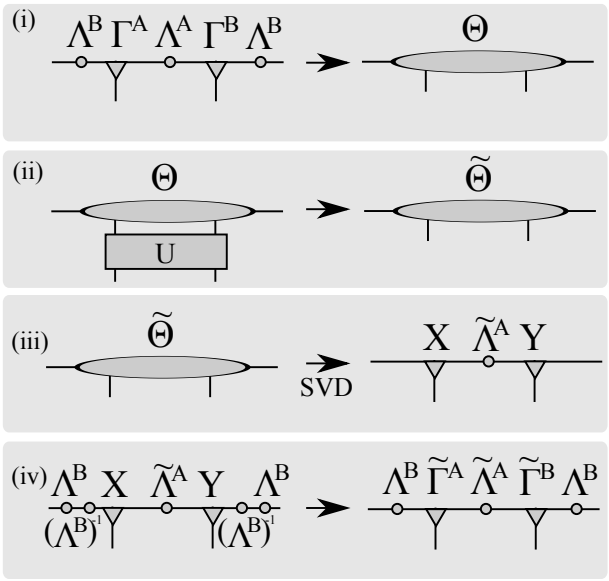

Figure 2.3: The iTEBD update scheme for a unitary two-site transformation of a two-site unit cell MPS in canonical form (see Sec. 2.2 for details).

This decomposition of the time evolution operator is shown pictorially in Fig. 2.2. One notices that even if the underlying system has a translation invariance of one site, the decomposition breaks this temporarily into a two site translation symmetry. Therefore, one needs to keep at least two sets of matrices Γ^A, Λ^A and Γ^B, Λ^B. The successive application of these two-site unitary operators to an MPS is the main part of the algorithm.

Local unitary updates of an MPS. One of the advantages of the MPS representation is that local transformations can be performed efficiently. Moreover, the canonical form discussed above is preserved if the transformations are unitary.[128]

A one-site unitary U simply transforms the tensors Γ of the MPS

$$\tilde{\Gamma}^{j}_{\alpha\beta} = \sum_{j'} U^{j}_{j'} \Gamma^{j'}_{\alpha\beta}. \tag{2.19}$$

If we consider an infinite, translational invariant MPS, this transformations implies the application of the unitary to *all* equivalent sites simultaneously. In such case the entanglement of the wave-function is not affected and thus the values of Λ do not change.

The update procedure for a two-site unitary transformation acting on two neighboring sites is shown in Fig. 2.3. We focus on an update of an AB bond between two neighboring sites n and $n+1$ for an MPS with a unit cell of size $N = 2$. The inequivalent BA bonds are updated similarly by simply exchanging A and B. The generalization to an L-site unit cell is straightforward. We first find the wave function in the basis spanned by the left Schmidt states on bond $n-1:n$, the 1-site Hilbert space of sites n and $n+1$, and the right Schmidt states on bond $n+1:n+2$, which together form an orthonormal basis $\{|\alpha_{n-1}\rangle_L, |j_n\rangle, |k_{n+1}\rangle, |\gamma_{n+1}\rangle_R\}$. Calling the wave function coefficients Θ, the state is expressed as

$$|\psi\rangle = \sum_{\alpha,j,k,\gamma} \Theta^{jk}_{\alpha\gamma} |\alpha_{n-1}\rangle_L |j_n\rangle |k_{n+1}\rangle |\gamma_{n+1}\rangle_R. \tag{2.20}$$

Using the definitions of $|\alpha\rangle_{L/R}$ shown in Fig. 2.1(b), Θ is given by

$$\Theta^{jk}_{\alpha\gamma} = \sum_{\beta} \Lambda^B_\alpha \Gamma^{A,j}_{\alpha\beta} \Lambda^A_\beta \Gamma^{B,k}_{\beta\gamma} \Lambda^B_\gamma. \tag{2.21}$$

Writing the wave function in this basis is useful because it is easy to apply the two-site unitary in step (ii) of the algorithm:

$$\tilde{\Theta}^{jk}_{\alpha\gamma} = \sum_{j'k'} U^{jk}_{j'k'} \Theta^{j'k'}_{\alpha\gamma}. \tag{2.22}$$

Next we have to extract the new tensors $\tilde{\Gamma}^A, \tilde{\Gamma}^B$ and $\tilde{\Lambda}^A$ from the transformed tensor $\tilde{\Theta}$ in a manner that preserves the canonical form. We first 'reshape' the tensor $\tilde{\Theta}$ by combining indices to obtain a $d\chi \times d\chi$ dimensional matrix $\Theta_{j\alpha;k\gamma}$. Because the basis $|\alpha_{n-1}\rangle_L |j_n\rangle$ is orthonormal, as for the right, it is natural to decompose the matrix using the singular value decomposition (SVD) in step (iii) into

$$\Theta_{j\alpha;k\gamma} = \sum_{\beta} X_{j\alpha;\beta} D_\beta Y_{\beta;k\gamma}, \tag{2.23}$$

where X, Y are isometries and D is a diagonal matrix. The isometry X relates the new Schmidt states $|\beta_n\rangle_L$ to the combined bases $|\alpha_{n-1}\rangle_L |j_n\rangle$. Analogously, the Schmidt states for the right site are obtained from the matrix Y. Thus the diagonal matrix D contains precisely the Schmidt values of the transformed state, i.e., $\tilde{\Lambda}^A = D$. The new tensors $\tilde{\Gamma}^A, \tilde{\Gamma}^B$ can be extracted directly from the matrices X, Y using the old matrices Λ^B and the definition of Θ in Eq. (2.21). In particular we obtain the new tensors in step (iv) by

$$\tilde{\Gamma}^{A,j}_{\alpha\beta} = (\Lambda^B)^{-1}_\alpha X_{j\alpha;\beta}, \tag{2.24a}$$

$$\tilde{\Gamma}^{B,j}_{\beta\gamma} = Y_{\beta;k\gamma} (\Lambda^B)^{-1}_\gamma. \tag{2.24b}$$

After the update, the new MPS is still in the canonical form. Note that as in the one-site update, if we apply the algorithm to an MPS, the update is performed simultaneously to all matrices at equivalent bonds. Thus the iTEBD algorithms exploits the translational invariance of the systems by effectively performing an infinite number of parallel updates at each step.

The entanglement at the bond $n, n+1$ has, in the update, changed and the bond dimension increased to $d\chi$. Thus the amount of information in the wave function grows exponentially if we successively apply unitaries to the state. To overcome this problem, we perform an approximation by fixing the maximal number of Schmidt terms to χ. After each step, only the χ most important states are kept, i.e., if we order the Schmidt states according to their size we simply truncate the range of the index β in (2.23) to be $1 \dots \chi$. This approximation limits the dimension of the MPS and the tensors Γ have at most a dimension of $d \times \chi \times \chi$. Given that the truncated weight is small, the normalization conditions for the canonical form will be fulfilled to a good approximation. In order to keep the wave function normalized, one should divide by the norm after the truncation, i.e., divide by $\mathcal{N} = \sqrt{\sum_{i,j,\alpha,\gamma} \left|\Theta^{ij}_{\alpha\gamma}\right|^2}$.

If we perform an imaginary time evolution of the state, the operator U is not unitary and thus it does not conserve the canonical form. It turns out, however, that the successive Schmidt decompositions assure a good approximation as long as the time steps are chosen small enough.[73] One way to obtain very accurate results is to decrease the size of the time steps successively. [126]

The simulation cost of this algorithm scales as $d^3\chi^3$ and the most time consuming part of the algorithm is the SVD in step (iii). If the Hamiltonian has symmetries, we can considerably accelerate this step by explicitly conserving the resulting constants of motion. The anisotropic spin model we study has for example a global $U(1)$ symmetry and conserves the total magnetization. Thus the matrix $\Theta_{i\alpha;j\gamma}$ has a block-diagonal form and the SVD can be performed in each block individually, yielding a considerable speed up. See Refs. [106, 105, 104] for details of an implementation of symmetries into the algorithm. Numerically, the algorithm can become unstable when the values of Λ become very small since the matrix has to be inverted in order to extract the new tensors in step (iv) of the algorithm. This problem can be avoided by applying a slightly modified version of this algorithm as introduced by Hastings in Ref. [49].

2.3 Matrix-Product Operators

The iDMRG algorithm explained in the next section relies on expressing the Hamiltonian of the system in terms of matrix product operator (MPO). An MPO

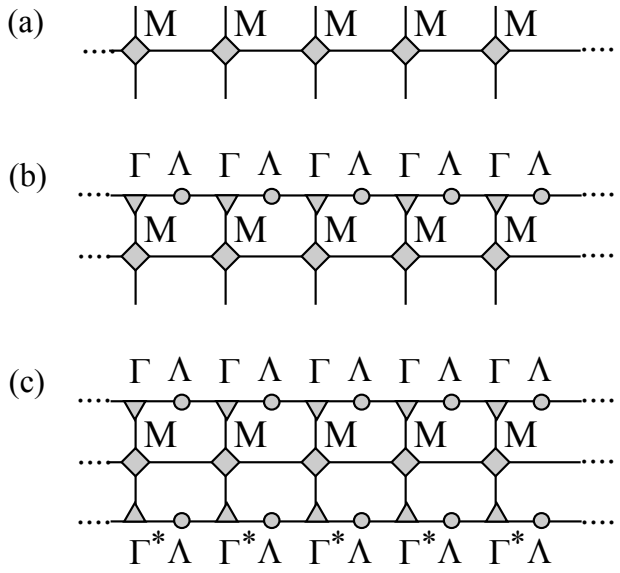

Figure 2.4: (a) An operator O acting on an entire chain expressed as a matrix product operator. (b) A matrix product operator acting on a matrix product state $O|\psi\rangle$. (c) The expectation value $\langle\psi|O|\psi\rangle$ expressed in an MPO form.

is a natural generalization of an MPS to the space of operators. An operator in an MPO form, acting on a chain with L sites, is given by

$$O = \sum_{\substack{j_1,\ldots,j_L \\ j'_1,\ldots,j'_L}} \vec{v}_{\text{left}}\, M^{[1]j_1 j'_1}\, M^{[2]j_2 j'_2} \cdots M^{[L]j_L j'_L}\, \vec{v}_{\text{right}} \times |j_1,\ldots,j_L\rangle\langle j'_1,\ldots,j'_L|\,, \tag{2.25}$$

where $M^{j_n j'_n,}$ are $D \times D$ matrices, and $|j_n\rangle$, $|j'_n\rangle$ represent local states at site n, as before. At the boundaries we initiate and terminate the MPO by the vectors $\vec{v}_{\text{left}}$ and $\vec{v}_{\text{right}}$.

A pictorial representation of an MPO is given in Fig. 2.4(a). The notation is very similar to the one for an MPS: the horizontal line corresponds to the indices of the virtual dimension and the vertical lines represent the physical states $|j_n\rangle$ (bottom) and $\langle j'_n|$ top. The advantage of the MPO is that it can be applied efficiently to a matrix product state as shown in Fig. 2.4(b). All local Hamiltonians with only short range interactions can be represented using an MPO of a small dimension D. Let us consider, for example, the MPO of the anisotropic Heisenberg model in the presence of an on-site anisotropy. Expressed as a tensor product, the Hamiltonian takes the

following form:

$$\begin{aligned} H &= S^x \otimes S^x \otimes \mathbb{1} \otimes \cdots \otimes \mathbb{1} + \mathbb{1} \otimes S^x \otimes S^x \otimes \cdots \otimes \mathbb{1} + \ldots \\ &+ S^y \otimes S^y \otimes \mathbb{1} \otimes \cdots \otimes \mathbb{1} + \mathbb{1} \otimes S^y \otimes S^y \otimes \cdots \otimes \mathbb{1} + \ldots \\ &+ \Delta S^z \otimes S^z \otimes \mathbb{1} \otimes \cdots \otimes \mathbb{1} + \ldots \\ &+ [D_2 (S^z)^2 + D_4 (S^z)^4] \otimes \mathbb{1} \otimes \mathbb{1} \otimes \cdots \otimes \mathbb{1} + \ldots \end{aligned} \tag{2.26}$$

The corresponding *exact* MPO has a dimension $D = 5$ and is given by

$$M^{[i]} = \begin{pmatrix} \mathbb{1} & 0 & 0 & 0 & 0 \\ S^x & 0 & 0 & 0 & 0 \\ S^y & 0 & 0 & 0 & 0 \\ \Delta S^z & 0 & 0 & 0 & 0 \\ D_2 (S^z)^2 + D_4 (S^z)^4 & S^x & S^y & S^z & \mathbb{1} \end{pmatrix}, \tag{2.27}$$

with

$$\vec{v}_{\text{left}} = \begin{pmatrix} 0, & 0, & 0, & 0, & 1 \end{pmatrix}, \quad \vec{v}_{\text{right}} = \begin{pmatrix} 1, & 0, & 0, & 0, & 0 \end{pmatrix}^T. \tag{2.28}$$

By multiplying the matrices (and taking tensor products of the operators), one can easily see that the product of the matrices does in fact yield the Hamiltonian (2.26). Further details of the MPO form of operators can be found in Refs. [97, 68].

2.4 Infinite Density Matrix Renormalization Group (iDMRG)

We now discuss the infinite Density Matrix Renormalization Group (iDMRG) algorithm. Unlike iTEBD, the iDMRG is a variational approach to optimizing the MPS, but the algorithms have many steps in common. One advantage of the iDMRG is that it does not rely on a Trotter-Suzuki decomposition of the Hamiltonian and thus applies to systems with longer range interactions. We assume only that the Hamiltonian has been written as an MPO. Secondly, the convergence of the iDMRG method to the ground state is in practice much faster. This is particularly the case if the gap above the ground state is small and the correlation length is long.

The schematic idea for the iDMRG algorithm is as follows (see Fig. 2.6). Like in iTEBD, the state at each step is represented by an MPS. We variationally optimize pairs of neighboring sites to minimize the ground state energy $\langle \psi | H | \psi \rangle$, while keeping the rest of the chain fixed. To do so, at each step we represent the initial wave function $|\psi\rangle$ using the two site tensor $\Theta^{jk}_{\alpha\gamma}$ (as previously defined in the iTEBD

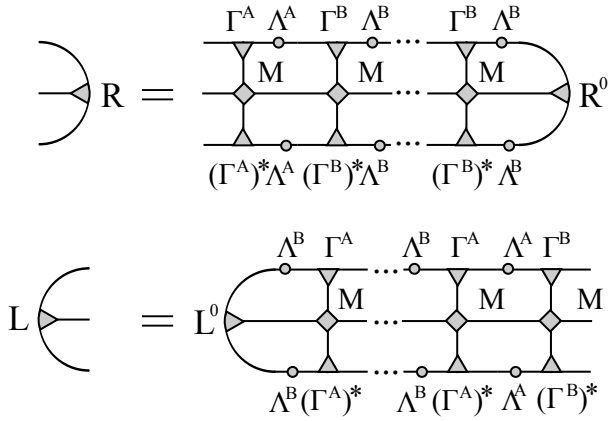

Figure 2.5: Pictorial representation of a contraction of the left and right environments. The boundaries are initiated by the tensors $R^0_{\alpha\bar{\alpha},a} = \delta_{\alpha\bar{\alpha}}\vec{v}_{\text{right};a}$ and $L^0_{\alpha\bar{\alpha},a} = \delta_{\alpha\bar{\alpha}}\vec{v}_{\text{left};a}$.

section), project the Hamiltonian into the space spanned by the basis set $|\alpha jk\beta\rangle$, and use an iterative algorithm (e.g. Lanczos) to lower the energy. Repeating this step for each pair, the wave function converges to the ground state. For simplicity, only the details of the algorithm with a unit cell of two sites, A and B, will be described below.

Two-site update algorithm. We start by describing the update of an AB bond between two neighboring sites n and $n+1$ (the update on a BA bond can be performed analogously by exchanging the role of A and B), and return later to the initialization procedure. Step (i) is identical to the first step in the iTEBD method; we contract the tensors for two neighboring sites to obtain the initial wave function $\Theta^{jk}_{\alpha\gamma}$. The orthonormal basis $|\alpha j\beta k\rangle$ spans the variational space $|\tilde{\psi}\rangle = \tilde{\Theta}^{jk}_{\alpha\gamma}|\alpha j\beta k\rangle$ of the update, in which we must minimize the energy $E = \langle\tilde{\psi}|H|\tilde{\psi}\rangle$ in order to determine the optimal $\tilde{\Theta}$. Because H is written as an infinite MPO, it appears at first that to evaluate the energy we will have to contract an infinite number of tensors starting from left and right infinity, as illustrated in Fig. 2.4(c). For the sake of induction, however, suppose we have already done this contraction on the left through bond $n-1:n$, and on the right through bond $n+1:n+2$. As illustrated in Fig. 2.5, the result of these contractions can be summarized in two three leg tensors we call the left and right "environments." The left environment $L_{\alpha\bar{\alpha},a}$ has three indices: the MPO index a, and the indices $\alpha, \bar{\alpha}$ corresponding to the bond indices of $|\tilde{\psi}\rangle$ and $\langle\tilde{\psi}|$. Likewise, on the right we have $R_{\gamma\bar{\gamma},c}$. Each bond of the system has a similarly defined environment;

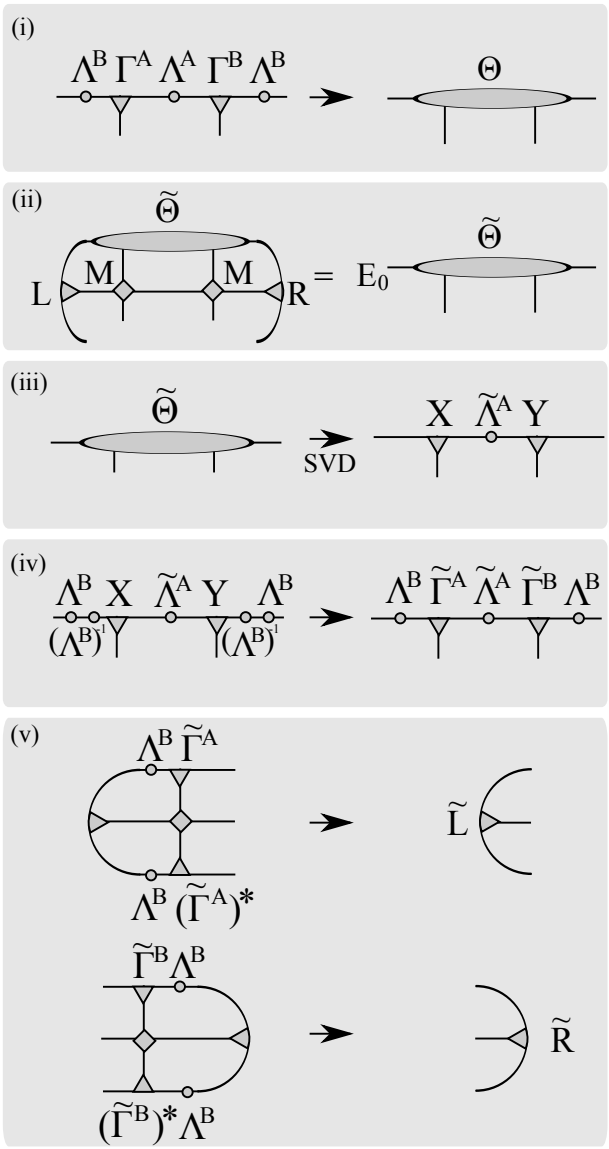

Figure 2.6: A pictorial representation of an iDRMG iteration step update. Refer to Sec. 2.4 for details.

for a unit cell of two, we have in total $\{L^A, L^B\}, \{R^A, R^B\}$. These environments are nothing other than the MPO for the Hamiltonian projected into the space of left and right Schmidt states about each bond.

With the environment in hand, we can project the Hamiltonian into the or-

thonormal basis $|\alpha j\gamma k\rangle$; to minimize the energy of Θ we find the ground state of the $\chi^2 d^2 \times \chi^2 d^2$ "Hamiltonian":

$$H_{\alpha jk\gamma;\bar{\alpha}\bar{j}\bar{k}\bar{\gamma}} = \sum_{a,b,c} L^B_{\alpha\bar{\alpha},a} M^{j,\bar{j}}_{ab} M^{k,\bar{k}}_{bc} R^B_{\gamma\bar{\gamma},c}. \tag{2.29}$$

To find this ground state, we use an iterative procedure such as Lanczos or Jacobi-Davidson at a cost of $\chi^3 D d^2$ per multiplication, as illustrated in step (ii) of Fig. 2.6, and obtain an improved guess for the wave function $\tilde{\Theta}$ and energy E_0. By using the initial wave function Θ as the starting vector for the minimization procedure, convergence is typically reached with only a couple of steps. This can be compared to the iTEBD optimization where we obtain a new wave-function $\tilde{\Theta}$ after applying the imaginary time-evolution operator. As with iTEBD, the bond dimension grows as $\chi \to d\chi$, which we must truncate using SVD, shown in step (iii). It is important that the left and right Schmidt basis about any bond remain orthogonal, because we assume $|\alpha j\beta k\rangle$ is an orthogonal basis at each step. Assuming this was the case on bonds of type B, the isometry properties of the SVD matrices X and Y imply that the orthogonality condition holds for the updated Schmidt states defined about the central bond A, and hence will remain so throughout the simulation. At this point, we have improved guesses for the matrices $\tilde{\Gamma}^{A/B}, \tilde{\Lambda}^A$ in step (iv).

The last step is to update the environment. At a minimum, we must update the environments on the bond which we just optimized by simply multiplying new tensors to the left and right as shown in Fig. 2.6 step (v):

$$\tilde{L}^A_{\beta\bar{\beta},b} = L^B_{\alpha\bar{\alpha},a} \Lambda^B_\alpha \tilde{\Gamma}^A_{\alpha\beta j} M^{j,\bar{j}}_{ab} \Lambda^B_{\bar{\alpha}} (\tilde{\Gamma}^A_{\bar{\alpha}\bar{\beta}\bar{j}})^*, \tag{2.30a}$$

$$\tilde{R}^A_{\beta\bar{\beta},b} = R^B_{\gamma\bar{\gamma},a} \tilde{\Gamma}^B_{\beta\gamma k} \Lambda^B_\gamma M^{k,\bar{k}}_{ab} (\tilde{\Gamma}^B_{\bar{\gamma}\bar{\beta}\bar{k}})^* \Lambda^B_{\bar{\gamma}}. \tag{2.30b}$$

This concludes the update on bond AB and we move over by one site, exchanging the roles of A and B, and repeat until convergence is reached.

Initializing the environment. We now return to the problem of initializing the algorithm. The initial MPS can be arbitrary (though it should be in canonical form). A fine choice is a $\chi = 1$ tensor product state which either preserves or breaks the symmetries as desired. To form the initial environment, we suppose when computing the left/right environment that $\hat{H}$ is zero to the left/right of the bond, which is captured by tensors of the form

$$R^{[n]}_{\alpha\bar{\alpha},a} = \delta_{\alpha\bar{\alpha}} \vec{v}_{\text{right};a}, \tag{2.31a}$$

$$L^{[n]}_{\alpha\bar{\alpha},a} = \delta_{\alpha\bar{\alpha}} \vec{v}_{\text{left};a}, \tag{2.31b}$$

where the $\vec{v}_{\text{left/right}}$ are the MPO terminal vectors defined in Eq. (2.25). Referring to Eq. (2.28) as an example, recall that $\vec{v}_{\text{right}}$ specifies the MPO index such that no further operators will be inserted to its right; likewise, $\vec{v}_{\text{left}}$ indicates no operators have been inserted to its left. Because all terms in the Hamiltonian then act as the identity to the left/right of the bond, the orthogonality of the Schmidt vectors implies that projecting the identity operator into the left/right Schmidt basis trivially gives $\delta_{\alpha\bar{\alpha}}$. When symmetry breaking is expected it is helpful to further initialize the environments by repeatedly performing the iDMRG update *without* performing the Lanczos optimization, which builds up environments using the initial symmetry broken MPS.

Ground state energy from iDMRG. One subtlety of the above prescription lies in the interpretation of the energy E_{GS} obtained during the diagonalization step. Is it the (infinite) energy of the infinite system? Using the initialization procedure just outlined, the Lanczos energy E_{GS} after the first step is the energy of the two-site problem. While we motivated the environments as representing infinite half chains, it is more accurate to assign them a length of 0 after the initialization procedure, and at each optimization step the length of the left/right environment about the central bond increases because a site has been appended. Keeping track of the length $\ell_{R/L}$ of each environment (for a unit cell of two, each grows on alternate steps), we see that the energy E_{GS} corresponds to a system of size $\ell = \ell_L + 2 + \ell_R$. By monitoring the change in E_{GS} with increased ℓ, we can extract the energy per site. This is convenient for problems in which there is no few-site Hamiltonian with which to evaluate the energy.

As for the iTEBD algorithm, we can achieve a considerable speed-up by using the symmetries of the Hamiltonian, which requires assigning quantum numbers to the tensors of the MPO in addition to the MPS.

2.5 Finite entanglement scaling

An advantage of the infinite system methods introduced above is that no artifacts from the boundary appear. On the other hand, finite size effects can be very useful for performing a scaling analysis. In this section we show that critical properties of the system can be extracted by performing a "finite-entanglement scaling" in the infinite systems. This means, one can perform simulations with different bond-dimensions χ at a critical point and use the induced *finite* correlation length ξ_χ as a scaling variable analogous to a finite system size.

To motivate this notion, consider the entanglement entropy S_E, which for an infinite system diverges logarithmically as a function of the correlation length as criticality is approached. [13] In an MPS, however, S_E is bounded by $S_E \leq \log \chi$, and an infinite χ is needed to accurately represent critical states. Clearly we cannot perform simulations with an infinite χ, raising the question: what happens if we nevertheless optimize a finite dimensional MPS for a critical system? This question has been addressed by a series of papers. [115, 84, 83] It turns out that simulating critical systems using finite χ cuts off long distance correlations a finite length ξ_χ. If we define the correlation length of the MPS ξ to be the length obtained from the second largest eigenvalue of the transfer matrix, Eq. (2.11), then *at criticality* the correlation length of the MPS scales as

$$\xi \propto \chi^\kappa \tag{2.32}$$

where $\kappa \approx \frac{1}{c}\frac{6}{\sqrt{\frac{12}{c}+1}}$. [84] Because χ introduces a length scale in a universal way, we can *define* the 'finite entanglement length' by $\xi_\chi \equiv C\chi^\kappa$, where C is independent of χ, and extract various quantities of interest using a finite ξ_χ scaling analysis, or "finite entanglement scaling." In an infinite system at criticality, the scaling relations are generally obtained from the analogous scaling relations in a finite size system by replacing the finite length L by ξ_χ. For example, for a critical point with central charge c, the entanglement entropy S_E between two halves of a finite system of length L scales as $S_E = \frac{c}{6}\log(L/a) + s_0$, with a the lattice spacing and s_0 a non-universal constant. If we instead measure S_E for an *infinite* system, but with finite χ, we can substitute $L \to \xi_\chi$, [13]

$$S_E = \frac{c}{6}\log(\xi_\chi/a) + s_0'. \tag{2.33}$$

The additive constant is again non-universal, and unrelated to s_0. One should note, though, that while ξ_χ and L have the same scaling dimension (i.e., that of length), the actual scaling functions are not guaranteed to be the same.

Another useful quantity at criticality for systems with a $U(1)$ symmetry is the 'stiffness,' here parameterized as the Luttinger parameter K. [36] For Hamiltonians that conserve the total magnetization, it can be obtained from the scaling of bipartite spin fluctuations of a half chain

$$F = \langle (S_L^z)^2 \rangle - \langle S_L^z \rangle^2, \tag{2.34}$$

where S_L^z is the z-component of the total spin to the left of a cut (for example, the total magnetization of the sites $i < 0$). The spin fluctuations satisfy [107, 108]

$$F = \frac{K}{2\pi^2}\log(\xi_\chi/a) + \text{const}, \tag{2.35}$$

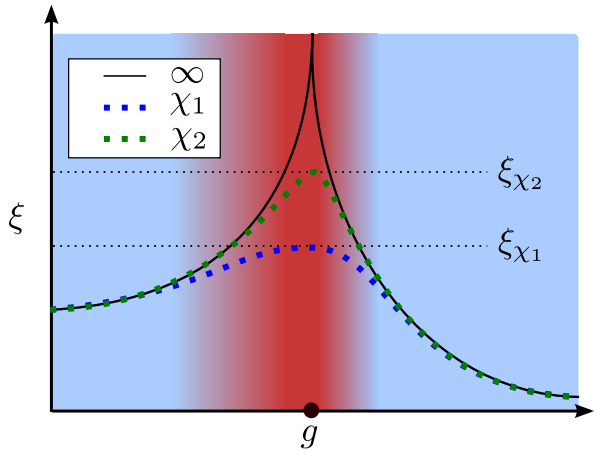

Figure 2.7: (Color online) A schematic plot illustrating the idea of finite-entanglement scaling. The black solid line shows the exact correlation length ξ_{phys} of the Hamiltonian, which diverges at the critical point. The dotted lines show the correlation lengths ξ of the optimized iMPS at a finite $\chi_2 > \chi_1$. The horizontal dashed lines are the correlation lengths $\xi_{\chi_1(\chi_2)}$ from Eq. (2.32), which are induced by the finite-entanglement cut-off at the critical point. The color shaded background indicates the two different regimes: Blue is the regime in which the iMPS is converged to the exact ground state using bond dimensions χ_1, χ_2 and red is the scaling regime which shrinks with increasing χ (see main text for further details).

allowing us to extract K by measuring the scaling of F with increased χ.

The above discussion holds at criticality. Next we discuss the situation in the vicinity of a critical point, where the physical correlation length ξ_{phys} is finite but much larger than the correlation length induced by finite χ, i.e. $\xi_\chi \ll \xi_{\text{phys}}$. For our purposes, we can define ξ_{phys} by the MPS correlation length ξ in the limit $\chi \to \infty$, where the MPS represents the true ground state. In this regime the MPS is still cutoff by ξ_χ, rather than the true correlation length ξ_{phys}, so the finite-entanglement scaling relations Eqs. (2.33) and (2.35) can still be used to obtain quantities like c and K. We will refer to this parameter range as the finite entanglement scaling region and it is shown as the red area in the schematic plot in Fig. 2.7.

Further away from criticality, as $\xi_{\text{phys}} \ll \xi_\chi$, we can fully converge the MPS and the state 'knows' it is not at the critical point. In this regime $\xi \to \xi_{\text{phys}}$ is independent of χ, and all other observables are converged in χ. If we measure the critical quantities c and K using Eq. (2.33) and Eq. (2.35), we find they renormalize

to zero.

The crossover can be analyzed by a general finite entanglement scaling form. Let g^i be a set of *physical* parameters, such as the coupling constants or the physical dimension of the system, and let $\mathcal{O}$ be a scaling observable. Near criticality, $\mathcal{O}(g)$ has a scaling form determined by the scaling dimensions of $\mathcal{O}$ and g^i. When the system is approximated by an MPS of finite χ, a new length scale ξ_χ is introduced. While χ itself has fixed scaling dimension, since $\xi_\chi \sim \chi^\kappa$, we find that it is numerically more stable to parameterize the effect of χ through the MPS correlation length ξ. We then measure $\mathcal{O}$ using the MPS, $\mathcal{O}(g;\xi)$.

The finite entanglement scaling procedure asserts that the usual scaling theory still applies to $\mathcal{O}(g;\xi)$, with the addition of a single parameter of mass dimension $[\xi] = -1$. As usual, the scaling hypothesis allows us to rescale $\mathcal{O}, g, \xi$ in order to eliminate the dependence on one parameter. In the usual case in which there are no marginal operators, we can linearize the renormalization flow equations to determine the scaling dimensions y_i, y_F, and find

$$\mathcal{O}(g^i,\xi) = e^{y_\mathcal{O}\ell}\mathcal{O}(e^{y_i\ell}g^i, e^{-\ell}\xi). \tag{2.36}$$

Note that ξ is in principle determined both by the physical correlation length ξ_{phys} and the finite entanglement length ξ_χ as discussed above; at criticality, $\xi = \xi_\chi$, while at infinite χ, $\xi = \xi_{\text{phys}}$. Regardless, (g^i, ξ) remains a valid coordinate system for the parameters.

In summary, in the finite entanglement scaling regime, $1 \ll \xi_\chi \ll \xi_{\text{phys}}$, we expect Eqs. (2.33) and (2.35) to produce the critical values c and K, but as $\xi_{\text{phys}} \ll \xi_\chi$, the MPS converges and we cross over to the true, non-critical values $c = K = 0$.

Chapter 3

Exact Matrix Product States for the Quantum Hall Effect

3.1 Introduction

The purpose of this chapter is to show that the venerable model wave functions for the fractional Quantum Hall effect, such as the Laughlin wave function, are MPSs in disguise. By this I mean that they have an exact, and very elegant, description as MPSs, and the entries of the tensors can be calculated analytically using the data of a conformal field theory. Many of the remarkable properties of these wavefunctions stem from their relationship to the CFT describing their edge theory, and in this chapter I show that this relationship implies precisely that they are MPSs. [1]

The fractional quantum Hall (FQH) effects are exotic phases of matter that appear when interacting 2D systems are subject to large magnetic fields. They are the foremost example of *topologically ordered* phases, which are characterized by long range entanglement rather than by local order parameters.[135] Topological order has many signatures such as gapless edge excitations, fractional or non-abelian statistics, and ground state degeneracy on a cylinder or torus. Many of these properties were discovered or demonstrated using "model wave functions" as ansatz for the ground state. The first example was Laughlin's wave function[64] at filling $\nu = 1/q$ argued to explain the first FQH experiments,[118] which has since been followed by many other successful ansatz.[45, 42, 70, 89] The model wave functions have also served as a diagnostic for exact diagonalization (ED) studies by checking the model states' overlap with the ED ground state.

Recently new ideas originating from quantum information, such as the entangle-

[1] Portions of this work appear in Phys. Rev. B 86, 245305

ment spectrum, have become important tools for detecting and characterizing the topological order of these phases.[58, 65, 2] Given a bipartition of the system into two sub-Hilbert spaces, $\mathfrak{H} = \mathfrak{H}_A \otimes \mathfrak{H}_B$, we can decompose any wave function $|\Psi\rangle$ in terms of wave functions which live solely in A or B:

$$|\Psi\rangle = \sum_a e^{-\frac{1}{2}E_a} |\Psi_a^A\rangle \otimes |\Psi_a^B\rangle, \tag{3.1}$$

with the restriction that the 'entanglement spectrum' E_a is real and that the 'Schmidt vectors' $|\Psi_a^A\rangle$ form an orthonormal set (as do the $|\Psi_a^B\rangle$). It was suggested in Ref. [58], and later thoroughly investigated in Ref. [66] that when A, B are chosen to be regions in space, the low lying entanglement spectrum of a FQH state can be identified with the energy spectrum of the conformal field theory (CFT) describing its gapless edge excitations.[86, 76] It was observed that for certain model wave functions, such as the Moore-Read (MR) state,[70] the *entire* entanglement spectrum could be identified as states of the edge CFT. [66]

A second realm in which entanglement has come to play an important role is for a set of variational wave functions called 'matrix products states' (MPS) [31] in one-dimension (1D) or 'tensor networks' [123] in higher dimensions. These are the variational states of the highly successful density matrix renormalization group (DMRG) method,[137, 75] which succeeds because MPS efficiently capture the structure of entanglement in many body wave functions.[78] The precise relationship between topological order and tensor network representations is a subject of ongoing work, but in 1D at least a complete classification of symmetry protected topological (SPT) order for both gapped 1D spin and fermion chains was recently accomplished using the MPS representation of the ground state. [16, 34, 119, 99] Given a set of sites labeled by i, each with local basis $|m_i\rangle$, an MPS $|\psi\rangle$ is defined by a set of 'B-matrices',

$$|\psi\rangle = \sum_{\{\alpha,m\}} \left[\cdots B^{m_2}_{\alpha_3\alpha_2} B^{m_1}_{\alpha_2\alpha_1} \cdots\right] |\cdots, m_2, m_1, \cdots\rangle. \tag{3.2}$$

The indices $0 \leq \alpha_i < \chi$ to be traced over are called 'auxiliary' indices, which we consider to be states in an 'auxiliary Hilbert space' defined on the bonds between sites. With the proper normalization, the auxiliary states are in one to one correspondence with the entanglement spectrum of a cut on the bond. An important insight from the classification scheme is that a suitable renormalization procedure [125, 16] can be defined which produces a representative state of the smallest possible χ. For example, the $\chi = 2$ state of Affleck, Lieb, Kennedy and Tasaki (AKLT) [1] is representative of the SPT ordered Haldane phase [43] of the spin-1 Heisenberg chain.

The observed simplicity of the FQH model states' entanglement spectrum suggests they play an analogous role for the FQH effects as the AKLT state does for the Haldane phase. To pursue the analogy further, the 1+1D AKLT wave function can be written as a time ordered correlation function of a single '0 + 1D' spin-$\frac{1}{2}$, which leads to its simple expression as an MPS whose $\chi = 2$ auxiliary Hilbert space is a spin-$\frac{1}{2}$.[4] The 2+1D FQH model wave functions can be written as the correlation function of a 1+1D CFT. Does it follow that the model FQH states have exact representations as an MPS with an auxiliary Hilbert space in one to one correspondence with the CFT, and if so, can they be implemented and manipulated numerically?

In this paper we show that the model FQH wave functions and their quasiparticle excitations indeed have exact representations as MPSs. As expected the requisite structure of the model states is that their wave functions are the correlation functions of a 1+1D CFT, which implies essentially by definition that they are MPSs whose auxiliary Hilbert space is the CFT. We also explain how the edge excitations and ground state degeneracy arise in the MPS picture.

Working on a cylinder in the Landau gauge, we can view the system as a 1D chain of orbitals for which the B-matrices of Eq. (3.2) are the matrix elements of local operators of the CFT. We have implemented these MPSs numerically for both the fermionic Laughlin and Moore-Read states on the geometry of an *infinitely* long cylinder of circumference L, allowing us to measure arbitrary real-space correlation functions using the standard infinite MPS algorithms. The infinite cylinder has a number numerical advantages, including the absence of boundaries, full translation invariance and no curvature effects. Compared to the torus geometry,[63, 62, 67] only a single cut is required to study the entanglement, greatly simplifying the identification of the entanglement spectrum. As we show in Sec. 3.3, the computational complexity of the MPS representation is on the order $\mathcal{O}(b^L)$ for $b \sim \mathcal{O}(1)$. However, to achieve the same type of scaling in the traditional Hilbert space representation (say on a sphere[47, 144, 66, 117, 110, 29]) would require $N \sim \mathcal{O}(L^2)$ particles and a Hilbert space dimension scaling as b^{L^2}. We note that previously a conceptually distinct approach found an MPS for the Laughlin state in which there is one matrix per *particle*, rather than per orbital.[52] However, the construction does not easily generalize to other FQH states and again results in a complexity b^N, which implies it cannot be implemented on the infinite cylinder geometry. A 2D tensor network construction for observables has also been constructed for lattice FQH states,[9] but the feasibility of its implementation is unclear.

Furthermore, we introduce an algorithm for calculating the real-space entanglement spectrum of any state given as an MPS in the orbital basis. We first use the larger system sizes provided by the MPS representation to extract the topological entanglement entropy (TEE) γ using four different methods; first using the conven-

tional scaling of the entanglement entropy,[58, 65]

$$S = \sum_a E_a e^{-E_a} = a_S L - \gamma + \mathcal{O}(L^{-1}), \tag{3.3}$$

and second from a similar scaling form we derive for the lowest entanglement energy, $E_0 = a_E L - \gamma + \mathcal{O}(L^{-1})$, for both the orbital and real-space cuts. [2] We find using E_0 in the orbital cut converges most quickly, and as this form is applicable to other topologically ordered phases, it may prove useful in cases where small system sizes are a constraint. We are able to definitively determine γ using all four methods for the $\nu = \frac{1}{3}, \frac{1}{5}$ and $\frac{1}{7}$ Laughlin states, as well as the $\nu = \frac{1}{2}$ Moore-Read state (*cf.* Tab. 3.1), which proved difficult in previous studies.[47, 144, 62, 110]

Finally, we perform a detailed scaling analysis of the spectrum for both the orbital and real-space cuts. During the final preparation of this work, a recent preprint [28] has conclusively demonstrated earlier arguments that the real-space entanglement spectrum of the model wave functions takes the form of the chiral Hamiltonian H perturbed by local, irrelevant boundary operators.[86, 29] This implies a scaling collapse of the entanglement spectrum in the limit $L \to \infty$ for fixed CFT level n. The large system sizes available here give the first detailed demonstration of this principle, allowing us to extract the entanglement velocities for both the Majorana and $U(1)$ modes of the MR state, as well as the form of the leading irrelevant corrections.

In contrast, in the orbital cut each entanglement eigenvalue scales as $E_a - E_0 \sim L^{-\zeta_a}$ which precludes the possibility of collapsing the spectrum. This is contrary to earlier indications that the orbital spectrum showed the same linear dispersion, [117] though the case studied there was the 'conformal limit' of bosonic $\nu = \frac{1}{2}$ wave function on a finite sphere.

3.2 Model Wavefunctions and Matrix Product States

A number of gapped model wave functions, including those of the FQH, can be written as the correlation functions of a field theory in one lower dimension.[101] In the 2+1D FQH effect, for example, the model wave functions are correlation functions of a 1+1D chiral conformal field theory (CFT).[70] Other examples with this structure include the AKLT states, the Toric code,[57] spin chains,[19, 72] and certain BCS superconductors.[130, 88, 27, 101] As we will illustrate in the case of the FQH effect, this structure implies that the state has an exact implementation as an

[2] The lowest entanglement energy E_0 is equal to the Rényi entropy[91] S_∞ at infinite order.

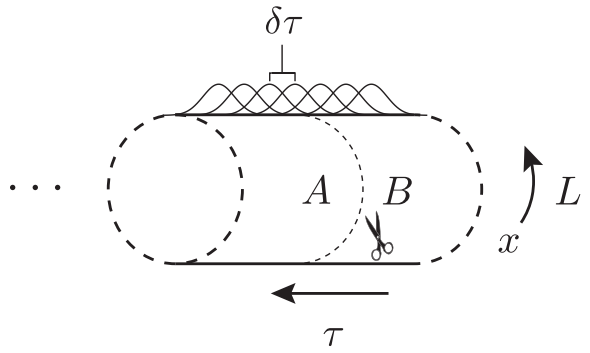

Figure 3.1: The infinite cylinder geometry for model FQH wave functions. L is the circumference, x and τ are the coordinates around and along the cylinder respectively. $\delta\tau = \frac{2\pi\ell_B^2}{L}$ is the spacing between Landau level orbitals, where $\ell_B = (\hbar/qB)^{1/2}$ is the magnetic length. A real-space entanglement cut between regions A, B would be made along some fixed τ.

	Filling	v_ϕ	v_χ	$\mathcal{D}^2 = e^{2\gamma}$
Laughlin	1	2.2568 ± 0.0003		$\lvert\gamma\rvert < 10^{-7}$
	1/3	1.2956 ± 0.0006		2.996
	1/5	0.672 ± 0.009		4.96
	1/7	0.28 ± 0.02		6.88
Moore-Read	1/2	1.33 ± 0.01	0.21 ± 0.01	7.77

Table 3.1: Extracted real-space entanglement velocities and TEE γ for various model wave functions. v_ϕ is the velocity of the chiral boson, and for the MR case, v_χ the velocity of the chiral Majorana, in units of the magnetic length ℓ_B. For the $\nu = 1$ integer quantum Hall state, the exact value of the velocity is known to be $4/\sqrt{\pi}$. In the column for total quantum dimension $\mathcal{D}$, we present the value extracted via the orbital cut E_0 around $L = 25\ell_B$. (For $\nu = 1$ integer case, we use the real-space cut S instead.) Refer to Sec. 3.6 for details on our numerical methods.

MPS or a tensor network. The auxiliary Hilbert space of the tensor network is in correspondence with the Hilbert space of the associated lower dimensional field theory. In turn, the edge excitations and the entanglement spectrum of tensor networks are known to be closely related; [20] this relationship takes a particularly elegant form for the FQH effect due to the stringent constraints of conformal invariance in 2D.[28]

The simplest example is the Laughlin state on an infinite cylinder, which can be written as the correlation function of a chiral boson $\phi(z)$ [3]

$$\begin{aligned}\Psi_L(z_a) &= \prod_{a<b}^{N} \sin\left((z_a - z_b)\tfrac{\pi}{L}\right)^q e^{-\frac{1}{2\ell_B^2}\sum_a \tau_a^2} \\ &= \left\langle \exp\left[i\sqrt{q}\sum_{a=1}^{N}\phi(z_a) - i\sqrt{q}\rho\int d^2z\,\phi(z)\right]\right\rangle_\phi\end{aligned} \tag{3.4}$$

as elucidated by Moore and Read.[70] Throughout we will use $z = x+i\tau$ as a complex coordinate on the cylinder, where x runs around its circumference of length L and τ runs along its length, as illustrated in Fig. 3.1. The filling fraction is $\nu = \frac{p}{q}$, the magnetic length is $\ell_B^2 = \frac{\hbar}{eB}$, and the density of electrons is $\rho = \frac{\nu}{2\pi\ell_B^2}$. The chiral boson ϕ is a free field characterized by its correlation function on the plane or cylinder,

$$\begin{aligned}\langle\phi(z)\phi(z')\rangle_{\text{plane}} &= -\log(z-z'), \\ \langle\phi(z)\phi(z')\rangle_{\text{cyl}} &= -\log\,\sin\left[\tfrac{\pi}{L}(z-z')\right].\end{aligned} \tag{3.5}$$

In the Laughlin state, for each electron we insert the operator $\mathcal{V}(z_a) = :e^{i\sqrt{q}\phi(z_a)}:$, where $::$ denotes normal ordering. Other quantum Hall states, such as the Moore-Read state or the Read-Rezayi sequence,[70, 89] can be obtained by letting $\mathcal{V}$ be an operator in a more general CFT. It is also necessary to include a neutralizing 'background charge' $\mathcal{O}_{bc} = -i\rho\int d^2z\,\phi(z)/\sqrt{\nu}$.The background charge introduces some subtleties, as the branch cut in the bosonic propagator has a phase ambiguity equivalent to a choice of gauge for the electrons, which we will address at a later point.

We write a second quantized version of Eq. (3.4) using a coherent state wave function in the variable ψ (which is a complex/Grassmann number for bosons/fermions), which in the thermodynamic limit is

$$\begin{aligned}\Psi_L[\psi] &= \langle 0|e^{\int d^2z\,\psi(z)\hat{\Psi}(z)}|\Psi_L\rangle \\ &= \left\langle e^{\int d^2z\left[\mathcal{V}(z)\,\psi(z) - i\rho\phi(z)/\sqrt{\nu}\right]}\right\rangle_{\text{CFT}}.\end{aligned} \tag{3.6}$$

The notation is rather subtle as we are tying together two theories: the physical particles in 2+1D, with coherent state coordinate $\psi(z)$, and the path integral over

[3] The normal ordering prescription is as follows. Each insertion $:e^{i\sqrt{q}\phi(z_a)}:$ is normal ordered, which eliminates a contraction that would produce $(z_a - z_a)^q = 0$, and the self interaction of the background charge $\int d^2z\,\phi(z)$ is ignored, which would contribute an overall divergent constant.

the auxiliary space of the 1+1D CFT, characterized by the correlation functions $\langle\cdot\rangle_{\mathrm{CFT}}$. Number conservation is enforced by the $U(1)$ symmetry of the chiral boson.

The structure of Eq. (3.6) is identical to that of a 'continuous matrix product state' (cMPS) defined in Ref. [121], which we review briefly. Starting with an MPS for a chain of bosons or fermions at sites with positions τ, we first pass from the occupation basis $\{|m_\tau\rangle\}$ to the coherent state basis $\{|\psi_\tau\rangle\}$ by defining

$$B_{\alpha\alpha'}[\psi_\tau] \equiv \sum_{m_\tau} \langle\psi_\tau|B^{m_\tau}_{\alpha\alpha'}|m_\tau\rangle. \tag{3.7}$$

Second, we note that the trace over the auxiliary states $\{\alpha\}$ is formally equivalent to a path integral over a 1D system, with the B playing the role of transfer matrices. Anticipating the continuum limit, we assume there are matrices H, V in the auxiliary Hilbert space such that $B[\psi(\tau)] = e^{H(\tau)+V(\tau)\psi(\tau)}$. We can then take the continuum limit of the MPS by analogy to the usual time-ordered path integral, which defines a cMPS,

$$\Psi[\psi] = \mathrm{Tr}_{\mathrm{aux}}\left[\mathcal{T}e^{\int_0^{L_\tau} d\tau[H(\tau)+V(\tau)\psi(\tau)]}\right]. \tag{3.8}$$

Comparing the cMPS to the second quantized version of the Laughlin state, (3.6), we see that they are equivalent if we take the *physical* Hilbert space at each slice to be that of particles on a ring of circumference L, and the auxiliary Hilbert space to be that of a chiral boson. In this case, H is precisely the Hamiltonian of the CFT (plus the background charge $\mathcal{O}_{bc}$), while V is the electron operator, $\mathcal{V}$. This structure was also recently noted in Ref. [28], where, in the MPS language, they find the dominant eigenvector of the 'transfer matrix'[78] of the cMPS, from which the entanglement Hamiltonian follows.

While the cMPS representation is convenient from an analytic perspective, computationally it is desirable to have the discrete version expressed in the basis of lowest Landau level (LLL) orbitals. Defining a coordinate $w = e^{-\frac{2\pi i}{L}z}$ for notational convenience, in Landau gauge the orbitals can be written as

$$\varphi_n(z) \propto e^{-\frac{1}{\ell_B^2}\left(i\tau_n x + \frac{1}{2}(\tau-\tau_n)^2\right)} = w^n e^{-\frac{1}{2\ell_B^2}\left(\tau_n^2+\tau^2\right)}, \tag{3.9}$$

where $\tau_n = \frac{2\pi n}{L}\ell_B^2$ is the guiding center for the n^{th} orbital. Viewing the orbitals as the sites of an infinite 1D chain, we want to arrive at a discrete MPS as defined in (3.2), which requires finding the appropriate matrices $B^m_{\alpha\alpha'}$. Based on the cMPS, we expect α will be in one-to-one correspondence with the states of the associated CFT.

In order to extract the occupation number at orbital n, we take advantage of the fact that orbitals of the LLL (in the Landau gauge) are labeled by momentum.

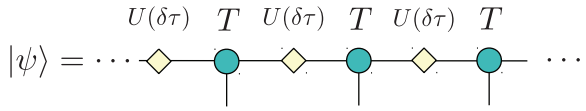

(a) Structure of the orbital MPS.

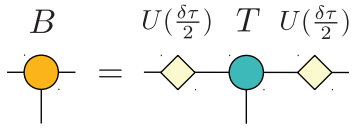

(b) Definition of the B-matrix.

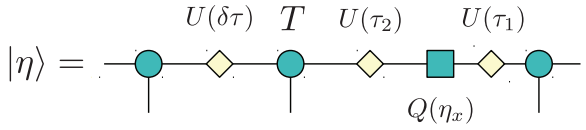

(c) Structure of MPS with a quasihole insertion Q.

Figure 3.2: The structure of the orbital MPS. (a) U is free time evolution of the CFT, punctuated by perturbations T at $\tau = \tau_n$. (b) The B-matrices in (3.2) are defined by combining U and T. (c) A quasiparticle is inserted by placing the matrix elements of the vertex operator Q in the correct time-ordered positions. It can be absorbed into either of the adjoining B-matrices.

When acting on a many-body state in the LLL, we can then replace the destruction operator $\hat{\psi}_n$ for orbital n with a contour integral around the cylinder,

$$\hat{\psi}_n \longrightarrow e^{\frac{\tau_n^2}{\ell_B^2}} \oint_{\tau=\tau_n} \frac{dw}{2\pi i}\, w^{-n-1} \hat{\psi}(w). \tag{3.10}$$

We chose to perform the integrals at τ_n, though with an appropriate change in normalization a different location could be chosen.

The gauge of the cMPS, however, depends on a branch cut prescription for the background charge. It is convenient to choose the cut to consistently occur at some fixed x coordinate, such as the boundary of $-L/2 < x < L/2$. This choice of gauge does not produce the Landau gauge; they differ by a phase $e^{ix\tau\ell_B^{-2}}$. Choosing this branch cut prescription for $\phi(z)$, but keeping ψ_n to be the destruction operators for the Landau gauge, we find Eq. (3.6) can be brought to the form

$$\Psi[\psi_n] = \left\langle e^{\sum_n \oint_{\tau=\tau_n} \frac{dw}{2\pi i}\, w^{-1}\left[\mathcal{V}(w)\psi_n - i\sqrt{\nu}\phi(w)\right]} \right\rangle_{\text{CFT}}. \tag{3.11}$$

Eq. (3.11) looks like unperturbed time evolution governed by the Hamiltonian of the chiral CFT, H, punctuated by interactions at τ_n. As orbital ordering coincides with

time ordering, we can pass to the Hamiltonian picture by inserting resolutions of the identity $\mathbb{1} = \sum_\alpha |\alpha\rangle\langle\alpha|$ at positions $\tau = \tau_n \pm \epsilon$, where α label all states of the CFT. A resulting unit cell looks like

$$\Psi[\psi_n] = \sum_{\{\alpha\}} \Big[\cdots \langle\alpha_{n+1}|e^{-\delta\tau H}|\alpha_n\rangle \\ \langle\alpha_n|e^{\mathcal{V}_0\psi_n - i\sqrt{\nu}\phi_0}|\alpha_{n-1}\rangle \cdots \Big], \tag{3.12}$$

where the operator [4]

$$\hat{\mathcal{V}}_0 \equiv \oint \frac{dw}{2\pi i}\, w^{-1}\mathcal{V}(w)$$

is precisely the '0^{th} mode' of the electron operator $\mathcal{V}(w)$, and likewise ϕ_0 is the zero-mode of the chiral boson. The resulting transfer operators are of two types. For the unperturbed segments $\tau \in (\tau_n, \tau_{n-1})$, the transfer operator is

$$U(\delta\tau) \equiv e^{-\delta\tau H}, \quad U(\delta\tau)_{\alpha\beta} = \delta_{\alpha\beta}e^{-\delta\tau E_\alpha} \tag{3.13}$$

where α again runs over states of the CFT, with energies E_α, and $\delta\tau = \frac{2\pi}{L}\ell_B^2$. At the location of each site we define a transfer operator [5]

$$T_{\alpha\beta}[\psi_n] \equiv \langle\alpha|e^{\hat{\mathcal{V}}_0\psi_n - i\sqrt{\nu}\phi_0}|\beta\rangle. \tag{3.14}$$

Stringing the transfer matrices together, we arrive at the exact MPS,

$$\Psi[\psi_n] = \prod_n U(\delta\tau)T[\psi_n] \tag{3.15}$$

as illustrated in Fig. 3.2a. We have suppressed the implicit summation over the CFT states α.

The above is in 'coherent state' form; to convert to the occupation basis $\{|m\rangle\}$, we define the B-matrices of Eq. (3.2) to be

$$\sum_m B^m (m!)^{\frac{3}{2}}\psi^m \equiv U(\tfrac{1}{2}\delta\tau)\, T[\psi]\, U(\tfrac{1}{2}\delta\tau) \tag{3.16}$$

[4] While we have expressed the definition in terms of the coordinate w, we are taking only a Fourier mode on the cylinder, not a conformal transformation to the plane. If we were to conformally map the expression to the plane we would recover the familiar modes of radial quantization, but that is not necessary here.

[5] Note that the boundary condition of the CFT on the auxiliary bond is not necessarily periodic, due to the zero mode which 'twists' the boundary condition.

as shown in Fig. 3.2b. Explicitly,

$$B^m = U(\tfrac{1}{2}\delta\tau)e^{-i\sqrt{\nu}\phi_0/2}\frac{\left(\hat{\mathcal{V}}_0\right)^m}{\sqrt{m!}}e^{-i\sqrt{\nu}\phi_0/2}U(\tfrac{1}{2}\delta\tau). \tag{3.17}$$

While the result is general, for the Laughlin and Moore-Read states, which are described by free CFTs with electron operators

$$\mathcal{V}(w) = :e^{i\sqrt{q}\phi(w)}: \text{ (Laughlin)}, \tag{3.18a}$$

$$\mathcal{V}(w) = \chi(w):e^{i\sqrt{q}\phi(w)}: \text{ (Moore-Read)}, \tag{3.18b}$$

(χ is a chiral Majorana field), both T and U, and hence B, can be calculated exactly at negligible numerical cost (for the details of this calculation, we refer to Appendices 3.9 and 3.10). For an arbitrary CFT, their calculation is more involved but nevertheless tractable using formulas developed for the 'truncated conformal space' approach to perturbed CFTs.[141]

In summary, we have demonstrated how to take a model wave function written in terms of a correlator of a CFT and convert it to a discrete MPS [Eq.(3.2)] in the orbital basis, characterized by a set of $B^m_{\alpha\beta}$. The auxiliary indices α, β label states of the CFT, such that each matrix B^m is an operator of the CFT. The operator B^m consists of three pieces: the (imaginary) time-evolution of the CFT (U), the background charge ($e^{-i\sqrt{\nu}\phi_0}$), and the insertion of m electron operators ($\mathcal{V}_0^m$). This is the chief result of this paper.

Discussion

In order to obtain wave functions on a half or finite cylinder, one simply truncates the MPS using the vacuum of the CFT as a boundary condition for the severed auxiliary bonds. If excited states are used as the boundary condition, these produce the corresponding model edge excitations.[133] This structure is analogous to the spin-$\frac{1}{2}$ degree of freedom at the boundary of an AKLT chain, which arises from the two choices of boundary condition for the $\chi = 2$ MPS.

To understand the ground state degeneracy of the phase, note that if the phase is $\mathfrak{m}$-fold degenerate on an infinite cylinder, there are $\mathfrak{m}$-primary fields in the CFT, and the states of the CFT partition into $\mathfrak{m}$ families which 'descend' from each of these primary fields.[33] Each family is invariant under the action of the electron operator $\mathcal{V}(w)$, so it follows that the CFT states on a given auxiliary bond can be consistently truncated to one of these $\mathfrak{m}$ families. The $\mathfrak{m}$ choices on the bond provide the $\mathfrak{m}$ 'minimal entanglement states'.[143]

The 'thin torus' wave functions are also a limiting case of our construction.[116, 8] As $L \to 0$, we can truncate the MPS by keeping only the states of the CFT with the lowest energy within each family (the 'highest weight states'), which generates a $\chi = 1$ MPS. The construction intuitively connects how the operator product expansions in the CFT are related to the orbital occupation numbers in the thin torus limit, the so called "pattern of zeros"[136] or the "root configuration."[10] We also note that an approximate $\chi = 2$ MPS for the Laughlin state was recently found;[71] in our language this results from a truncation of the CFT to the states $|P| \leq 1$.

We now explain how the two conserved quantities of the LLL problem, particle number and momentum (sometimes called 'center of mass'), can be assigned to the states of the CFT. In the orbital basis we define the conserved quantities to be

$$\hat{C} = \sum_j (q\hat{N}_j - p) \quad \text{(particle number)}, \tag{3.19a}$$

$$\hat{K} = \sum_j j(q\hat{N}_j - p) \quad \text{(momentum)}, \tag{3.19b}$$

where j is the orbital index and we have included a filling factor dependent scaling ($\nu = p/q$) so that both remain finite in the thermodynamic limit. If a state is invariant under a $U(1)$ symmetry transformation, the states of the Schmidt spectrum can be assigned definite charge. Consequently, the entanglement spectrum on bond $\bar{n} \in \mathbb{Z} + \frac{1}{2}$ can be labeled by pairs $(C_{\bar{n}}, K_{\bar{n}})$. The states of the auxiliary CFT have quantum numbers as well, in particular the total momentum $|P|$ of the CFT and the winding number N of the boson (see Appendix 3.9 for detailed definitions). The pairs $(N, |P|)$ and $(C_{\bar{n}}, K_{\bar{n}})$ are related by

$$C_{\bar{n}} = N, \tag{3.20a}$$

$$K_{\bar{n}} = q|P| + \frac{1}{2}N^2 + \bar{n}N, \tag{3.20b}$$

which explains how the previously observed offsets of the $|P| = 0$ levels depend on the number sector and bond location.

3.3 Convergence properties and computational complexity

For numerical purposes we must truncate the MPS by keeping only the χ most important states in the entanglement spectrum. Most MPS algorithms (such as

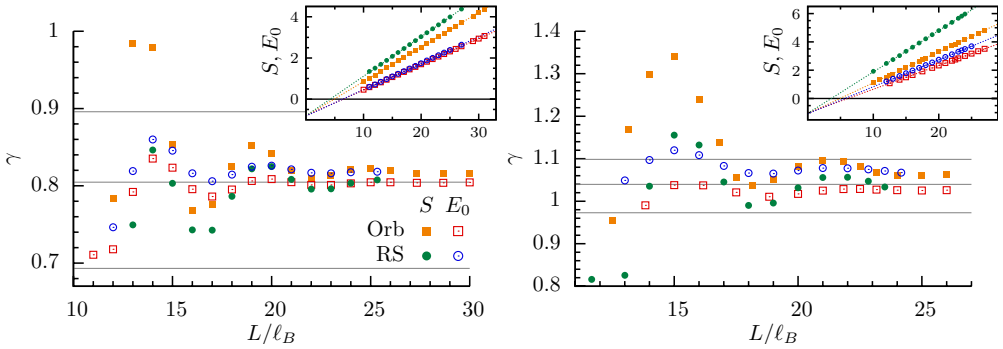

Figure 3.3: Numerically computing the TEE γ for the $\nu = 1/5$ Laughlin state (top) and the $\nu = 1/2$ Moore-Read state (bottom). γ is extracted from both orbital (squares) and real-space (circles) cut, via the entanglement entropy S (filled) and the lowest entanglement energy E_0 (empty), by performing windowed fits to the form $S(L), E_0(L) = a_{S,E}L - \gamma$ at various circumferences L. The horizontal lines marks the values of $\gamma = \log \mathcal{D}$ where $\mathcal{D}^2 = 4, 5, 6$ (top) and $7, 8, 9$ (bottom). As $L \to \infty$, the extracted value of γ approaches their theoretical values of $\frac{1}{2}\log 5$ and $\frac{1}{2}\log 8$ respectively. In the latter case we can see that $L \gtrsim 20\ell_B$ is required for the TEE to be extracted with reasonable accuracy. (Insets) S vs. L/ℓ_B for the four cases.

measuring correlation functions) can then be computed with time $\mathcal{O}(M\chi^3)$ and storage $\mathcal{O}(\chi^2)$, where M is the number of sites involved in the measurement. In this section we argue that to simulate the state at some fixed precision we must keep $\chi \sim e^{\alpha cL/v}(cL/v)^{-1/2}$ where c is the central charge of the entanglement spectrum, v is its 'entanglement velocity,' and α is a non-universal constant of order 1. In contrast to exact diagonalization, the complexity scales exponentially only in the circumference of the cylinder, rather than its area. Use of the conserved quantum numbers drastically reduces the computational time, but does not alter the exponential complexity.

Following Kitaev and Preskill's derivation of the topological entanglement entropy,[58] we proceed under the assumption that the 'thermodynamic' properties of the entanglement spectrum, such as the entanglement entropy, take the same form as those of the auxiliary CFT. However, there is no reason to expect the velocities that appear will be universal, so in what follows all powers of L/v should be understood to have non-universal coefficients. The exact status of this assumption for the orbital basis is somewhat unclear, because as we will show the orbital spectrum does not collapse to the CFT; nevertheless the appearance of γ in the entropy S, the scaling form of the lowest eigenvalue E_0, and the collapse we find for the convergence of S with increased χ appear to behave as expected.

The density of states $\rho(E)$ for a modularly invariant CFT is given by the 'Cardy' formula.[15] However, when working with the 'minimally entangled'[143] ground states naturally provided by the MPS construction, we must take into account the fact that only one sector of the CFT, 'a,' belongs to the entanglement spectrum, where the sector a depends on a choice of one of the $\mathfrak{m}$ ground states. The corresponding partition function and density operator are defined as

$$\mathcal{Z}_a = \mathrm{Tr}_a\, e^{-\beta H_e}, \tag{3.21}$$

$$\hat{\rho} = \mathcal{Z}_a^{-1}\, \mathrm{Tr}_a\, e^{-H_e}. \tag{3.22}$$

The derivation of the Cardy formula requires a modular transformation, but the required partition function is not modularly invariant. This results in the explicit appearance of the modular $\mathcal{S}$ matrix, $-\log(\mathcal{S}_a^{\mathbb{1}}) = \gamma_a$, where γ_a is the topological entanglement entropy of the ground state a. Taking this term into account, the density of states is

$$\rho(E)dE = \frac{dE}{4E}\sqrt{\frac{2}{\pi}} e^{-\gamma_a} e^{\sqrt{\frac{\pi(c+\bar{c})EL}{3v}}} \left(\frac{\pi(c+\bar{c})EL}{3v}\right)^{1/4}. \tag{3.23}$$

All the other thermodynamic properties follow from $\rho(E)$. It is convenient to introduce the dimensionless variable μ,

$$\mu \equiv \left(\frac{\pi(c+\bar{c})EL}{3v}\right)^{1/4}. \tag{3.24}$$

We can calculate the partition function and entanglement entropy,

$$\begin{aligned} \mathcal{Z}_a(\beta) &= \int \rho(E) e^{-\beta E} dE \\ &= \sqrt{\frac{2}{\pi}} e^{-\gamma_a} \int e^{\mu^2 - \frac{3v}{\pi(c+\bar{c})}\frac{\beta}{L}\mu^4} d\mu \\ &= e^{\frac{\pi(c+\bar{c})}{12}\frac{L}{\beta v} - \gamma_a + \cdots}, \end{aligned} \tag{3.25}$$

$$\begin{aligned} S &= \partial_{\beta^{-1}}(-\beta^{-1} \ln \mathcal{Z}_a)\big|_{\beta=1} \\ &= \frac{\pi(c+\bar{c})}{6}\frac{L}{v} - \gamma_a + \ldots. \end{aligned} \tag{3.26}$$

The partition function (3.25) is evaluated via steepest descent about the saddle point $\mu_* = \sqrt{\frac{\pi(c+\bar{c})}{6v}\frac{L}{\beta}}$. As the entanglement spectrum is $p_i = e^{-E_i}/\mathcal{Z}_a(1)$, a particular consequence of Eq. (3.25) is that the lowest entanglement level is $p_0 = e^{-[a_E L - \gamma_a]}$ for

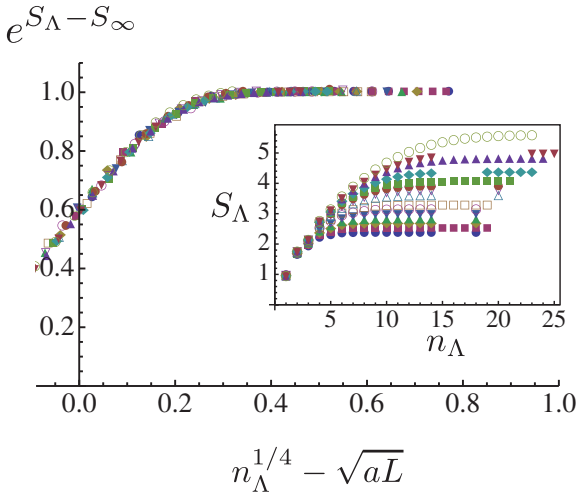

Figure 3.4: Convergence of the orbital entanglement entropy S_Λ for the $q = 3$ Laughlin state as the number of Virasoro levels kept (n_Λ) is increased. (Inset) For various circumferences $19\ell_B \leq L \leq 40\ell_B$, we calculate the entanglement S_Λ of the MPS keeping only the lowest n_Λ Virasoro levels of the CFT. For large enough n_Λ, S_Λ converges to the exact entanglement entropy S_∞. We expect the convergence to be controlled by the parameter $\mu - \mu_* \propto n_\Lambda^{1/4} - (aL)^{1/2}$ for some a. (Main figure) We plot the convergence of the entanglement entropy, $e^{S_\Lambda - S_\infty}$ as a function of $n_\Lambda^{1/4} - (aL)^{1/2}$, with $a \approx 0.0875$ giving a good collapse.

some non-universal a_E. A similar result was recently obtained in [28]. As illustrated in Fig. 3.3, for both the orbital and real-space cuts γ can be extracted from the scaling of p_0 with equivalent or better accuracy as from S.

The steepest descent analysis shows that the bulk of the probability comes from a region within $\mathcal{O}(1)$ of the saddle point μ_*. Up to this point the number of states χ with $E < E_*$ is

$$\chi(E_*) = \int^{E_*} \rho(E)\, dE\,. \tag{3.27}$$

Alternately, we can define the number of CFT Virasoro levels n_* required above the vacuum state,

$$n_* \equiv n(E_*) = \frac{E_* L}{2\pi v} = \frac{(c + \bar{c})}{24} \left(\frac{L}{v}\right)^2 . \tag{3.28}$$

To study the convergence properties, suppose we only keep states such that $E < E_\Lambda$. The cutoff partition function $\mathcal{Z}_\Lambda$ is

$$\begin{aligned}\mathcal{Z}_\Lambda(\beta) &= \int^{E_\Lambda} dE\, \rho(E)\, e^{-\beta E} \\ &\sim \mathcal{Z}_\infty(\beta)\, \frac{1}{2}\, \mathrm{erfc}\left(-\sqrt{2}(\mu_\Lambda - \mu_*)\right),\end{aligned} \tag{3.29}$$

with resulting truncation error

$$\epsilon_\Lambda \equiv 1 - \frac{\mathcal{Z}_\Lambda(1)}{\mathcal{Z}_\infty(1)} = \frac{1}{2}\, \mathrm{erfc}\left(\sqrt{2}(\mu_\Lambda - \mu_*)\right). \tag{3.30}$$

While the specific functional form may not remain universal, it suggests that convergence is controlled by the dimensionless factor $\mu_\Lambda - \mu_* \sim n_\Lambda^{1/4} - (aL)^{1/2}$. In the inset of Fig. 3.4, we plot the convergence of the entanglement entropy S_Λ as a function of the number of Virasoro levels n_Λ kept at various circumferences L. We then scale the data horizontally by plotting as a function of $n_\Lambda^{1/4} - (aL)^{1/2}$ for a numerically fit value of a. Without any further *vertical* scaling, the data appears to collapse. This is somewhat surprising given the irregular structure of the orbital spectrum, but does validate the predicted form $n_\Lambda \sim L^2$. Choosing an acceptable fractional error for S_Λ, in large L limit we then conclude from the Cardy formula the required dimension of the MPS to simulate at fixed accuracy is

$$\chi \sim e^{\alpha c L/v} (cL/v)^{-1/2} \tag{3.31}$$

as claimed. Equivalently the number of Virasoro levels required is $\sim \mathcal{O}(L^2)$.

3.4 Quasi-particle excitations

We now discuss how to introduce quasiparticles into the MPS. In the 'conformal block' approach to model wave functions,[70] a quasiparticle excitation at η is introduced by inserting an appropriate operator $\mathcal{Q}(\eta)$ into the CFT correlator,

$$\Psi[\psi_n; \eta] = \left\langle \mathcal{Q}(\eta)\, e^{\sum_n \left[\mathcal{V}_0(\tau_n)\psi_n - i\sqrt{\nu}\phi_0(\tau_n)\right]} \right\rangle_{\mathrm{CFT}}. \tag{3.32}$$

We will focus on the Laughlin and Moore-Read quasiholes, for which $\mathcal{Q}$ is a *local* operator that takes a particularly simple form,

$$\mathcal{Q}(\eta) = :e^{i\phi(\eta)/\sqrt{q}}: \quad \text{(Laughlin)}, \tag{3.33a}$$

$$\mathcal{Q}(\eta) = \sigma(\eta) :e^{i\phi(\eta)/2\sqrt{q}}: \quad \text{(Moore-Read)}. \tag{3.33b}$$

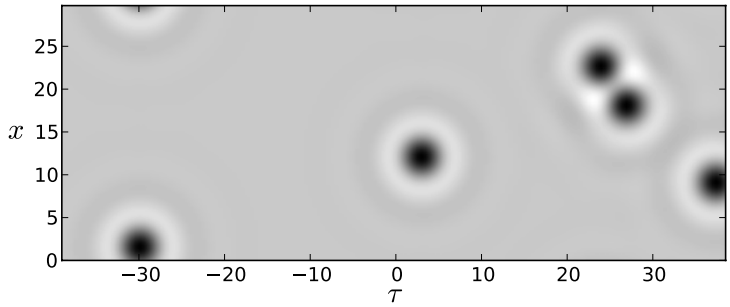

Figure 3.5: The real-space density $\rho(\tau, x)$ of a $q = 5$ Laughlin state with five quasiholes on an infinite cylinder of circumference $L = 30\ell_B$. Distances are measured in units of ℓ_B. (The top and bottom edges are identified.)

Here $\sigma(\eta)$ is the chiral part of the Ising order operator. Quasiparticles require 'quasi-local' operators,[46] which can also be included in the MPS, but we have deferred their implementation.

To incorporate the quasihole into the MPS, we first explicitly time order Eq. (3.32) by bringing the insertion $\mathcal{Q}(\eta)$ between the orbitals $\tau_{n+1} \geq \eta_\tau \geq \tau_n$. For fermions, this introduces a sign for each electron in the region $\tau > \eta_\tau$. As detailed in Appendix 3.12, this sign can be written as $s^{\hat{\pi}_0/\sqrt{q}}$, where $\hat{\pi}_0$ is conjugate to the bosonic zero-mode and $s = \pm 1$ for bosons and fermions respectively.

We calculate the matrix elements of $\mathcal{Q}$ at $\tau = 0$,

$$Q_{\alpha,\beta} = \langle \alpha | s^{\hat{\pi}_0/\sqrt{q}} \mathcal{Q}(\eta_x) | \beta \rangle, \tag{3.34}$$

and then insert Q into the 'unperturbed' evolution on the bond between sites $n, n+1$,

$$U(\delta\tau) \to U(\tau_a)\, Q\, U(\tau_b), \quad \tau_a + \tau_b = \delta\tau, \tag{3.35}$$

where $\tau_a = \tau_{n+1} - \eta_\tau$. The structure of the resulting MPS is illustrated in Fig. 3.2c. For further details on calculating Q for the Laughlin and MR states we refer to Appendix 3.12.

We have implemented the Laughlin quasiholes numerically, with a resulting density profile for a collection of quasiholes in the $q = 5$ state shown in Fig. 3.5. As a simple test of the result, we can explicitly evaluate the Berry connection associated with the transport of one $q = 3$ Laughlin quasihole around another,

$$\theta = \oint dA = \oint d\eta \, \langle \eta | (-i\partial_\eta) | \eta \rangle. \tag{3.36}$$

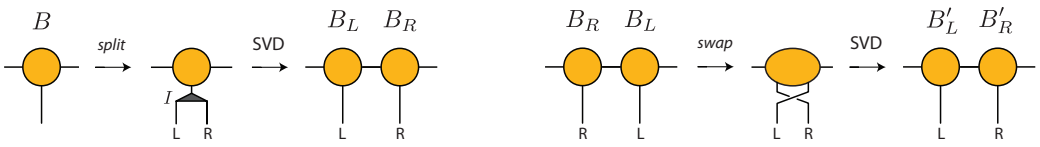

(a) Split operation. (b) Swap operation.

Figure 3.6: The splitting and swapping[103] procedure performed on an MPS. The two operations allow us to compute the real-space entanglement cut from an orbital MPS.

We keep one quasihole fixed at $\eta = 0$, while a second follows a discretized path η_i chosen to wind around the other, which defines a discretized connection $e^{iA_{ij}} = \langle \eta_i \rangle \eta_j$. We then integrate the connection after subtracting out a similar phase in the absence of the second particle. Calculating the inner product between two matrix product states can be computed with complexity $\mathcal{O}(A/\ell_B^2\ \chi^3)$, where A is the area of the region enclosing the quasiholes in question. Working on an $L = 16\ell_B$ cylinder and ensuring the quasiparticles remain at least a distance of $8\ell_B$ apart, we find a statistical angle $\theta_{q=3} = 2.0992$, compared to the prediction of $\frac{2\pi}{3} \approx 2.0944$. The computation takes about 1 minute.

While the result is already well established for the Laughlin states,[5] it would be worthwhile to explicitly calculate the non-abelian Berry connection for the Moore-Read quasiparticles. As we have computed the form of the Q-matrices, we believe this would be tractable.

3.5 Real-space entanglement spectrum

Finally, we present an algorithm for computing the real-space entanglement spectrum (RSES) of quantum Hall states on both finite and infinite cylinders. In contrast to the orbital cut which divides the system into two sets of LLL orbitals,[47] the real-space cut partitions the system into two regions of physical space. Previously this was accomplished analytically for the free $\nu = 1$ case, [120, 92] and numerically using Monte Carlo[93] and large scale singular value decomposition (SVD) of explicit wave functions.[29, 110] Our technique is not specific to the model wave functions, and provides a means for computing the RSES of non-model states calculated from DMRG. As the scaling form of the entanglement spectrum only appears for the real-space cut, this may prove an important diagnostic for non-model states. For simplicity, we assume a wave function in the LLL, and consider an entanglement cut running around the cylinder at $\tau = \tau_c$.

The first step of the algorithm is to 'split' each orbital $\varphi_n(z)$ [Eq. (3.9)] into components $\varphi_{nR/L}$ supported on the right and left of a cut at τ_c,

$$\begin{aligned}\varphi_n(z) &= \theta(\tau-\tau_c)\varphi_n(z) + \theta(\tau_c-\tau)\varphi_n(z) \\ &= g_{nL}\varphi_{nL}(z) + g_{nR}\varphi_{nR}(z).\end{aligned} \tag{3.37}$$

We normalize the split orbitals by factors $g_{L/R}$ such that $\{\varphi_{nL}, \varphi_{nR}\}$ remains an orthonormal basis. Expressing the state in terms of the 'split' basis amount to appending isometries I onto the B-matrices,

$$B^m_{\alpha\beta} \to B^m_{\alpha\beta} I^{kl}_m, \quad I^{kl}_m = \sqrt{\binom{m}{k}}\, g^k_L\, g^l_R\, \delta_{k+l,m}, \tag{3.38}$$

where the factors g implicitly depend on the orbital location. Because the orbitals φ_n are exponentially localized about $\tau_n = \frac{2\pi\ell_B^2}{L}n$, we can work at some fixed accuracy by splitting only the $M \sim \mathcal{O}\big(\frac{L}{\ell_B}\big)$ orbitals nearest to the cut. In practice, we find $M = 1.5L/\ell_B$ is sufficient to obtain a converged spectrum. As illustrated in Fig. 3.6a, the affected B matrices are then split using a SVD equivalent to the truncation step of time evolving block decimation (TEBD).[126] As with TEBD, the splitting step preserves the 'canonical' form of the MPS, implying that the bipartition about the new bond is a Schmidt decomposition.

After the splitting step we have added M B-matrices to the chain, with orbitals alternating between the left and right sides of the cut. Choosing some particular bond to represent the location of the cut (usually the bond at the center of the set of sites we have split), we sort the MPS through a series of $\mathcal{O}(M^2)$ swapping procedures, bringing all indices associated to the left region to the left of the cut, and likewise for the right. To accomplish this, we employ the swapping algorithm described in Ref. [103] to exchange each pair of neighboring sites in the MPS. As illustrated in Fig. 3.6b, for each swap we form a two-site wave function, permute the right and left legs to bring them to the desired order, and then split the wave function using SVD to obtain a new pair of B-matrices. Again, the canonical form of the MPS is preserved during this procedure, so after performing the required swaps the bond designated as the cut gives the real-space Schmidt decomposition.

Depending on the initial bond dimension χ, it may be necessary to truncate the new B-matrices by keeping only the largest singular values of the SVD. It appears that the low lying states are not affected by truncation of the highest lying states, but the convergence with increased χ should be checked on a case by case basis.

3.6 Entanglement spectrum: orbital cut vs. real-space cut

In this section we study the scaling form of the RSES, then contrast it to the orbital spectrum. As illustrated for the $q = 3$ Laughlin state in Figs. 3.7, and for the MR state in Figs. 3.11, the orbital and real-space cuts agree in their counting, which is that of the CFT, but differ in the scaling of the energy levels E_i present in the spectrum.

Kitaev and Preskill[58] first noted that the known universal features of topological entanglement entropy could be explained if the *energies* of the entanglement spectrum coincided with those of the chiral CFT. A physical argument was later provided in Ref. [86]. Recall that the states of the CFT are grouped into 'families' associated with each primary field ϕ_h,[33] in this context one per degenerate ground state on a cylinder, and let $\hat{P}_{\phi_h}$ denote a projection operator onto the corresponding family. The basic conclusion of Ref. [86] was that the reduced *real-space* density matrix of a topological state with gapless chiral edge modes takes the form

$$\hat{\rho}_L = \sum_h p_h \hat{P}_{\phi_h} e^{-v\hat{H}+\mathcal{O}(k\ell_B)} \hat{P}_{\phi_h}. \tag{3.39}$$

Here $\hat{H}$ is the Hamiltonian of the CFT, which we will take to have velocity 1, so an 'entanglement velocity' is included as a factor v. $\hat{H}$ is perturbed by more irrelevant boundary operators of order $(k\ell_B)^\delta$ for $\delta > 1$. The coefficients p_h depend on the degenerate ground state being considered. During the final preparation of this work, this scaling form was put on firm footing for the model FQH states.[28]

While the irrelevant operators generally introduce 'interaction terms' to the entanglement Hamiltonian, to illustrate the expected behavior we consider the simplest type of correction, a dispersive term. For the Laughlin state this takes the form

$$\tilde{E}_a \equiv E_a - E_0 \sim v \left[\sum_{n>0} \epsilon(k_n) a_n^\dagger a_n + \frac{2\pi}{L} \frac{\hat{N}^2}{2q} \right], \tag{3.40}$$

$$\epsilon(k) = k[1 + u_2 k^2 + u_4 k^4 + \cdots], \quad k_n = \frac{2\pi}{L} n. \tag{3.41}$$

which accounts for the 'branches' apparent in the real-space spectrum (Fig. 3.7 right), each of which is associated with the presence of a new mode $a_n^\dagger$. The dispersion relation can be fit from the heights of these branches. Note that only odd powers of k can appear in the dispersion of a chiral boson. In general, if the irrelevant perturbations descend from the identity boundary operator, only odd powers in k should appear.

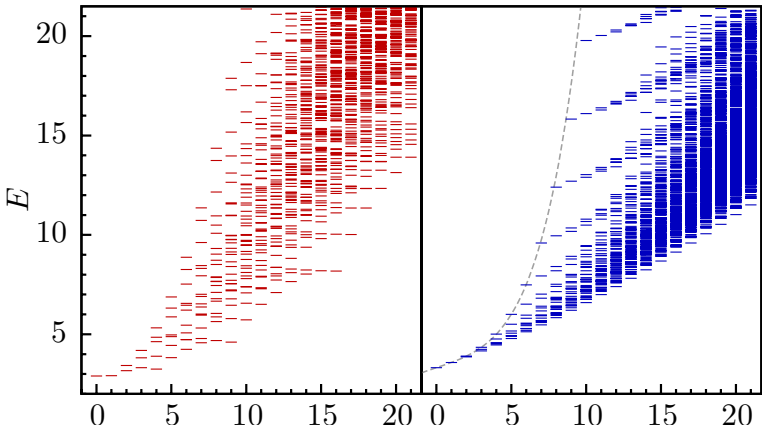

Figure 3.7: Entanglement spectra (in the neutral charge sector) of the orbital (left) and real-space (right) cut of the $q = 3$ Laughlin state at $L = 32\ell_B$. The energies E are plot against their momentum in units of $\Delta k = \frac{2\pi}{L}$. Both spectra have the counting 1, 1, 2, 3, 5, 7, 11, *etc.*, consistent with that of a chiral boson CFT. However, the energy levels E have vastly different quantitative behaviors in the two cases, which we investigate in Fig. 3.8. The dashed line on the right is of the form $v\epsilon(k) = vk[1 + u_2k^2 + u_4k^4]$, with u_2, u_4 fit from the highest level of each sector, which we associate to the state $a_n^\dagger|0\rangle$. The fits appear to rule out a similar term u_1, but larger sizes and a treatment of the 'interactions' would be required to rule out u_3 if it is indeed absent.

In order to accurately extract the entanglement velocity, we consider the scaling of the shifted spectrum $\frac{\tilde{E}L}{2\pi}$ with increased L. Based on these scaling ideas, a state with momentum $k = \frac{2\pi}{L}(n_\phi + n_\chi)$ should have an energy

$$\frac{\tilde{E}_a L}{2\pi} = v_\phi(\Delta_{\phi h} + n_\phi) + v_\chi(\Delta_{\chi h} + n_\chi) + t_{2a}L^{-2} + t_{4a}L^{-4} + \cdots \quad (3.42)$$

where n_ϕ and n_χ are integers corresponding to the momenta of the $U(1)$ and Majorana sectors. The offsets $\Delta_{\phi/\chi h}$ are the scaling dimensions of the highest weight state in the sector, which depends on the bond and number sector in question (for the Laughlin states, it is $\frac{N^2}{2q}$). For the MR case we have included a detailed exposition of this structure in Appendix 3.11.

Focusing on the identity sector $\Delta_h = 0$ of the *real-space* $q = 3$ Laughlin cut, Fig. 3.8a tracks the scaled relative entanglement energy levels $\frac{\tilde{E}L}{2\pi}$ as a function of L^{-2}, extrapolating their value as the circumference approaches infinity. As indicated by

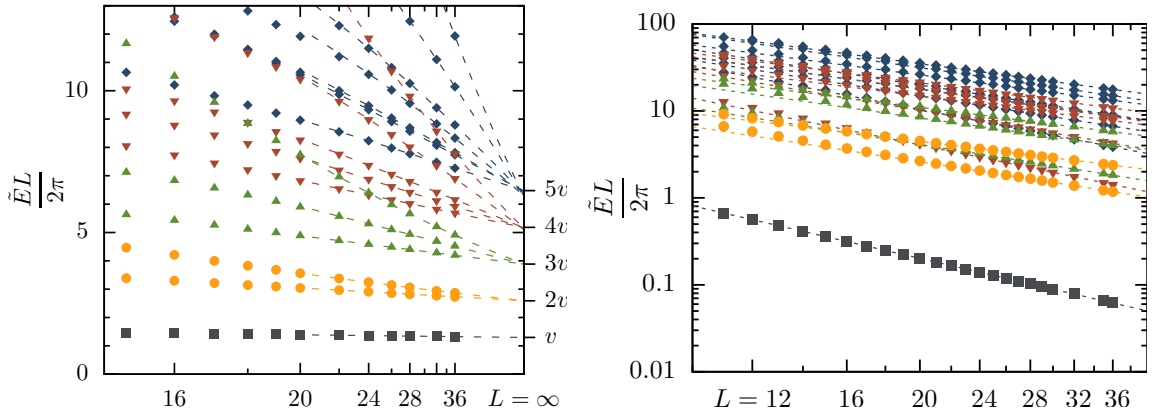

(a) Real-space cut: plot of $\tilde{E}L/2\pi$ vs. $-1/L^2$. (b) Orbital cut: log-log plot of $\tilde{E}L/2\pi$ vs. L.

Figure 3.8: The relative entanglement energies for the real-space cut and orbital cut of the Laughlin state at $\nu = 1/3$. (Data shown for the charge neutral sector, L shown in units of ℓ_B.) The states at different momenta are distinguished by their colored symbols. (a) For the real-space cut, we plot $\frac{\tilde{E}L}{2\pi}$; the relative entanglement energy (relative to E_0) times the cylinder radius, as a function of $-1/L^2$. The energies are extrapolated to $L = \infty$ using a quadratic fit $t_0+t_2L^{-2}+t_4L^{-4}$, and land on multiples of the entanglement velocity $v \approx 1.2956$. (b) For the orbital cut, we show $\frac{\tilde{E}L}{2\pi}$ on a log-log plot, showing that the data has a linear behavior with negative slopes. The lines shown results from a linear fit to the last few data points. This demonstrates a power-law relation $\tilde{E}_a \propto L^{-\zeta_a}$ with $\zeta_a > 1$.

the right-most tics of the figure, $\frac{\tilde{E}L}{2\pi}$ approaches $n_\phi v_\phi$ for large L, where $v_\phi \approx 1.2956$. The data clearly confirms that the real-space entanglement spectrum approaches a linear dispersion with fixed velocity, and the success of the fit justifies the absence of L^{-1} and L^{-3} perturbative terms. We have tabulated the velocities for the $q = 1$, 3, 5 and 7 in Tab. 3.1. The relation $v_{q=1}/v_{q=3} \approx \sqrt{3}$ noted previously[110] appears not to continue to higher q.

This same technique can be used for more complicated wave functions such as the Moore-Read state, as shown in Fig. 3.9. We extrapolate the velocities of both the charge and neutral modes to be $v_\phi \approx 1.33$ and $v_\chi \approx 0.21$ respectively. We note that the extrapolation is only possible for sufficiently large circumferences $L \gtrsim 20\ell_B$, which is well within reach using the MPS representation of the wave function.

Figure 3.8b shows that in the orbital-cut, $\tilde{E}$ does not extrapolate to the CFT linear dispersion. Rather, they appear to follow power law decays $\tilde{E}_a \sim L^{-\zeta_a}$ with different ζ_a for each state a. For example, the fit for $k = \frac{2\pi}{L}$ gives $\zeta \approx 3.0$, while $\zeta \approx 2.3$, 2.1 for the two set of states at $k = 2\frac{2\pi}{L}$. (In the real-space case, $\zeta = 1$ for

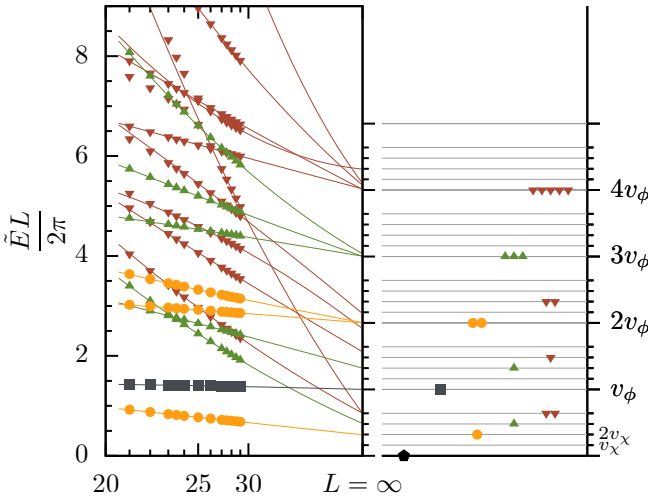

Figure 3.9: Extrapolating the entanglement energies $\tilde{E}L/2\pi$ for the Moore-Read state at $\nu = 1/2$, using a cut associated with counting 1, 1, 3, 5, 10, *etc.* for $N = 0$ charge sector (*cf.* App. 3.11). (Left) Here we show that the energies for the first three momenta extrapolate to integral combinations of v_ϕ and v_χ, the velocities of the chiral boson and Majorana mode respectively. The major tics on the vertical axis labels multiples of v_ϕ, the minor tics label combinations $n_\phi v_\phi + n_\chi v_\chi$ for integers n_ϕ and n_χ (and ℓ_B set to 1). States with momentum $4\frac{2\pi}{L}$ extrapolate near, but not exactly, to the theoretical prediction, which we attribute to smallness of the system sizes. The superimposed lines are quadratic fits over the largest few circumferences, extrapolating to give $v_\phi \approx 1.33$, $v_\chi \approx 0.21$. (Right) The theoretical placement of the energy levels for the state. Here the boson counting (1,1,2,3,5) and the Majorana counting (1,0,1,1,2) are apparent. See App. 3.11 for detailed explanation of the counting in this plot and data for other charge sectors.

all the levels.) Unfortunately, the range of data available is insufficient to draw any conclusions.

Finally, we note that one can extract the topological entanglement entropy in either types of cut. This was shown in Fig. 3.3 where we used both the entropy S and the zero momentum state E_0 as a function of L. For each L we perform a windowed fit; presenting the intercept of the best line fit through the neighboring points. While it is possible to extract γ from any of the four computed quantities, we can see that the real-space cut is less oscillatory than the orbital cut. At the same time, using the orbital cut E_0 seems to give a much better convergence of γ than any of the other methods, *i.e.*, the system size L required to computed $\mathcal{D} = e^\gamma$ via the orbital E_0 to accuracy ± 0.5 is the smallest. Table 3.1 lists the entanglement

velocities and TEE for various Laughlin states and the $q = 2$ MR state, as well as the velocities extracted via the method used in Figs. 3.8a and 3.9.

3.7 Conclusion

We have shown how the CFT structure in model FQH wave functions enable us to represent them as matrix product states. These MPSs can be evaluated numerically on an infinite cylinder; the distinct advantages of this geometry, as well as the efficiency of the MPS, allow us to study in detail the scaling properties of the Moore-Read entanglement spectrum, including a definitive identification of the $U(1)$ and Majorana modes and their velocities.

There are several future directions. The MPS representation is well suited for studying the screening properties of the states as well as their Berry connections, so it would be valuable to numerically implement the MR quasiholes in order to verify various screening arguments.[87, 11] As we have noted, our construction also generalizes to other topological phases whose model states can be expressed as a correlation function of a lower dimensional field theory. The resulting picture is strikingly similar to the 'entanglement renormalization' classification of 1D phases exemplified in the AKLT state. In particular, it would appear that the fixed points of the entanglement renormalization scheme may be interpreted as some form of fixed point for the auxiliary field theory when expressed as a tensor network – for topological phases, a massless fixed point, while for trivial phases, a massive fixed point. Making this connection precise would be an intriguing development.

We would like to acknowledge helpful conversations with Joel E. Moore, Tarun Grover, Frank Pollmann, Sid Parameswaran, and Jérôme Dubail, as well as support from NSF GRFP Grant DGE 1106400 (MZ) and NSF DMR-0804413 (RM).

3.8 Appendix A. Details on the conversion from real space to orbital space MPS

Here I go over the technical details required to prove that the CFT wavefunctions can be brought from real space form, in which the wave function is obtained in the position basis, to an orbital form, in the basis of the LLL orbitals. The basic intuition is that because the LLL orbitals are distinguished by momentum, we do not need to perform the full 2D overlap integrals to extract the occupation number of an orbital - we can do a contour integral. The chief technical difficulty is figuring out what gauge the CFT state is actually in.

Recall the 'coherent state' wave functional of the CFT wave functions is

$$\Psi[\psi(z)] = \left\langle e^{\int d^2z \left[\mathcal{V}_e(z)\psi(z) - i\rho\phi(z)/\sqrt{\nu}\right]} \right\rangle_{CFT}, \tag{3.43}$$

where $\psi(z)$ is the coherent state coordinate (it is Grassmann or complex valued for fermions and bosons respectively). The electron operator is generally of the form $\mathcal{V}_e = e^{i\phi/\sqrt{\nu}}\chi$. The first part is the '$U(1)$' part, which generates a Jastrow term $(z_i - z_j)^{1/\nu}$, while χ is the 'statistics' part, such as a Majorana for the Pfaffian state. All of the subtleties in what follows arise from the $U(1)$ part and its background charge, so I will assume the Laughlin case $\chi = 1$.

Introducing the orbitals

The usual way to convert between bases is with overlap integrals using the LLL basis states

$$\phi_n \propto e^{-ik_n x - \frac{1}{2}(\tau - k_n)^2} = e^{-ik_n z} e^{-\frac{1}{2}\left(k_n^2 + \tau^2\right)}, \quad k_n = \frac{2\pi n}{L}. \tag{3.44}$$

But if the state is already entirely in the LLL, it is sufficient to do a contour integral, because the states are labeled by momentum. When acting on a state that is in Landau gauge, and entirely in the LLL, you can replace the destruction operator of orbital n with a contour integral around the cylinder,

$$\hat{\psi}_n \Rightarrow \oint_{\tau=\tau_n} \frac{dx}{L}\, e^{ik_n x} \hat{\psi}(x, \tau_n), \quad \tau_n = \frac{2\pi n}{L} = k_n \tag{3.45}$$

$$= e^{\tau_n^2} \oint_{\tau=\tau_n} \frac{dw}{2\pi i}\, w^{-n-1} \hat{\psi}(w) \tag{3.46}$$

up to an n independent normalization. I have chosen to perform the integrals at τ_n, though with an appropriate change in normalization a different location could

be chosen. However - we can't just substitute in this mode expansion and be done. First, we wouldn't get an equation that was manifestly translation invariant (due to the n dependence). Second it's not obvious what gauge the state Eq. (3.43) is actually in!

Branch cuts and the background charge

We first need to understand how the background charge makes a gauge choice. The correlation function on a cylinder can be decomposed into the fluctuating part (first) and zero mode (second):

$$\langle\phi(w_1)\phi(w_2)\rangle_{cyl} = -\log(1-\frac{w_2}{w_1}) + \frac{1}{2}\log(\frac{w_2}{w_1}) \text{ for } \tau_1 > \tau_2 \tag{3.47}$$

In Sec.3.8 I have included the mode expansion of the boson from which this can be derived. For $\tau_1 < \tau_2$, we exchange $1 \leftrightarrow 2$. The fluctuating part does not have a branch cut, but the zero mode does. The $\mathcal{V}_e\mathcal{V}_e$ interaction doesn't see the branch cut, but because $\mathcal{O}_{bc}$ is a continuous smear of charge, there is a branch cut in the $\mathcal{V}_e e^{\mathcal{O}_{bc}}$ interaction. This ambiguity is what determines the gauge of the state, which we can fix by a choice of branch cut.

Let's consider the interaction between an electron at w_1 and the background charge at w_2, with $\tau_1 > \tau_2$. Because we will eventually integrate around $\int dx_2$, we can *ignore* the fluctuating part of the background charge, leaving

$$\left\langle e^{i\phi(w_1)/\sqrt{\nu} - i\rho\phi(w_2)/\sqrt{\nu}} \right\rangle_\phi = e^{-\frac{1}{2\nu}\rho\log(\frac{w_2}{w_1})} = e^{-\frac{1}{2L}[\tau_1-\tau_2-i(x_1-x_2)]} \quad \text{for } \tau_1 > \tau_2 \tag{3.48}$$

Note the result is not periodic in x_1 - this is the branch. The most natural choice for the CFT is to consistently choose the discontinuity at some fixed x, say, $x = \pm L/2$. As a result, the total interaction with the background charge, given by integrating over d^2z, is

$$\left\langle e^{i\phi(z)/\sqrt{\nu} - i\rho\int d^2u\phi(u)/\sqrt{\nu}} \right\rangle_\phi = e^{-\frac{\tau^2}{2}} e^{ix\tau} \tag{3.49}$$

We see that the background charge properly produces the Gaussian $e^{-\frac{\tau^2}{2}}$, but includes a phase as well! Apparently our choice has produced a state in the gauge $A = (0, x)$ rather than $A = (-\tau, 0)$. The CFT gauge ('CFT') use related to the Landau gauge ('LG') according to

$$\Psi_{CFT}(w_i) = \Psi_{LG}(w_i)\prod_i w_i^{-L\tau_i/2\pi}\ e^{\sum_i \tau_i^2}. \tag{3.50}$$

Note that here τ_i is the location of the ith particle - not $\tau_n = k_n$.

Comparing with Eq. (3.45), this is actually convenient at the ring locations τ_n, where $L\tau_n/2\pi = n$. So if we let ψ_n still denote orbitals in the Landau gauge, but *act on a state in the CFT gauge*, we can replace the destruction operator of orbital n with a contour integral around the cylinder,

$$\hat{\psi}_n \Rightarrow \oint_{\tau=\tau_n} \frac{dw}{2\pi i} w^{-1}\, \hat{\psi}(w) \ \text{(CFT gauge)} \tag{3.51}$$

This expansion is manifestly translation invariant.

At this stage we have the form

$$\Psi[\psi_n] = \left\langle e^{\sum_n \int \frac{dx}{L} \mathcal{V}_e(x,\tau_n)\psi_n - i\sqrt{\nu^{-1}}\rho \int d^2z \phi(z)} \right\rangle_{CFT}, \tag{3.52}$$

The last trick is to make the background charge discrete as well. Because we chose contours at τ_n, it will be sufficient to reproduce the wave function *only at* τ_n. With this in mind, we can redistribute the uniform background charge into a set of discrete rings at locations τ_n:

$$\rho \int d^2z \phi(z)/\sqrt{\nu} \to \frac{\sqrt{\nu}}{L} \sum_n \int dx \phi(x, \tau_n) \tag{3.53}$$

Just to check we get the correct result, we do an elementary electrostatics calculation to find the potential of a set of charged rings:

$$\left\langle e^{i\phi(w)/\sqrt{\nu} - \frac{i\sqrt{\nu}}{L}\sum_n \int dx_2 \phi(x_2 + i\tau_n)} \right\rangle_\phi \Bigg|_{w=x+i\tau_m} = e^{-\tau_m^2/2} e^{ix\tau_m} = w^{-m} e^{\tau_m^2} \tag{3.54}$$

which is identical to the continuous case, so the same substitution for $\hat{\psi}_n$ applies. Technical point - the expression must be Weyl ordered on the slice τ_m, distributing the background charge 50/50 on either side of $\mathcal{V}_e$.

All together,

$$\Psi[\psi_n] = \left\langle e^{\sum_n \oint \frac{dx}{L} \left[\mathcal{V}_e(x,\tau_n)\psi_n - i\sqrt{\nu}\phi(x,\tau_n)\right]} \right\rangle_{CFT} \tag{3.55}$$

$$= \left\langle e^{\sum_n \left[\mathcal{V}_{e;0}\psi_n - i\sqrt{\nu}\phi_0\right]_{\tau_n}} \right\rangle_{CFT} \tag{3.56}$$

where $\mathcal{O}_0 = \oint \frac{dx}{L} \mathcal{O}(x)$ are the 'zero modes' of an operator.

Reference for chiral boson conventions

At $g = \frac{1}{4\pi}$, where $G(z) = -\log(z)$ (on the plane), we have the following mode expansion on a cylinder:

$$\phi(w) = \sum_{n\neq 0} \frac{w^{-n}}{\sqrt{|n|}} a_n + \phi_0 + \frac{\pi_0}{i}\log(w), \tag{3.57}$$
$$[\phi_0, \pi_0] = i, \quad [a_n, a_m] = \delta_{n+m}.$$

The field is composed of the fluctuating part $\phi'(w)$ and the 'zero mode',

$$\phi(w) = \phi'(w) + \phi_0 + \frac{\pi_0}{i}\log(w)\,. \tag{3.58}$$

The Hamiltonian is

$$H = \frac{2\pi}{L}\left[\sum_{n>0} n\ a_{-n}a_n + \frac{1}{2}\pi_0^2\right] \tag{3.59}$$

3.9 Appendix B. Evaluation of B-matrices for Laughlin states

Here we provide more detail on the precise form of the Laughlin MPS and its numerical implementation. The mode expansion of the chiral boson is

$$\phi(w) = \sum_{n\neq 0} \frac{w^{-n}}{\sqrt{|n|}} a_n + \phi_0 + \frac{\pi_0}{i}\log(w), \tag{3.60}$$
$$[\phi_0, \pi_0] = i, \quad [a_n, a_m] = \delta_{n+m}.$$

The field is composed of the fluctuating part $\phi'(w)$ and the 'zero mode',

$$\phi(w) = \phi'(w) + \phi_0 + \frac{\pi_0}{i}\log(w)\,. \tag{3.61}$$

The states of the fluctuating sector can be labeled by occupation numbers, which we denote by a string of positive integers P. For example, $|0\rangle$ denotes the ground state, $|221\rangle = \frac{1}{\sqrt{2}} a_2^\dagger a_2^\dagger a_1^\dagger |0\rangle$, *etc.* We define $|P|$ to be the total momentum of the fluctuations in $|P\rangle$, given by the sum of the integers. The states of the zero-mode sector are labeled by the eigenvalues of π_0. For convenience, we define 'charge' by $\hat{N} = \sqrt{q}\pi_0$, chosen such that the electron has charge q. The states of the zero-mode sector are labeled by $|N\rangle$, so the full CFT is then spanned by $|P, N\rangle$.

Treating first the 'free' evolution U, we find

$$H = \frac{2\pi}{L}\left[|P| + \frac{N^2}{2q}\right], \frac{2\pi}{L}\left[|P| + \frac{1}{2q}N^2\right], \tag{3.62}$$

$$U(\delta\tau)_{P,N;P',N'} = \delta_{P,P'}\delta_{N,N'} e^{-(2\pi\ell_B/L)^2\left[|P|+\frac{1}{2q}N^2\right]}. \tag{3.63}$$

Now we calculate the on-site term T, first by converting from the coherent state form $T[\psi]$ to the occupation basis, T^m:

$$\begin{aligned} T[\psi] &= e^{-\frac{i}{2\sqrt{q}}\phi_0} e^{\hat{\mathcal{V}}_0\psi} e^{-\frac{i}{2\sqrt{q}}\phi_0} \\ &= \sum_m T^m (m!)^{3/2} \psi^m. \end{aligned} \tag{3.64}$$

$$T^m \equiv \frac{1}{\sqrt{m!}} e^{-\frac{i}{2\sqrt{q}}\phi_0} \left(\hat{\mathcal{V}}_0\right)^m e^{-\frac{i}{2\sqrt{q}}\phi_0}. \tag{3.65}$$

We next compute the matrix elements of the vertex operator,

$$\begin{aligned} &\langle P, N|\hat{\mathcal{V}}_0|P', N'\rangle \\ &\quad = \langle P, N|e^{i\sqrt{q}\phi'(w)+i\sqrt{q}\phi_0+N\log(w)]}|P', N'\rangle. \end{aligned} \tag{3.66}$$

The zero-mode part depends only on N,

$$\langle N|e^{i\sqrt{q}\phi_0+\hat{N}\log(w)}|N'\rangle = \delta_{N-N',q}\, w^{N+N'/2}. \tag{3.67}$$

The fluctuating part depends only on the oscillators $|P\rangle$, so we define

$$A^n_{P,P'} = \langle P| \oint \frac{dw}{2\pi i}\, w^{-n-1} e^{i\sqrt{q}\phi'(w)}|P'\rangle. \tag{3.68}$$

Hence A^n is simply the nth coefficient of a Taylor expansion in w. The matrices A are non-zero only for $P - P' = -(N + N')/2$, due to momentum conservation. Numerically, we impose a cutoff Λ such that we only keep states $|P\rangle$ with $|P| \leq \Lambda$, which allows us to evaluate A for only a finite number of states. The time to compute A is proportional to its number of entries, so the construction of the MPS is an insignificant part of the computational cost (*i.e.*, compared to matrix multiplication). Combining the zero-mode and fluctuations,

$$\langle P, N|\hat{\mathcal{V}}_0|P', N'\rangle = A^{-\frac{N+N'}{2}}_{PP'} \delta_{N-N',q}. \tag{3.69}$$

Finally, the sandwiching background charge contributes $e^{-\frac{i}{\sqrt{q}}\phi_0} = \delta_{P,P'}\delta_{N-N',-1}$ to each site.

Focusing on the case of fermions where there is at most one particle per orbital,

$$T^0_{P,N;P',N'} = \delta_{P,P'}\delta_{N-N',-1} \qquad \text{(unoccupied)}, \tag{3.70a}$$

$$T^1_{P,N;P',N'} = A_{PP'}^{-\frac{N+N'}{2}}\delta_{N-N',q-1} \qquad \text{(occupied)}. \tag{3.70b}$$

For case of bosons, the higher occupation states involve products of the A's.

The q fold ground state degeneracy of the Laughlin states can be seen by noting that on a particular bond, $e^{2\pi i N/q}$ is a constant, and can be chosen to take one of q values.

3.10 Appendix C. Evaluation of B-matrices for Moore-Read state

The CFT associated with the Moore-Read state is a tensor product of a chiral boson ϕ and a Majorana mode χ. We first give a brief review of the structure of the chiral Majorana CFT on a cylinder.[37] The states form four sectors according to their boundary condition (bc), (periodic '**P**' or antiperiodic '**AP**') and number parity (even '+1' or odd '−1'). We denote the lowest energy states of these four sectors by '$|\mathbb{1}\rangle$' for **AP**/1, '$|\chi\rangle$' for **AP**/−1, '$|\sigma\rangle$' for **P**/1 and '$|\mu\rangle$' for **P**/−1. In the periodic sector the Majorana has modes $\chi_n : n \in \mathbb{Z}$, while in the anti-periodic sector it has modes $\chi_m : m \in \mathbb{Z} + \frac{1}{2}$. The states of the **P**/**AP** sectors can be obtained by acting with the **P**/**AP** modes χ_{-m} on $|\sigma\rangle/|\mathbb{1}\rangle$ respectively. Within a given sector, the states can then be labeled by a string of numbers P_χ; they are either integers or half-integers depending on the bc, and do not repeat because of the fermionic statistics. Letting $|P_\chi|$ denote the total momentum of the Majorana,

$$H_\chi = \frac{2\pi}{L}\left[|P_\chi| + \Delta\right] \tag{3.71}$$

where $\Delta = \{0, \frac{1}{16}\}$ for the **AP** and **P** sectors respectively, though Δ can be ignored as it only changes the normalization of the state.

The operator $e^{i\sqrt{q}\phi(z)}\chi(z)$ must be periodic in z at the location of the Landau orbitals τ_n (our choice of gauge has a twist boundary condition in between). This introduces a constraint between the zero mode of the boson, $\hat{N} = \sqrt{q}\hat{\pi}_0$, and the boundary condition of the Majorana. We find that for q even (the fermionic case), at the *bond* of the MPS the CFT boundary condition is such that if the Majorana is in **P**, we must have $N \in \mathbb{Z} + \frac{1}{2}$, while for **AP**, we must have $N \in \mathbb{Z}$. The boundary conditions will correspond to different degenerate ground states, with 4 states of type

AP and 2 of type **P**, for a total of 6 on the infinite cylinder (for a torus, the **P** sector acquires an additional 2 states depending on the parity of the electron number).[88]

The total energy of the combined CFT is

$$H = \frac{2\pi}{L}\left[|P_\chi| + |P_\phi| + \frac{1}{2q}N^2\right] \tag{3.72}$$

with $|P_\phi|$ and N arising for the boson. As for the Laughlin state, $U = e^{-\delta\tau H}$ is diagonal if we work in the occupation basis. Constructing the T matrices proceeds as for the Laughlin case, but we must include the Majorana sector in the computation of $\hat{\mathcal{V}}_0 = \oint \frac{dw}{2\pi i} w^{-1}\chi(w)e^{i\sqrt{q}\phi(w)}$. Letting

$$\chi^m_{P_\chi,P'_\chi} = \langle P_\chi|\chi_m|P'_\chi\rangle \tag{3.73}$$

denote the matrix elements of the Majorana operators, the required matrix element is

$$\langle P_\phi, P_\chi, N|\hat{\mathcal{V}}_0|P'_\phi, P'_\chi, N'\rangle = \sum_m \chi^{-m}_{P_\chi,P'_\chi} A^{m-\frac{N+N'}{2}}_{P_\phi,P'_\phi}\,\delta_{N-N',q}\,, \tag{3.74}$$

with A defined as for the Laughlin case.

For fermions, where there is at most one particle per orbital,

$$T^0_{(P_\phi,P_\chi,N),(P',P'_\chi,N')} = \delta_{P_\phi,P'_\phi}\delta_{P_\chi,P'_\chi}\delta_{N-N',-1} \quad \text{(unoccupied)}, \tag{3.75a}$$

$$T^1_{(P_\phi,P_\chi,N),(P',P'_\chi,N')} = \sum_m \chi^{-m}_{P_\chi,P'_\chi} A^{m-\frac{N+N'}{2}}_{P_\phi,P'_\phi}\delta_{N-N',q-1} \quad \text{(occupied)}. \tag{3.75b}$$

For the case of bosons, the higher occupation states involve products of the $\mathcal{V}_0$'s.

The $3q$ fold ground state degeneracy of the MR states can be seen by first choosing a bc sector for the Majorana, **P** or **AP**. In the **AP** sector, on any given bond $(-1)^F e^{i\pi N/q}$ is constant, with $N \in \mathbb{Z}$ and F the Majorana number. The quantity has $2q$ allowed values, each leading to a distinct state. $(-1)^F e^{i\pi N/q}$ is also constant in the **P** sector, where $N \in \mathbb{Z} + \frac{1}{2}$. However, here the $2q$ values only lead to q distinct states. This is because while inserting the Majorana zero-mode χ_0 at past infinity changes the assignment of F, it does *not* actually change the physical state. As

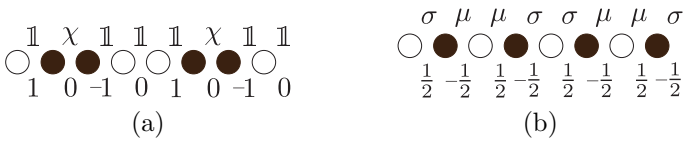

Figure 3.10: The thin torus orbital wave functions for the (a) antiperiodic and (b) periodic sectors. Each site corresponds to an orbital, which is either filled (black) or empty (white). Each bond has only a single state of the CFT, which we decompose into the Majorana part, shown above the bond, and zero mode of the boson N, shown below the bond.

illustrated in Fig. 3.10, this can be understood as a simple relabeling $\mu \leftrightarrow \sigma$, which are equivalent so produces the same state.

In the small L limit, these $3q$ states evolve into 'thin torus' wave functions.[8] In this limit, we restrict the Majorana CFT to the states $\{|\mathbb{1}\rangle, |\chi\rangle, |\sigma\rangle, |\mu\rangle\}$, and fix $|P_\phi| = 0$ for the boson, which projects onto the charges $N = \{-1, -\frac{1}{2}, 0, \frac{1}{2}, 1\}$. The 6 resulting states are precisely the 'highest weight' states of the CFT, as illustrated in Fig. 3.10.

3.11 Appendix D. The counting of the Moore-Read state

As explained in the last section, the chiral Majorana CFT may be separated into four sectors, by periodicity of the boundary as well as the particle number parity.

In the periodic sectors σ and μ, the excitations have momenta which are integral multiples of $\Delta k = \frac{2\pi}{L}$, hence the counting of level n is the number of partitions of n into an even/odd number of distinct non-negative integers. The number of states at momenta $0, \Delta k, 2\Delta k, ...$ are as follows,[6]

$$\mu, \sigma : \qquad 1, 1, 1, 2, 2, 3, 4, 5, 6, 8, 10, 12, 15, 18, ... \tag{3.76a}$$

(Because the presence of the zero-momentum mode, the counting of the two **P** sectors are identical.)

In the antiperiodic sectors the excitations have momenta which are integer-plus-half multiples of Δk, or in other words, twice the momentum is always an odd multiple of Δk. Hence in the $\mathbb{1}$ sector the counting of level n is given by the partitions

[6]The sequence (3.76a) is given at oeis.org/A000009.

of $2n$ into positive odd integers. [7]

$$\mathbb{1}: \qquad 1,0,1,1,2,2,3,3,5,5,7,8,11,12,... \tag{3.76b}$$

The same definition also hold for the χ sector, with counting as follows,[8]

$$\chi: \qquad 1,1,1,1,2,2,3,4,5,6,8,9,12,... \tag{3.76c}$$

Note that since there are an odd number of excitations, the lowest energy state is $|\chi\rangle = \chi_{1/2}|\mathbb{1}\rangle$ with momentum $\frac{1}{2}\Delta k$. The counting in this sector corresponds to the number of states at momenta $\frac{1}{2}\Delta k, \frac{3}{2}\Delta k, \frac{5}{2}\Delta k, ...$

Combined with the chiral boson, the counting of the Moore-Read edge spectra are[134][9]

$$\mathbb{1}: \qquad 1,1,3,5,10,16,28,43,70,..., \tag{3.77a}$$

$$\chi: \qquad 1,2,4,7,13,21,35,55,86,..., \tag{3.77b}$$

$$\mu,\sigma: \qquad 1,2,4,8,14,24,40,64,100,.... \tag{3.77c}$$

(Again, in the χ sector, the momenta are shifted by $\frac{1}{2}\Delta k$.) Figure 3.11 shows the orbital and real-space cut of the $q = 2$ MR state giving the $\mathbb{1}$ sector.

Notice that in the **AP** case, the Majorana sector alternates between $\mathbb{1}$ and χ sectors whenever an orbital is filled (see Fig. 3.10). Hence the entanglement spectrum with different charges would also alternate between the countings (3.77a) and (3.77b), shown clearly in Fig. 3.11. Figure 3.12 shows the relative entanglement energies of $q = 2$ MR state at the $N = \pm q$ charge sectors, contrast this to the $N = 0$ sector of Fig. 3.9.

3.12 Appendix E. Evaluation of $\mathcal{Q}$-matrices for Laughlin and Moore-Read quasiholes

Evaluation of the Q-matrices for the Laughlin state can be done in a similar manner to the bulk B-matrices, but omitting the contour integration:

$$Q_{P,N;P',N'} = \delta_{N-N',1}\,(sw)^{\frac{N+N'}{2q}}\langle P|e^{i\phi'(w)/\sqrt{q}}|P'\rangle \tag{3.78}$$

[7] The fact that we require an even number of integers in the partition is automatically enforced. The sequence (3.76b) is given at oeis.org/A069910.

[8] The sequence (3.76c) is given at oeis.org/A069911.

[9] The sequence (3.77c) is given at oeis.org/A015128. The sequences (3.77a) and (3.77b) interlaced together is given at oeis.org/A006950.

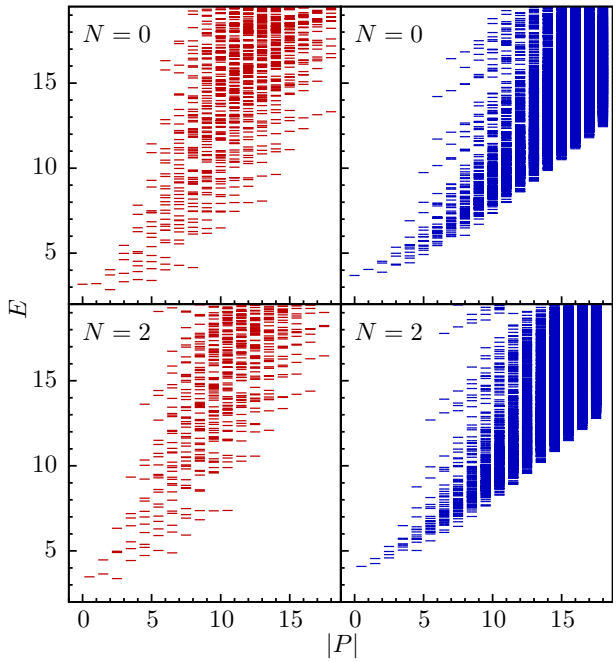

Figure 3.11: The entanglement spectra of the $q = 2$ Moore-Read state at $L = 25\ell_B$, with the orbital (left) and real-space (right) cut, in the $N = 0$ (top) and $N = 2$ (bottom) charge sectors. In the orbital case, the cut takes place on the bond with $|\mathbb{1}\rangle$ Majorana and $N = 0$ boson state in the thin torus limit (*cf.* Fig. 3.10). The real-space cut takes place at the τ centered on that bond. For $N = 0$, the counting of the states are 1, 1, 3, 5, 10, 16, *etc*, while for $N = 2$, the counting are 1, 2, 4, 7, 13, *etc*.

where $w = e^{-\frac{2\pi i}{L}\eta_x}$ and $s = \pm 1$ for bosons or fermions respectively. Note that the momentum is no longer conserved.

The Moore-Read case is more complex. In the context of the Majorana CFT, the Ising order and disorder fields σ, μ are 'twist' fields, interpolating between **AP** and **P** periodic bc's. We take the point of view that the fields σ and μ have fixed fermion parity $+1$ and -1 respectively. The resulting fusion rules are

$$[\sigma][\sigma] = [\mu][\mu] = [\chi][\chi] = [\mathbb{1}], \tag{3.79a}$$

$$[\mu][\sigma] = \chi, \ [\mu][\chi] = [\sigma], \ [\sigma][\chi] = [\mu]. \tag{3.79b}$$

In this approach, there are *two* possible quasihole insertions, $\sigma(\eta)e^{i\phi/\sqrt{q}}$, and $\mu(\eta)e^{i\phi/\sqrt{q}}$. As $\chi_0\sigma \sim \mu$, this is a direct realization of the picture in which each vortex has a Majorana zero-mode. The non-trivial vector space of quasihole excitations arises from

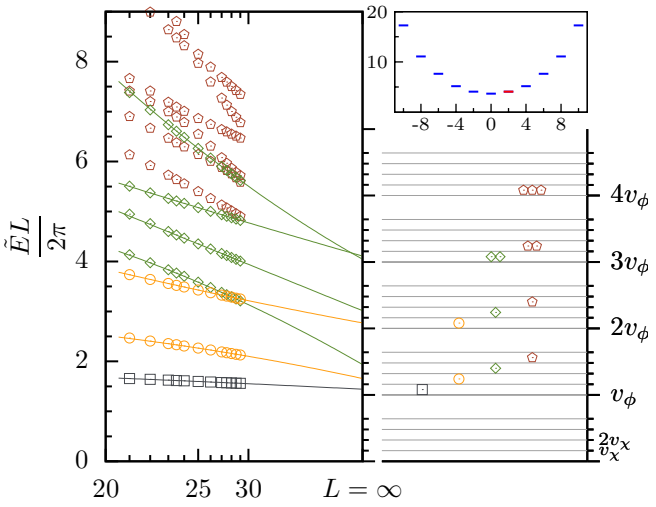

Figure 3.12

the freedom of choosing σ or μ, subject to the constraint that they fuse properly to the vacuum.

Fortunately the techniques for evaluating matrix elements of the type

$$\sigma_{P_\chi,P'_\chi} = \langle P_\chi|\sigma(0)|P'_\chi\rangle \tag{3.80}$$

have already been developed in the 'truncated-fermionic-space-approach' to the perturbed Ising CFT.[142]

Consider, for example, the **AP** to **P** case. Arbitrary states can be built by acting with the modes χ_{-n}, so without loss of generality we consider the matrix element

$$\langle\sigma| \prod_{\{m_i\in P_\chi\}} \chi_{m_i}\sigma(\eta) \prod_{\{n_i\in P'_\chi\}} \chi_{-n_i}|\mathbb{1}\rangle. \tag{3.81}$$

The chief technical result of Ref. [142] Eqs. 2.9-2.13 is that there exists an easily computed matrix $C(\eta)$ such that

$$\langle\sigma|\cdots\chi_m\sigma(\eta)\cdots|\mathbb{1}\rangle = \langle\sigma|\cdots\sigma(\eta)C_{mn}(\eta)\chi_n\cdots|\mathbb{1}\rangle. \tag{3.82}$$

After commuting all χ across the insertion, the Majoranas are brought to normal ordered form, reducing the problem to Wick contractions and the matrix elements

$$\langle\sigma|\sigma|\mathbb{1}\rangle = C_{\sigma\sigma 1} \tag{3.83a}$$

$$\langle\sigma|\mu|\chi\rangle = C_{\sigma\mu\chi} \quad etc. \tag{3.83b}$$

We have not as of yet implement the MR quasiholes numerically, which would be a worthwhile check given the subtleties of this case.

Chapter 4

Exact Matrix Product States for Quantum Spin Liquids and BCS Superconductors

4.1 Introduction

The parton construction [7, 132] allows for a mean field description of spin systems. While a mean field theory is usually only capable of describing ordered (symmetry broken) phases, remarkably the parton construction provides a mean field theory of *spin liquids*, which lack any order parameter.[132] The particular parton approach considered here constructs a spin-1/2 from spin-1/2 fermions by substituting

$$\mathbf{S}_x \Rightarrow f^\dagger_{x,\sigma} \mathbf{S}_{\sigma\rho} f_{x,\rho} \tag{4.1}$$

and restricting the fermions to an occupation of one per site, $\sum_\sigma n_{x,\sigma} = 1$. After this substitution, the Hamiltonian is quartic in fermions, so isn't any easier to solve exactly than the original spin system. However, we can try treating the fermions using a (free) mean field Hamiltonian. A mean field Hamiltonian introduces fluctuations in $\sum_\sigma n_{x,\sigma}$, so to get back a sensible spin wave function $|\Psi\rangle$ we must Gutzwiller project the mean-field fermion wavefunction $|\mathrm{MF}\rangle$:

$$\langle\{\sigma\}|\Psi\rangle = \Psi[\sigma_x] = \langle 0| \prod_x f_{x,\sigma_x} |\mathrm{MF}\rangle. \tag{4.2}$$

The resulting wavefunctions can be treated as a variational class parameterized by the mean-field Hamiltonian. After Gutzwiller projection, the states are no longer free, and computing their microscopic properties is non-trivial.

There are two reasons tensor network representations of parton states would be useful. First, one can use tensor network methods to efficiently evaluate variational energies (usually done using variational Monte-Carlo) in order to estimate gaps, obtain length scales, or other microscopic details. Second (and more importantly), the 'model' tensor networks can be use to initialize DMRG and its higher dimensional generalizations. The reliability of the current algorithms for finding the tensor network representation of a 2D ground-state is *much* more suspect than in 1D. Among other reasons, tensor networks can have qualitatively different structures depending on the patterns of entanglement; for example their auxiliary bonds may develop gauge symmetries, projective representations of the physical symmetries, etc. Since the existing algorithms are iterative and local, it is reasonable (and currently an open question!) to suspect that the existing algorithms can get stuck in metastable states if the initial guess has an incompatible entanglement structure. These metastability issues could be examined in detail if the algorithm can be initialized by a representative in each topological class; the parton states serve this purpose perfectly.

The special case of free-fermion states with a nearest neighbor pairing function has been discussed elsewhere.[39] In this Chapter I consider MPS representations for arbitrary states, even though the relevant states are in 2D and higher. For a state on a 2D cylinder, we can always turn it into a 1D system by choosing an ordering of sites (the 'snake'). Despite the ugliness of this procedure, currently the most competetive tensor network approach for 2D systems is currently DMRG on cylinders.[112] Finding the optimal 2D tensor network is a very interesting (and more difficult) item for future study.

The particular class of spin liquids I will consider here are the gapped, $\mathbb{Z}_2$-spin liquids. The topological order of these models is $\mathbb{Z}_2$ gauge theory, where the 'electric charges' carry spin-1/2 and are called spinons. The parton construction for these states is a Gutzwiller projected BCS wave function:

$$|\Psi\rangle = \langle \mathcal{P}|\mathrm{MF}\rangle = \langle \mathcal{P} e^{\frac{1}{2}\sum c^\dagger G c^\dagger}|0\rangle. \tag{4.3}$$

Here $c^\dagger$ denotes a vector of creation operators for the single-particle states, and G is an anti-symmetric matrix, the pairing function (I suppress indices). The Gutzwiller projection

$$\langle \mathcal{P} = \langle 0| \prod_i f_{i\sigma_i} |\mathrm{MF}\rangle. \tag{4.4}$$

is an on-site isometry, so is trivial to apply once given an MPS for $|\mathrm{MF}\rangle$ (as it is on-site).

This bring us to our main question: how do we obtain an MPS for $|\mathrm{MF}\rangle$?

4.2 General approach for finding an analytic MPS representation

Our central tool is what I will call a 'bipartition' of a state. Let $\mathcal{H} = \mathcal{H}_{L_i} \otimes \mathcal{H}_{R_i}$ be the division of the Hilbert space into the sites to the left/right of bond i. We have a rank χ_i 'bipartition' of Ψ if we can find χ_i states $\{|\eta\rangle_{L_i}\}, \{|\eta\rangle_{R_i}\}$, *not necessarily orthonormal*, such that

$$|\Psi\rangle = \sum_{\eta=1}^{\chi_i} |\eta\rangle_{L_i} \otimes |\eta\rangle_{R_i}. \tag{4.5}$$

This is similar to a Schmidt decomposition, but we have relaxed the requirement of orthonormality, and in fact the rank of the Schmidt decomposition is bounded from above by χ_i. Now suppose we have such a bipartition on each bond i. The Hilbert spaces of $\mathcal{H}_{R_i}, \mathcal{H}_{R_{i+1}}$ differ by the addition of one site (which I will call $i+1$), spanned by an orthornormal basis $|\xi\rangle_{i+1}$ of dimension d. There must be a recursion relation between the bases defined on each bond:

$$|\eta\rangle_{R_i} = \sum_{\xi=1}^{d} \sum_{\eta'=1}^{\chi_{i+1}} W^{\xi}_{\eta\eta'} |\xi\rangle_i |\eta'\rangle_{R_{i+1}}, \tag{4.6}$$

which defines the tensor W. If the state is translation invariant, with a unit-cell of 1, W defines an equivalent recursion on bond $i+1, i+2$, etc. So, repeating for $|\eta'\rangle_{R_{i+1}}$ ad infinitum, we obtain

$$|\Psi\rangle = \sum_{\{\xi_i\},\{\eta_i\}} \left[\cdots W^{\xi_i}_{\eta_{i-1}\eta_i} W^{\xi_{i+1}}_{\eta_i\eta_{i+1}} \cdots \right] |\cdots \xi_i \xi_{i+1} \cdots\rangle \tag{4.7}$$

where $|\cdots \xi_i \xi_{i+1} \cdots\rangle$ is a basis for the entire physical Hilbert space.

If there is a non-trivial unit cell of L, then there are L distinct recursions of the form Eq. (4.6), defining $W^{[n]}$ for $n = 1, \cdots L$, which are inserted periodically into Eq. (4.7)

In summary, our general plan of attack is to a) find a bipartition on each bond b) find the recursion relation W between the bipartitions. These W are the desired MPS.

4.3 MPS for BCS states

We assume the sites are given an ordering i, and each site contains arbitrary orbital degrees of freedom (such as spin). Because we're dealing with fermionic

states, I find it most natural to use the formalism of Grassmann tensor networks, which ensures the fermionic sign structure is handled properly. [60, 39] Our goal is to find an fermionic MPS representation for $|\mathrm{MF}\rangle$, with one matrix 'W' per site i.

For notational simplicity, we find an MPS for the coherent state wavefunction. Recall the coherent states are defined by $|\xi\rangle \equiv e^{\xi c^\dagger}|0\rangle$, where $\xi = (\xi_1, \xi_2, \cdots)$ is a vector of Grassmann numbers, one for each single-particle state. Actually - we let ξ_i denote all degrees of freedom on site i (such as spin), so it is itself a vector, but we will suppress these internal indices. The coherent wave function is

$$\Psi^\xi = \langle \xi | \mathrm{MF} \rangle = e^{\frac{1}{2}\sum \xi G \xi}. \tag{4.8}$$

and we want to find matrices W such that

$$\Psi^\xi = \sum_{\{n\}} \left[\cdots W^{\xi_1}_{n_0 n_1} W^{\xi_2}_{n_1 n_2} \cdots \right] \tag{4.9}$$

I'll use an indexing scheme in which bond i is to the right of site i. This coherent state rewriting is entirely trivial, you can always make the replacement $\xi_i \to c_i^\dagger$ within Ψ and let it act on the Fock vacuum.

Finding the bipartition

To find a bipartition, start at a bond i which cuts the system into halves L_i, R_i. The pairing function G (which is anti-symmetric) splits into sub matrices for the inter/intra-region pairing:

$$\xi G \xi = (\xi_{L_i}, \xi_{R_i}) \begin{pmatrix} G_{L_i} & G_{LR_i} \\ -G_{LR_i}^T & G_{R_i} \end{pmatrix} \begin{pmatrix} \xi_{L_i} \\ \xi_{R_i} \end{pmatrix} \tag{4.10}$$

Here ξ_{L_i} is a Grassmann basis for the left (and likewise for the right). We now SVD the inter-region pairing:

$$G_{LR_i} = \bar{V}_i S_i V_i \tag{4.11}$$

There is no relation between $V, \bar{V}$ absent other symmetries. The singular value decomposition isolates the degrees of freedom entangling the two edges:

$$\Psi^\xi = e^{\frac{1}{2}\xi_{L_i} G_{L_i} \xi_{L_i}} \; e^{\xi_{L_i} \bar{V}_i S_i V_i \xi_{R_i}} \; e^{\frac{1}{2}\xi_{R_i} G_{R_i} \xi_{R_i}} \tag{4.12}$$

$$e^{\xi_{L_i} \bar{V}_i S_i V_i \xi_{R_i}} = \prod_b (1 + \sum_{a,c} \xi_{L_i,a} \bar{V}_{i,ab} S_{i,b} V_{i,bc} \xi_{R_i,c}) \tag{4.13}$$

The Taylor expansion of Eq. (4.13) holds because the ξ are Grassmann numbers and $V, \bar{V}$ are unitary. For each state b in the SVD, upon expanding the exponential we obtain two contributions to the wave function, so if the rank of the SVD is $\dim(S_i) = N_i$ we have obtained a rank $\chi_i = 2^{N_i}$ bipartition of the state. Note, however, that the above is not precisely a Schmidt decomposition as the contributions need not be orthonormal.

The single particle states b of the SVD are a bit like the *single-particle* orbitals of the entanglement spectrum. Corresponding to these states b, let us introduce N_i complex Grassmann variables on each bond i, $\eta_i = (\eta_{i,1}, \cdots \eta_{i,N_i})$, $\bar{\eta}_i = (\bar{\eta}_{i,1}, \cdots \bar{\eta}_{i,N_i})$. We define a set of wave functions Ψ_{η_i} on the right and $\Psi_{\bar{\eta}_i}$ to the left by

$$\Psi_{\eta_i}^{\xi_{R_i}} = e^{\eta_i V_i \xi_{R_i} + \frac{1}{2}\xi_{R_i} G_{R_i} \xi_{R_i}} \tag{4.14}$$

$$\Psi_{\bar{\eta}_i}^{\xi_{L_i}} = e^{\xi_{L_i} \bar{V}_i \bar{\eta}_i + \frac{1}{2}\xi_{L_i} G_{L_i} \xi_{L_i}} \tag{4.15}$$

Using the rules of Grassmann integration, we obtain a bipartition:

$$\Psi^{\xi} = \int d\eta_i d\bar{\eta}_i \Psi_{\bar{\eta}_i}^{\xi_{L_i}} e^{\bar{\eta} S_i^{-1} \eta_i} \Psi_{\eta_i}^{\xi_{R_i}} \tag{4.16}$$

(strictly speaking there is a factor of $|S|$ here but it will be canceled later). While the Grassmann notation may be unfamiliar, the integration over N_i complex Grassmann variables is entirely equivalent to tensor contraction on the Hilbert space of an N_i-particle fermion system, with dimension 2^{N_i}, which enumerate the 2^{N_i} terms in Eqn. (4.13). Compared to our earlier discussion, Eq.(4.5), we have weighted the sum with the diagonal factor S, but this could be absorbed into either the left or right so doesn't change the required structure.

Finding the recursion

Now consider two bonds $i, j = i+1$. There must exist a tensor $\Gamma_{\eta_i, \bar{\eta}_j}^{\xi_i}$ which relates the basis defined on bonds i, j, which differ by the addition of site ξ_j:

$$\Psi_{\eta_i}^{\xi_{R_i}} = \int d\bar{\eta}_j d\eta_j \Gamma_{\eta_i \bar{\eta}_j}^{\xi_j} e^{\bar{\eta}_j S_j^{-1} \eta_j} \Psi_{\eta_j}^{\xi_{R_j}}. \tag{4.17}$$

By repeating Eqn.(4.17), we will obtain an fermionic MPS of the form

$$\Psi^{\xi} = \int \mathcal{D}[\eta, \bar{\eta}] \cdots \Gamma_{\eta_{-1} \bar{\eta}_0}^{\xi_0} e^{\bar{\eta}_0 S_0^{-1} \eta_0} \Gamma_{\eta_0 \bar{\eta}_1}^{\xi_1} e^{\bar{\eta}_1 S_1^{-1} \eta_1} \Gamma_{\eta_1 \bar{\eta}_2}^{\xi_2} \cdots \tag{4.18}$$

which I will later rewrite in the usual MPS form.

To find Γ, we isolate the contribution of site $i+1=j$, using $\xi_{R_i}=(\xi_j,\xi_{R_j})$, $\xi_{L_j}=(\xi_j,\xi_{L_i})$:

$$\eta_i V_i \xi_{R_i} = \eta_i C_j \xi_j + \eta_i Y_j \xi_{R_j}, \qquad V_i = \left(\begin{array}{c|c} C_j & Y_j \end{array}\right) \tag{4.19}$$

$$\xi_{L_j} \bar{V}_j \bar{\eta}_j = \xi_j B_j \bar{\eta}_j + \xi_{L_i} \bar{Y}_j \bar{\eta}_j, \qquad \bar{V}_j = \left(\begin{array}{c} B_j \\ \hline \bar{Y}_j \end{array}\right) \tag{4.20}$$

$$\xi_{R_i} G_{R_i} \xi_{R_i} = \xi_j D_j \xi_j + 2\xi_j T_j \xi_{R_j} + \xi_{R_j} G_{R_j} \xi_{R_j}, \qquad G_{R_i} = \left(\begin{array}{c|c} D_j & T_j \\ \hline -T_j^T & G_{R_j} \end{array}\right) \tag{4.21}$$

From the above data we define

$$A_j \equiv Y_j V_j^\dagger S_j^{-1} = S_i^{-1} \bar{V}_i^\dagger \bar{Y}_j \tag{4.22}$$

Then substituting these definitions into Eqn. (4.17), we find:

$$\Gamma^{\xi_j}_{\eta_i \bar{\eta}_j} = \exp\left[\eta_i A_j \bar{\eta}_j + \xi_j B_j \bar{\eta}_j + \eta_i C_j \xi_j + \tfrac{1}{2}\xi_j D_j \xi_j\right] \tag{4.23}$$

Combined with the the diagonal operator $e^{\bar{\eta} S_i^{-1} \eta_i}$ on each bond, these Γ make up the fermionic MPS. I will obtain the explicit matrix elements for $W \sim \Gamma e^S$ later.

4.4 Non-optimal truncation and relation to Hankel SVD and control theory

If the rank of the singular value decomposition is $N_i = \mathrm{rank}(S_i)$, the required MPS bond dimension is $m_i = 2^{N_i}$. For a generic pairing function, $N_i = \infty$. So some form of truncation is necessary.

The optimal approximation would be to find the Schmidt spectrum and drop the high lying states - we return to this shortly. In the meantime, suppose G is very small; then, to lowest order in G, Eq. (4.13) is a Schmidt decomposition, so we expect for a gapped system S will fall off rapidly (depending on the circumference of the system), and a good approximation is obtained by keeping the most significant

singular values. This corresponds to dropping the corresponding rows and columns of A, B, C, D, reducing the rank of Γ.

For a translation invariant system, the approximation obtained by keeping the most significant S is related to a technique in control theory. When the system is translation invariant, the pairing function has the form $G_{ij} = G(i-j)$. Each $G(i-j)$ is a $p \times p$ matrix in the internal space of sites i, j. We can view this sequence as a signal in time $t = i - j$ and ask what 'state space system' (see Wikipedia) gives an optimal approximation to the $p \times p$ signal $G(t)$. A state space system represents a linear system with inputs and outputs (like a first order ODE or its discrete generalization) through a set of matrices denoted (A, B, C, D). For a rank-N system, A is a $N \times N$ matrix, B is a $p \times N$ matrix, C is $N \times p$, and D is $p \times p$. We want the signal G to be the Green's function for the linear system, which is given by

$$G(t) = \theta(t > 0) B A^{t-1} C + D\delta_{t=0} \tag{4.24}$$

For a generic G, we might need a system of infinite rank, so we can instead look for the optimal rank-N approximation. For a particular definition of optimal (defined by the 'Hankel norm'), the solution is given by a technique called balanced model reduction. [61] The intra-region pairing is a *Hankel matrix*, $G_{LR,ij} \equiv G(i + j)$. The SVD of a Hankel matrix determines the 'Hankel singular values,' which we have called S. It turns out that the optimal (A, B, C, D) spit out by balanced model reduction is *precisely* the (A, B, C, D) defined in Eq. (4.23) for Γ, after a) truncating to the N rows and columns corresponding to the most significant Hankel singular values S; b) rescaling rows and columns to incorporate S into (A, B, C, D).

So apparently the MPS approximation to a BCS states is closely related to applying balanced model reduction to the pairing function $G(i-j)$. To my knowledge, there is no (developed) generalization of balanced model reduction to a '2D signal' - this would be worth pursuing.

For *strong-pairing* phases (short ranged G) it appears that the Hankel singular values S are in indeed *very* close to the true single-body entanglement eigenvalues. Hence, in addition to keeping only a finite number of the S (equivalent to truncating the single-particle entanglement Hilbert space), one should further perform a truncation in the *many-body* entanglement space, with weights approximately proportional to by

$$e^{-E_{\{n_\beta\}}} \sim e^{-\sum_\beta E_\beta n_\beta} = \prod_\beta (S_\beta)^{2n_\beta}. \tag{4.25}$$

For *weak-pairing* phases, G is long ranged: $\lim_{r\to\infty} G(r) \neq 0$. This can lead to topological Majorana modes at the boundary. Numerically one has to treat this special case carefully.

4.5 Converting the fMPS to the usual bosonic MPS matrices.

We've written the MPS in a fancy, obfuscating Grassmann notation, but all can be converted to a bosonic MPS for the Jordan-Wigner representation of the fermions. Recall that any Grassmann tensor in N Grassmann variables γ_a can be written as usual rank-N tensor of total size 2^N via Taylor expansion:

$$M[\gamma_1, \gamma_2, \cdots, \gamma_N] = \sum_{\{n_a\}} M_{n_1,n_2,\cdots} \prod_{a=1}^{N} \gamma_a^{n_a}, \quad n_a \in \{0,1\} \tag{4.26}$$

Note that changing the order of expansion for the indices $a = 1, \cdots$ will change the sign structure. The rules for Grassmann integration are $\int d\eta\, \eta = 1, \int d\eta = 0$. So for a single variable,

$$\int d\gamma d\bar{\gamma} A_{\bar{\gamma}} e^{\bar{\gamma}\gamma} B_\gamma = \sum_{n,\bar{n}=0}^{1} A_{\bar{n}} B_n \int d\gamma d\bar{\gamma}\, \bar{\gamma}^{\bar{n}} (1 + \bar{\gamma}\gamma) \gamma^n \tag{4.27}$$

$$= \sum_{n=0}^{1} A_n B_n \tag{4.28}$$

Now for several variables, let us choose our expansion to run in opposing orders, so that

$$\int d\gamma d\bar{\gamma} A_{\bar{\gamma}} B_\gamma = \sum_{\{n\},\{\bar{n}\}} A_{\bar{n}_N,\cdots,\bar{n}_1} B_{n_1,\cdots,n_N} \bar{\gamma}_N^{n_N} \cdots \bar{\gamma}_1^{n_1} e^{\bar{\gamma}\gamma} \gamma_1^{n_1} \cdots \gamma_N^{n_B} \tag{4.29}$$

$$= \sum_{\{n\}} A_{\{n\}} B_{\{n\}} \tag{4.30}$$

This is the usual tensor contraction over a fermionic Hilbert space of dimension 2^N.

So to put the fMPS on a computer, we need to calculate this expansion for Γ. The key equation is

$$e^{\frac{1}{2}\gamma H \gamma} = \sum_{\{n_a\}} \mathrm{Pf}(H|_{n_a}) \prod_a \gamma_a^{n_a} \tag{4.31}$$

where $H|_{n_a}$ is a matrix formed from H by keeping all rows and columns for which $n_a = 1$ and Pf is the Pfaffian. Note that it is *very* important that if the rows/columns of H are ordered $a = 1, 2, \cdots$, then $\prod_a \gamma_a^{n_a} = \gamma_1^{n_1} \gamma_2^{n_2} \cdots$. As far as I can tell, these 2^N

coefficients can be computed in a *total* time of $\mathcal{O}(N2^N)$ using the recursive properties of the Pfaffian.

Carefully consideration of the Grassmann integrals in the fMPS, Eq. (4.18), reveals it is very important that we compute the expansion (4.31) for the ordering

$$\gamma = (\eta_i, \xi_j, \bar{\eta}_j) = (\eta_{i,1}, \cdots, \eta_{i,N_i}, \xi_{j,1}, \cdots, \xi_{j,d_j}, \bar{\eta}_{N_j}, \cdots, \bar{\eta}_1). \tag{4.32}$$

Note the $\bar{\eta}$ are inverted compared to η. Applying Eqn. (4.31) to Γ,

$$\Gamma = e^{\frac{1}{2}(\eta_i,\xi_j,\bar{\eta}_j)H(\eta_i,\xi_j,\bar{\eta}_j)}, \quad H = \begin{pmatrix} 0 & C & A \\ -C^T & D_j & B \\ -A^T & -B^T & 0 \end{pmatrix} \tag{4.33}$$

we obtain a rank-3 tensor $\Gamma^{m_j}_{n_i,\bar{n}_j}$, where m_j is the physical occupation index. Likewise, on the bonds we define

$$s_{\bar{n}_j,n_j} = \delta_{\bar{n}_j,n_j} \prod_b (S_{j,b})^{n_{j,b}}. \tag{4.34}$$

Then

$$W^{m_j}_{n_{j-1},n_j} = \Gamma^{m_j}_{n_i,n_j} \prod_b (S_{j,b})^{n_{j,b}} \tag{4.35}$$

are the bosonic matrices of the MPS in the Jordan-Wigner transformed occupation basis $\{m_j\}$.

4.6 Simplification for S= 1/2 Gutzwiller projection.

The pairing ansatz for a $\mathcal{T}$ and SU(2) symmetric BCS state is

$$|\mathrm{MF}\rangle = e^{\sum_{i,j} c^\dagger_{i\uparrow} g_{ij} c^\dagger_{i\downarrow}} \tag{4.36}$$

$$G = g \otimes i\sigma^y \tag{4.37}$$

with g real symmetric. Since the system has a tensor product structure between site and spin, we define from the lowercase g the same data as in Eqn.(4.17), all denoted

in lowercase. We have

$$G_{LR} = \bar{v}sv \otimes \sigma^z\sigma^x \tag{4.38}$$
$$S = s \otimes \mathbb{1} \tag{4.39}$$
$$D = g_{jj} \otimes i\sigma^y \tag{4.40}$$
$$C = c \otimes \sigma^x \tag{4.41}$$
$$B = b \otimes \sigma^z \tag{4.42}$$
$$A = a \otimes \mathbb{1} \tag{4.43}$$

4.7 Optimal approximation

Finally we briefly discuss the problem of finding the optimal truncation, which requires us to compute the Schmidt spectrum. While this is in some sense 'trivial' since the state is free, the standard algorithm requires inverting a matrix the size of the system. [128, 81] We want an algorithm that works in the thermodynamic limit. The key is to find the Gram matrix which encodes the non-orthonomality of the bipartition $|\eta\rangle_{L/R}$ in Eq. (4.5). Defining Gram matrices for the left / right of the by $X^{L/R}_{\bar{\alpha},\alpha} = \langle\bar{\alpha}|\alpha\rangle_{L/R}$, we can verify that the entanglement Hamiltonian H_E is isospectral to $e^{-H_E} \sim \sqrt{X^L}X^R\sqrt{X^L}$. Hence if we can compute the X, we can recover the entanglement spectrum and hence the optimal basis in which to truncate the MPS.

For simplicity, we will consider only the case when $D = 0$, and assume a unit cell of 1. To calculate the Gram matrix, we calculate the overlap of Γ matrices on a single site,

$$\int d\bar{\xi}d\xi\bar{\Gamma}^{\bar{\xi}}_{\bar{\alpha}\bar{\beta}}e^{-\bar{\xi}\xi}\Gamma^{\xi}_{\alpha\beta}, \quad \bar{J} = \alpha C + \beta B^T, J = \bar{\alpha}C^* + \bar{\beta}B^\dagger \tag{4.44}$$
$$= \int d\bar{\xi}d\xi \exp\left[\alpha A\beta + \bar{\alpha}A^*\bar{\beta} + \bar{J}\xi + J\bar{\xi} - \bar{\xi}\xi\right] \tag{4.45}$$
$$= \exp\left[\alpha A\beta + \bar{\alpha}A^*\bar{\beta} - (\alpha C + \beta B^T)(C^\dagger\bar{\alpha} + B^*\bar{\beta})\right] \tag{4.46}$$

Now we wish to treat entries $r = (\alpha, \bar{\alpha})$ as a row in $N+N$ dimensional Hilbert space, and $c = (\beta, \bar{\beta})$ as a column. The overlap takes the general form

$$\bar{\Gamma}.\Gamma = \exp\left[-\alpha CC^\dagger\bar{\alpha}\right]\exp\left[\begin{pmatrix} \alpha & \bar{\alpha} \end{pmatrix}\begin{pmatrix} A & -CB^* \\ C^*B & A^* \end{pmatrix}\begin{pmatrix} \beta \\ \bar{\beta} \end{pmatrix}\right]\exp\left[-\beta B^T B^*\bar{\beta}\right] \tag{4.47}$$

The full MPS is a combination of Γ with the diagonal bond contribution S. We can rescale fields all fields by $\eta \to \sqrt{S}\eta$, taking $A \to \sqrt{S}A\sqrt{S}, B \to B\sqrt{S}, C \to \sqrt{S}C$. Then, after this rescaling,

$$T_{\alpha\bar{\alpha};\beta\bar{\beta}} = (\bar{W}.W)_{\alpha\bar{\alpha};\beta\bar{\beta}} = \exp\left[-\alpha CC^\dagger\bar{\alpha}\right] \exp\left[\begin{pmatrix} \alpha & \bar{\alpha} \end{pmatrix} \begin{pmatrix} A & -CB^* \\ C^*B & A^* \end{pmatrix} \begin{pmatrix} \beta \\ \bar{\beta} \end{pmatrix}\right] \exp\left[-\beta B^T B^* \bar{\beta}\right] \tag{4.48}$$

is the *transfer matrix* of the MPS. The left / right dominant eigenvectors of T are the Gram matrices $X^{L/R}$, from which we can find the entanglement spectrum and optimal MPS truncation.

4.8 Conclusion

I have proposed a method to obtain MPS for a variety of quantum spin liquids and BCS superconductors. This result can be extended to bosonic parton states as well as fermionic band insulators (as would be relevant to the chiral-spin liquid phase). In the future, it will be useful to work out the most efficient representation in terms of 2D tensor networks, which may shed light on the behavior of realistic 2D tensor networks and their optimization.

Chapter 5

Exact and good enough Matrix Product Operators for time evolving long range Hamiltonians

5.1 Introduction

The ability to study dynamical properties in and out of equilibrium is essential for understanding the physics of strongly interacting systems. Following the success of the density-matrix renormalization group (DMRG) for finding one-dimensional (1D) ground states [137], a number of closely related techniques have been developed to explore the dynamical properties of short-ranged 1D systems [127, 138, 24, 96, 53]. This exciting development has given access to experimentally relevant observables, such as dynamical correlation functions which can be compared with data from neutron scattering and ultracold atomic gasses, and non-equilibrium dynamics, providing insight into long standing questions about thermalization [97]. Simultaneously, large-scale DMRG has begun to study ground-state properties of quasi-two dimensional (2D) quantum systems, such as strips and cylinders, allowing one to probe much larger systems than accessible to exact diagonalization [112]. For example, DMRG studies provide solid evidence for the existence of a spin-liquid ground state in the $S = 1/2$ kagome antiferromagnet [140, 25]. The 2D-DMRG method orders the sites of a 2D lattice into a 1D chain with long-ranged interactions; truly 2D tensor network methods may eventually supplant this approach [54, 21], but 2D-DMRG is currently a standard tool due to its reliability.

It is desirable to combine these two developments in order to evaluate dynamical properties of quasi-2D systems (e.g., the time evolution of bosons in a 2D optical trap

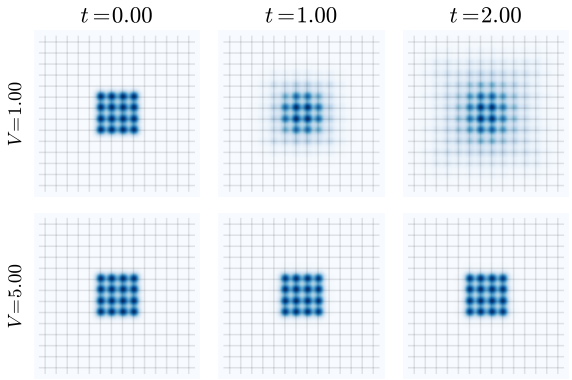

Figure 5.1: Quasi-exact time evolution of interacting hard-core bosons in a 14×14 lattice trap. The bosons hop with bandwidth $t = 1$ and interact with nearest-neighbor repulsion V. 16 bosons begin in an un-entangled product state, and evolve in time from left to right. In the top row, $V = 1$, and the bosons expand outward. In the bottom row, $t < V = 5$, the bosons remain trapped in a bound state due to the strong interactions. A similar effect has been observed experimentally in cold-atom optical lattices [139, 95].

as shown in Fig. 5.1). However, the existing DMRG-based time-evolution methods cannot be easily applied to a quasi-2D system. This is mainly due to the long-ranged interactions that occur when representing a 2D system as a 1D chain; a similar difficulty exists for 1D systems with power-law Coulombic and dipolar interactions.

In this work we address this problem by providing a method to time-evolve long-ranged Hamiltonians. The unique advantage of the method is that it simultaneously (a) can be applied to any long-ranged Hamiltonian while preserving all symmetries, (b) has a constant error per site in the thermodynamic limit at fixed computational effort, (c) can be applied to an infinitely long system assuming translation invariance and (d) can be easily implemented using standard DMRG methods.

Like other 1D methods, we work in the framework of matrix product states (MPSs) [31, 75, 94], a variational ansatz for finitely entangled states within which we wish to simulate the full many-body dynamics.The structure of an MPS can be generalized to operators, called matrix product operators (MPOs) [124]. An MPO can be efficiently applied to an MPS using standard methods [82, 111, 97]. If a long-ranged Hamiltonian H has a compact MPO approximation for e^{tH}, then the time evolution can be efficiently simulated by successively applying the MPO to the MPS. The most naive time-stepper, an Euler step $1 + tH$, as well as its Runge-Kutta [32] and Krylov [96, 55, 131] improvements, indeed have an efficient MPO representation.

But these global methods have an error per *site* which diverges with the system size L, for example as $\mathcal{O}(Lt^2)$ for the Euler step, which eventually renders them impractical as $L \to \infty$. For certain simple H, such as a nearest neighbor interactions or a sum of commuting terms[82], a compact MPO with *finite* error per site exists, which is the basis behind the highly successful time evolving block decimation (TEBD) [127] and tDMRG [24, 138]. However, these methods do not generalize well for long-ranged Hamiltonians, which is the focus of this work.

The basic insight of this work is that a Hamiltonian which is expressed as a sum of terms $H = \sum_x H_x$ admits a *local* version of a Runge-Kutta step; for instance we could improve the Euler step by taking

$$1 + t\sum_x H_x \to \prod_x (1 + tH_x). \tag{5.1}$$

The error is still at $\mathcal{O}(t^2)$, so it is formally a 1^{st}-order time stepper. But any set of distant regions all receive the correct 1^{st}-order step in parallel. Hence, in contrast to the naive Euler step, the total error scales as Lt^2, rather than as L^2t^2. The main result of this work is that an improved version of Eq. (5.1) has a very compact MPO representation which can easily be extended to higher-order approximations in $\mathcal{O}(t^p)$.

In Fig. 5.2, we compare the accuracy of the methods proposed here, called W^{I} and W^{II}, against TEBD and global 2^{nd} order Runge-Kutta. TEBD works for short-ranged Hamiltonians, so we compare by quenching from product states into the spin-1/2 nearest-neighbor Heisenberg chain, where a high order TEBD calculation serves as a quasi-exact reference. Runge-Kutta is orders of magnitude less accurate, with an error that scales as L^5 compared to L for TEBD and $W^{I/II}$. Both TEBD and $W^{I/II}$ are comparable in accuracy; for evolution starting from a Neel state, W^{II} is slightly more accurate than TEBD, while from a random state TEBD is more accurate. Any such difference can be easily mitigated by a small decrease in time step. But unlike TEBD, $W^{I/II}$ can be immediately applied to a long-ranged problem without a Trotter decomposition.

To our knowledge, the other existing method which can time-evolve long-ranged interactions with a constant error per site is the recently developed time dependent variation principle (TDVP), which projects the exact Schrödinger equation into the MPS variational space and numerically integrates the resulting equations [40, 26]. While the method has yet to be applied to quasi-2D systems, a version was successfully applied to the long-ranged transverse field Ising model [50]. However, in contrast to the proposal here, which involves the standard tensor network technique of applying an MPO, the TDVP requires one to implement an entirely distinct and relatively complex set of algorithms. It will be a useful subject for future work to make a detailed comparison between TDVP and the present MPO approach.

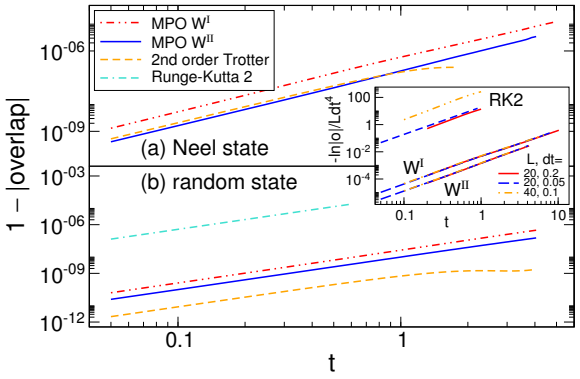

Figure 5.2: Comparison of 2^{nd}-order MPOs W^{I}, W^{II}, TEBD, and global Runge-Kutta for the spin-1/2 Heisenberg chain. 4^{th}-order TEBD serves as a quasi-exact reference for calculating errors. Panels (a), (b) show quenches starting from a $L = 20$ Neel state and random state respectively. In the inset, we show the scaling of the errors for system sizes $L = 20, 40$. For $W^{I/II}$ we find perfect collapse to the expected scaling Lt^4, as the error per site remains constant in the thermodynamic limit. In contrast, for global Runge-Kutta the error increases as L^5t^4.

The first application presented here is a calculation of a dynamical correlation function of the Haldane-Shastry spin chain, which is a 1D spin-half antiferromagnet with power-law long-ranged interactions [41, 102]. Our numerical simulations agree with the analytic exact results [44] up to long times, which serves as a check of the method's accuracy , and show a ballistic spreading of correlations consistent with the model's integrability. The second application is the simulation of dynamics in a 2D Bose-Hubbard model. Here we focus on a class of experiments with ultracold atomic gases that study expansion of a cloud that is initially confined to a small region of the lattice [139, 95]. The main qualitative surprise in the experiments is that even repulsive interactions can lead to self-trapped states, which is reproduced in our model calculation along with several other features, shown in Fig 5.1. We will further elaborate on these applications later.

5.2 Matrix product operators

In order to understand our main result, we review some basic facts regarding MPOs. An operator Z acting on a 1D chain with physical sites labeled by i has an MPO representation

$$Z = \cdots \hat{W}_{(1)}\hat{W}_{(2)}\hat{W}_{(3)} \cdots \tag{5.2}$$

where each $\hat{W}_{(i)}$ is a matrix of operators acting on the Hilbert space of site-i (with physical indicides m_i, m_i'),

$$[\hat{W}_{(i)}]_{a_{i-1}a_i} = \sum_{m_i,m_i'} [W_{(i)}]^{m_i m_i'}_{a_{i-1}a_i} |m_i\rangle\langle m_i'|, \tag{5.3}$$

with $[W_{(i)}]^{m_i m_i'}_{a_{i-1}a_i} \in \mathbb{C}$. In Eq. (5.2), the matrices are contracted by summing over all indices $a_i = 1, \ldots, \chi_i$. These indices live in the space between sites $(i, i+1)$, which refer to as a *bond*. The χ_is are called the MPO bond dimensions, and they denote the size of the $\hat{W}$ matrices. Several algorithms have been developed for efficiently applying an MPO to an MPS, with effort of either $\mathcal{O}(\chi^2)$ or $\mathcal{O}(\chi^3)$ [82, 111, 97].

Two classes are of interest to us; sums of local operators (such as a Hamiltonian), and exponentials of such sums (evolution operators). We first review the structure of the former. For the bond between sites $(i, i+1)$ that divides the system into regions L_i and R_i, any Hamiltonian H can be decomposed as

$$H = H_{L_i} \otimes \mathbb{1}_{R_i} + \mathbb{1}_{L_i} \otimes H_{R_i} + \sum_{a_i=1}^{N_i} h_{L_i,a_i} \otimes h_{R_i,a_i}. \tag{5.4}$$

Here H_{L_i/R_i} are the components of the Hamiltonian localized purely to the left/right of the bond, while the $h_{L_i,a_i} \otimes h_{R_i,a_i}$ run over N_i interaction terms which cross the bond. There is a recursion between the decompositions on bond $(i-1, i)$ and $(i, i+1)$, which differ by the addition of site i:

$$\begin{pmatrix} H_{R_{i-1}} \\ h_{R_{i-1},a_{i-1}} \\ \mathbb{1}_{R_{i-1}} \end{pmatrix} = \begin{matrix} 1 \\ N_{i-1} \\ 1 \end{matrix} \overset{\begin{matrix} 1 & N_i & 1 \end{matrix}}{\begin{pmatrix} \hat{\mathbb{1}} & \hat{C} & \hat{D} \\ 0 & \hat{A} & \hat{B} \\ 0 & 0 & \hat{\mathbb{1}} \end{pmatrix}_{(i)}} \otimes \begin{pmatrix} H_{R_i} \\ h_{R_i,a_i} \\ \mathbb{1}_{R_i} \end{pmatrix}. \tag{5.5}$$

Here $(\hat{A}, \hat{B}, \hat{C}, \hat{D})_{(i)}$ are matrices of operators acting on site i, with dimensions indicated on the border. This recursion is in fact the MPO: the block matrix in the middle is $\hat{W}_{(i)}$, with size $\chi_i = N_i + 2$. (See App. 5.6 for explicit examples of MPOs.) The optimal $(\hat{A}, \hat{B}, \hat{C}, \hat{D})_{(i)}$ can be obtained using the block Hankel singular value decomposition, a well known technique in control theory known as balanced model reduction [61].

We can view the recursion relation of Eq. (5.5) as a finite state machine [22]; the transitions of the machine sequentially place the operators at each site, as illustrated in Fig. 5.3a. The first/last indices of the MPO, which we denote by L/R respectively, play a special role, as they indicate that no non-trivial operators have been placed to

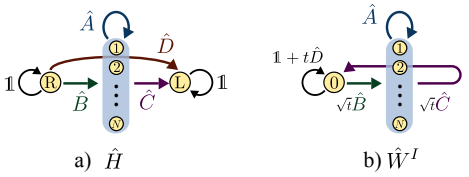

Figure 5.3: Graphical depictions of MPOs for (a) the Hamiltonian H and (b) the time-stepper $\hat{W}^I(t)$. As explained in Ref. [22], by analogy to a finite-state-machine the indices of the MPO (labeling rows and columns) are represented as nodes of a graph, while the entries of the MPO are edges.

the left/right of the bond. Due to the block-triangular structure of $\hat{W}$, once the MPO state transitions into the first index L, it remains there in perpetuity, placing only the identity operator $\hat{\mathbb{1}}$ with each $\hat{W}$. The transition from R to L (not necessarily in one step) places some local operator H_x; the sum over all such paths generates the Hamiltonian.

5.3 Time evolution operators

Given the decomposition $H = \sum_x H_x$, our goal is to find an efficient MPO for

$$U(t) = 1 + t\sum_x H_x + \frac{1}{2}t^2 \sum_{x,y} H_x H_y + \cdots . \tag{5.6}$$

In the most general case, an approximation for $U(t)$ is necessary, which brings us to our main result.

While the local Euler step defined in Eq. (5.1) does not have a simple MPO representation, a slight modification does. Let us define $x < y$ if the sites affected by H_x are strictly to the left of those affected by H_y. Consider an evolution operator which keeps all non-overlapping terms:

$$\begin{aligned} U^I(t) = 1 + t\sum_x H_x + t^2 \sum_{x<y} H_x H_y \\ + t^3 \sum_{x<y<z} H_x H_y H_z + \ldots \end{aligned} \tag{5.7}$$

These contributions are a subset of Eqs. (5.1) and (5.6). The first error occurs at order t^2, for terms H_x, H_y which overlap. For a system of length L, there are $\mathcal{O}(L)$ such terms, so the error is $\mathcal{O}(Lt^2)$; a constant error per *site*. Remarkably, U^I

has an exact compact MPO description "W^I", and is trivial to construct from the (A, B, C, D) of H, illustrated in Fig. 5.3b. It has a block structure of total dimension $\chi_i = N_i + 1$:

$$\hat{W}^I_{(i)}(t) = \begin{matrix} \\ {\scriptstyle 1} \\ {\scriptstyle N_{i-1}} \end{matrix} \begin{matrix} \begin{matrix} {\scriptstyle 1} & \quad {\scriptstyle N_i} \end{matrix} \\ \begin{pmatrix} \hat{\mathbb{1}}_{(i)} + t\hat{D}_{(i)} & \sqrt{t}\hat{C}_{(i)} \\ \sqrt{t}\hat{B}_{(i)} & \hat{A}_{(i)} \end{pmatrix} \end{matrix}. \tag{5.8}$$

The MPO bond dimension of $\hat{W}^I$ is one less than that of H, so it can be simply constructed and efficiently applied to the state.

While $\hat{W}^I$ is trivial to construct and performs well, it is not quite optimal. For example, a purely onsite Hamiltonian has a trivial $\chi = 1$ MPO representation for e^{tH}. Yet the MPO constructed from $\hat{W}^I$ would only produce the approximation $U^I = \prod_x (1 + tH_x)$ in this case.

We can improve Eq. (5.7), by keeping terms which may overlap by one site. Let $\langle x, \ldots, z \rangle$ denote a collection of terms in which no two cross the same bond. Arbitrarily high powers of a single site term, for example, can appear in these collections. Consider an evolution operator which keeps all such terms:

$$\begin{aligned} U^{II}(t) = 1 + t\sum_x H_x + \frac{t^2}{2}\sum_{\langle x,y\rangle} H_x H_y \\ + \frac{t^3}{6}\sum_{\langle x,y,z\rangle} H_x H_y H_z + \ldots \ . \end{aligned} \tag{5.9}$$

Again, the first error occurs at t^2, with L such terms, so the error is still formally $\mathcal{O}(Lt^2)$. But for typical interactions far fewer terms are dropped than in U^I; in particular onsite terms are captured to *all* orders. While there is not an exact compact MPO representation for U^{II}, we can construct an MPO approximation $\hat{W}^{II}$ which differs from U^{II} at $\mathcal{O}(Lt^3)$. Because the difference is at higher order than the accuracy of U^{II}, $\hat{W}^{II}$ still gives a noticeably better approximation than $\hat{W}^I$, and retains the feature that an onsite interaction is kept exactly. As $\hat{W}^{II}$ is just as compact as $\hat{W}^I$, it is always the preferred choice.

The MPO $\hat{W}^{II}$ is more complicated to construct, so for a detailed derivation of $\hat{W}^{II}$ and an algorithm to compute it we refer to App. 5.8. It takes the form

$$\hat{W}^{II} = \begin{matrix} \\ {\scriptstyle 1} \\ {\scriptstyle N_{i-1}} \end{matrix} \begin{matrix} \begin{matrix} {\scriptstyle 1} & \quad {\scriptstyle N_i} \end{matrix} \\ \begin{pmatrix} \hat{W}^{II}_D & \hat{W}^{II}_C \\ \hat{W}^{II}_B & \hat{W}^{II}_A \end{pmatrix} \end{matrix}. \tag{5.10}$$

To define the sub-blocks, introduce two vectors of formal parameters $\phi_a, \bar{\phi}_b$, with $a = 1, \ldots, N_{i-1}$, $b = 1, \ldots, N_i$. Let $\phi \cdot \hat{A}_{(i)} \cdot \bar{\phi}$ denote a dot product of these formal parameters into the MPO indices of $\hat{A}_{(i)}$. The sub-blocks are defined by a Taylor expansion in terms of ϕ, $\bar{\phi}$,

$$\begin{aligned} & e^{\phi\cdot\hat{A}\cdot\bar{\phi}+\phi\cdot\hat{B}\sqrt{t}+\sqrt{t}\hat{C}\cdot\bar{\phi}+t\hat{D}} \\ & \quad = \hat{W}^{II}_D + \hat{W}^{II}_C \cdot \bar{\phi} + \phi \cdot \hat{W}^{II}_B + \phi \cdot \hat{W}^{II}_A \cdot \bar{\phi} + \ldots \end{aligned} \tag{5.11}$$

Notice $\hat{W}^{II}_D = e^{t\hat{D}}$ is simply the onsite term, which is kept exactly. We also note that H has many different MPO representations, and at 2nd-order $\hat{W}^{II}$ is not invariant under different choices. This choice can be exploited to further reduce errors (cf. App. 5.11). Finally, if H is a sum of commuting terms, there is an analytic MPO representation for e^{tH} given in App. 5.9.

As with TEBD, we want to construct approximations with errors at higher order $\mathcal{O}(Lt^p)$ in t, which allow one to use much larger time steps. In fact, simply by cycling through a carefully chosen set of step constants $\{t_a\}$ we can obtain approximations of arbitrarily high order. MPS compression can be applied between steps so that the over-all complexity of the algorithm increases only linearly in the number of stages, though higher-order approximations presumably depend more sensitively on the accuracy of the intervening compression. In particular, there is a 2nd-order order approximation which alternates between two complex time steps t_1, t_2.

Each stage of the approximation should have a compact MPO expression (otherwise the increased complexity cancels the gains of a larger time step), so we consider an ansatz of the form

$$W^{II}(t_1)W^{II}(t_2)\cdots W^{II}(t_n) = U(t) + \mathcal{O}(Lt^p), \tag{5.12}$$

where $p-1$ is the approximation order. Our goal is to determine a set of step constants $\{t_a\}$ which produce the desired order. For example, to find a 2nd-order step ($p = 3$), we expand Eq. (5.12) order by order and find constraints

$$\sum_a t_a = t, \quad \sum_{a<b} t_a t_b = \frac{1}{2}t^2, \quad \sum_a t_a^2 = 0 \tag{5.13}$$

which can be solved by $t_1 = \frac{1+i}{2}t, t_2 = \frac{1-i}{2}t$. One can continue to arbitrary order; a set of 4 t_a's is required at 3rd order, a set of 7 at 4th order. Thus, by alternating between two compact MPOs, $W^{II}(t_1)$ and $W^{II}(t_2)$, we obtain a 2nd-order approximation. The same result folds for W^I. As shown in Fig. 5.2, the 2nd-order behavior is preserved even when truncation to the MPS ansatz intervenes between steps, so the 2nd-order time step is no more demanding than the 1st-order one.

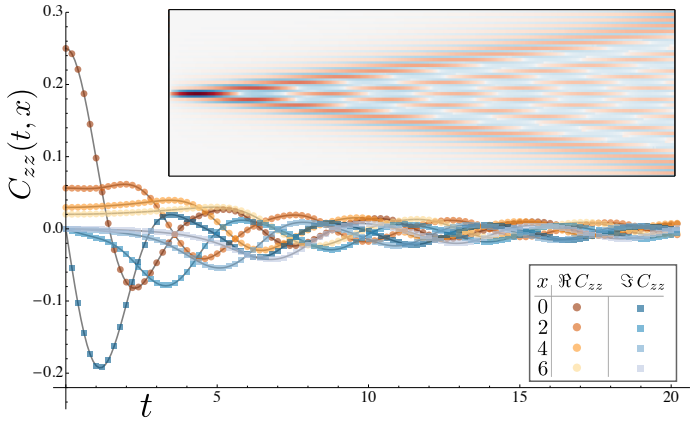

Figure 5.4: Time evolution of the response function $C_{zz}(t,x) = \langle 0|S^z(t,x)S^z(0,0)|0\rangle$ for the Haldane-Shastry model. Discrete data points are evaluated numerically using the 2nd-order MPO time stepper W^{II} ($dt = 0.025$), shown here for positions $x = 0, 2, 4, 6$. The exact analytic prediction shown in solid curves, giving beautiful agreement with the MPO. The inset shows a density plot of $C_{zz}(t,x)$ in the t–x plane.

5.4 Applications

Our first system beyond the reach of TEBD is the spin-1/2 Haldane-Shastry model, an exactly solvable critical spin chain with long-ranged Hamiltonian

$$H_{\text{HS}} = \sum_{x,r>0} \frac{\mathbf{S}_x \cdot \mathbf{S}_{x+r}}{r^2}. \tag{5.14}$$

The model can be viewed as a lattice form of the Calogero-Sutherland continuum model of fractional statistics [14, 113] and is connected to the Laughlin fractional quantum Hall wavefunction with an exact MPS representation [19]. The dynamical correlation function $C_{zz}(t,x)$ was first calculated analytically by Haldane and Zirnbauer [44]. As the system is critical and the Hamiltonian long-ranged, numerically obtaining C_{zz} is a stringent test of the proposed method. We use an MPO approximation of the Hamiltonian to capture the r^{-2} power law with high accuracy out to about 200 sites [23]. After using infinite DMRG [68, 23, 59] to obtain the ground state with infinite boundary conditions, we act with S^z and time evolve via W^{II}. As described in Fig. 5.4, the numerically computed C_{zz} is nearly identical to the analytic prediction (cf. App. 5.12) out to significant time scales.

Finally, one of the most interesting potential applications is time-evolving finitely-entangled 2D systems. We make a preliminary study by considering the 2D Bose-Hubbard model with a hard-core interaction and nearest neighbor repulsion V. Re-

cently there have been several experimental and theoretical studies of the expansion of strongly-interacting clouds [139, 95, 35, 129, 90]. The repulsion V can generate many-body bound states if it exceeds the bandwidth t, because there is no way for the interaction energy to transform into kinetic energy. Here we let a 16-boson $n = 1$ product state expand into a 14×14 grid. As shown in Fig. 5.1, the repulsion V has a dramatic effect on the expansion, trapping the bosons into a bound state. Because the 2D lattice has been turned into a 1D chain, the errors in W^{II} are highly anisotropic. Nevertheless we find that with a time step $dt = 0.01$, the density remains rotationally symmetric to within 4% at $t = 2$.

5.5 Conclusion

We have introduced an MPO based algorithm to simulate the time-evolution of long-ranged Hamiltonians. Our method was benchmarked against existing numerical methods for 1D short ranged models, as well as analytic results for the long-ranged Haldane-Shastry model. We also presented results of a preliminary study of the expansion of interacting bosons in a 2D trap. Given the recent successes of DMRG for investigating gapped 2D ground state and their gapless edges, the techniques presented here could open the door to numerically calculating experimentally relevant dynamic quantities such as spectral functions.

We are grateful to J. H. Bardarson, E. M. Stoudenmire, D. Varjas for helpful conversations. The authors wish to thank NSF DMR-1206515 (M.Z. and J.E.M.), the Sherman Fairchild Foundation (R.M.), the Nanostructured Thermoelectrics program of DOE BES (C.K.), and the Simons Foundation (J.E.M.).

5.6 MPO examples

In this section, we provide explicit examples of MPOs for pedagogical purposes.

To reiterate from the main text, an MPO describes an operators written as a product of $\hat{W}$'s

$$\cdots \hat{W}_{(1)}\hat{W}_{(2)}\hat{W}_{(3)} \cdots , \tag{5.15}$$

where each $\hat{W}_{(i)}$ is a matrix of operators acting on site i. An MPO for a Hamiltonain

can always be casted in the form

$$\hat{W}_{(i)} = \begin{array}{c} \\ 1 \\ N_{i-1} \\ 1 \end{array} \begin{array}{c} \begin{array}{ccc} 1 & N_i & 1 \end{array} \\ \begin{pmatrix} \hat{\mathbb{1}} & \hat{C} & \hat{D} \\ 0 & \hat{A} & \hat{B} \\ 0 & 0 & \hat{\mathbb{1}} \end{pmatrix}_{(i)} \end{array} . \tag{5.16}$$

$\hat{D}$ is simply an operator, $\hat{C}$ and $\hat{B}$ are, respectively, a row and column vector, an $\hat{A}$ is an $N_{i-1} \times N_i$ matrix of operators.

Consider the transverse field Ising model with Hamiltonian

$$H_{\mathrm{TFI}} = -J \sum_i \hat{Z}_i \hat{Z}_{i+1} - h \sum_i \hat{X}_i, \tag{5.17}$$

where $\hat{X}$ and $\hat{Z}$ are Pauli operators. This Hamiltonian may be constructed as an MPO with

$$\hat{W}_{(i)} = \begin{pmatrix} \hat{\mathbb{1}} & \hat{Z} & -h\hat{X} \\ 0 & 0 & -J\hat{Z} \\ 0 & 0 & \hat{\mathbb{1}} \end{pmatrix}_{(i)} . \tag{5.18}$$

Hence $N_i = 1$ for all bonds, and the MPO has bond dimension $\chi_i = 3$. We can also read off the $(\hat{A}, \hat{B}, \hat{C}, \hat{D})$ operators as $(0, -J\hat{Z}, \hat{Z}, -h\hat{X})$. We note that this MPO is not unique for Hamiltonian Eq. (5.17) (cf. App. 5.11). Due to the absence of $\hat{A}$, the Hamiltonian consists of only onsite and nearest-neighbor terms. Here $\hat{D}$ always denote the onsite term, and the pair terms are given by $\hat{C}_i \hat{B}_{i+1}$.

Our second example is a long-ranged XY-chain, with exponentially decaying couplings.

$$H = J \sum_{i<j} e^{-\alpha|i-j|} \big(\hat{X}_i \hat{X}_j + \hat{Y}_i \hat{Y}_j \big). \tag{5.19}$$

A corresponding MPO with $N_i = 2$ is as follows,

$$\hat{W}_{(i)} = \begin{pmatrix} \hat{\mathbb{1}} & e^{-\alpha}\hat{X} & e^{-\alpha}\hat{Y} & 0 \\ 0 & e^{-\alpha}\hat{\mathbb{1}} & 0 & J\hat{X} \\ 0 & 0 & e^{-\alpha}\hat{\mathbb{1}} & J\hat{Y} \\ 0 & 0 & 0 & \hat{\mathbb{1}} \end{pmatrix}_{(i)} . \tag{5.20}$$

Here $\hat{A}$ is a non-trivial 2×2 matrix of operators, which allows terms to reach beyond two neighboring sites. Each insertion of the $\hat{A}$ matrix increases the separation of the bookends $\hat{X}/\hat{Y}$ by 1 site, and also reduces its amplitude by $e^{-\alpha}$ factor.

5.7 Characterizing errors

Here we make a brief remark on the correct way to characterize the errors in an approximation $\tilde{U}(t)$ to the exact evolution $U(t)$. We say an approximation has an error *per site* of order t^p if

$$U(-t)\tilde{U}(t) = e^{\sum_{j=p}^{\infty} t^j O_j} \sim e^{L(a_p t^p + a_{p+1} t^{p+1} + \cdots)} \tag{5.21}$$

where each operator O_j is a sum of *local* terms, so its spectral radius goes as $|O_j| \sim L$. One can see that Suzuki-Trotter and W^I follow this form, while global Runge-Kutta does not. The locality of the operator generating the error implies that (after normalizing the state) the error in local observables should scale as t^p.

Now consider the expansion of $U(t) - \tilde{U}(t)$, which is more natural to calculate:

$$U(t) - \tilde{U}(t) \sim \sum_{nm} t_{nm} L^n t^m \tag{5.22}$$

where $L^n t^m$ denotes a term of spectral radius L^n and order t^m. For an approximation with constant error t^p per site, we see that $t_{nm} \neq 0$ only if $m - n \geq p - 1$. Order $p-1$ Runge-Kutta has errors of the form $L^m t^m$ for $m \geq p$, which violates this constraint.

5.8 Computing W_{II}

We defer the derivation of $\hat{W}^{II}$ until after App. 5.9, but first give an algorithm to compute it. We must compute objects of the form

$$\begin{aligned} \hat{W}[\phi, \bar{\phi}] &= e^{\phi \cdot \hat{A} \cdot \bar{\phi} + \phi \cdot \hat{B} \sqrt{t} + \sqrt{t} \hat{C} \cdot \bar{\phi} + t\hat{D}} \\ &= \hat{W}_D + \hat{W}_C \cdot \bar{\phi} + \phi \cdot \hat{W}_B + \phi \cdot \hat{W}_A \cdot \bar{\phi} + \cdots \end{aligned} \tag{5.23}$$

For certain cases where the Hamiltonian is free, so that A contains no field operators, B, C are linear in field operators, and D is quadratic in field operators, the result can be obtained using Pfaffians or permanents for fermionic and bosonic theories respectively. Here we discuss only the most general case, where the result must be obtained numerically.

Let's compute $\hat{W}_{A;a\bar{a}}$, where $a, \bar{a}$ index the rows and columns in correspondence with $\phi_a, \bar{\phi}_{\bar{a}}$. At this order, we can consider $\phi_a, \bar{\phi}_{\bar{a}}$ to be formal objects defined by the property $\phi_a^2 = \bar{\phi}_{\bar{a}}^2 = 0$, and they commute with all other objects. For computational purposes, we can then represent ϕ_a as a hard-core boson creation operator $\phi_a \to c_a^\dagger$, and likewise $\bar{\phi}_{\bar{a}} \to \bar{c}_{\bar{a}}^\dagger$, restricted to an occupation of at most 1 c-type and 1 $\bar{c}$-type

boson. We denote the Hilbert space of the $c/\bar{c}$ type bosons by $\mathcal{H}_{c/\bar{c}}$, and $\mathcal{H}_{\text{phys}}$ the Hilbert space of the physical site. The desired entries of $\hat{W}_A$, which are *operators* in $\mathcal{H}_{\text{phys}}$, can be obtained by calculating a vacuum expectation values in the Hilbert space of the $\mathcal{H}_{c/\bar{c}}$ coupled to the physical site:

$$\begin{aligned}\hat{W}_{A;a\bar{a}} &= \langle 0,\bar{0}|c_a\bar{c}_{\bar{a}}e^{c^\dagger\cdot\hat{A}\cdot\bar{c}^\dagger+c^\dagger\cdot\hat{B}\sqrt{t}+\sqrt{t}\hat{C}\cdot\bar{c}^\dagger+t\hat{D}}|0,\bar{0}\rangle \\ &= \langle 0,\bar{0}|c_a\bar{c}_{\bar{a}}e^{c_a^\dagger\bar{c}_{\bar{a}}^\dagger\hat{A}_{ab}+c_a^\dagger\hat{B}_a\sqrt{t}+\sqrt{t}\hat{C}_b\bar{c}_{\bar{a}}^\dagger+t\hat{D}}|0,\bar{0}\rangle\end{aligned} \tag{5.24}$$

To be more explicit, the argument of the exponential is an operator in the space $\mathcal{H}_c\otimes\mathcal{H}_{\bar{c}}\otimes\mathcal{H}_{\text{phys}}$. The desired entry $\hat{W}_{A;a,\bar{a}}$ is the transition amplitude from the vacuum $|0,\bar{0}\rangle$ of the $\mathcal{H}_c\otimes\mathcal{H}_{\bar{c}}$ into the occupied state $\langle 0,\bar{0}|c_a\bar{c}_{\bar{a}}$. Because the operators are restricted to single occupation, $c^2=\bar{c}^2=0$, when computing the particular entry $\hat{W}_{A;a\bar{a}}$ we only need the Hilbert space of two hard-core bosons $c_a,\bar{c}_{\bar{a}}$ as well as the physical Hilbert space of a single site; if the latter dimension is d, the total dimension is 2^2d. Thus the matrix elements can be obtained by exponentiating a matrix of dimension $4d$, which is trivial. This is repeated for the N^2 entries of $\hat{W}_{A;a\bar{a}}$. Results for $\hat{W}_{B;a}$ follow as a byproduct by calculating the transition into $\langle 0,\bar{0}|c_a$, and similarly for C,D.

All together, $\hat{W}^{II}$ can be computed with complexity $\mathcal{O}(N^2d^3)$.

5.9 Exact MPO exponentiation for commuting Hamiltonians

Here we obtain the exact MPO description for e^H when H is a sum of commuting terms such as $\sum_{i,j}\hat{X}_i\hat{X}_jt_{ij}$. This result generalizes the nearest-neighbor case investigated in Ref. [82]. to long range interactions. First, we address the stricter case in which $\hat{A},\hat{B},\hat{C},\hat{D}$ all commute, then comment briefly on the more general case.

Suppose the data $(A,B,C,D)_{(i)}$ of the MPO representation for H is given, with bond dimensions $\chi_i=2+N_i$. On each bond $(i,i+1)$, introduce a vector of complex fields $\phi_i=(\phi_{i,1},\ldots,\phi_{i,N_i})$, with complex conjugate $\bar{\phi}_i$ and indices $a_i=1,\ldots,N_i$ in correspondence with the non-trivial MPO indices in H. (That is, any MPO indices that is not L or R.) Using the fundamental rule of complex Gaussian integrals,

$$\frac{1}{\pi}\int d^2\phi\, e^{-\bar{\phi}\phi+J\bar{\phi}+\phi\bar{J}}=e^{J\bar{J}}, \tag{5.25}$$

the exponential factors as

$$e^H=\int\mathcal{D}[\phi_i,\bar{\phi}_i]\; e^{H_{L_i}+h_{L_i}\cdot\bar{\phi}_i}e^{-\bar{\phi}_i\cdot\phi_i}e^{\phi_i\cdot h_{R_i}+H_{R_i}} \tag{5.26}$$

where the dot-product is the sum $\sum_{a_i=1}^{N_i}$, and $\mathcal{D}[\phi_i, \bar{\phi}_i]$ is shorthand for $\prod_{a_i}(d^2\phi_{i,a_i}/\pi)$. This identity requires that all terms commute; otherwise discrepancies arise at second-order in H.

Now using the MPO recursion of Eq. (5.5), we can peel off one site:

$$H_{R_i} + \phi_i \cdot h_{R_i} = \phi_i \cdot \hat{A}_{i+1} \cdot h_{R_{i+1}} + \phi_i \cdot \hat{B}_{i+1} + \hat{C}_{i+1} \cdot h_{R_{i+1}} + \hat{D}_{i+1} + H_{R_{i+1}}. \quad (5.27)$$

Thus if we introduce a new vector of fields $\phi_{i+1,a_{i+1}}$ which runs over $a_{i+1} = 1, \ldots, N_{i+1}$, we can write

$$\begin{aligned} e^{\phi_i \cdot h_{R_i} + H_{R_i}} &= \int \mathcal{D}[\phi_{i+1}, \bar{\phi}_{i+1}]\ \hat{U}_{\phi_i, \bar{\phi}_{i+1}} e^{-\bar{\phi}_{i+1}\phi_{i+1}} e^{\phi_{i+1} \cdot h_{R_{i+1}} + H_{R_{i+1}}}, \\ &\text{where} \quad \hat{U}_{\phi_i, \bar{\phi}_{i+1}} \equiv e^{\phi_i \cdot \hat{A}_{i+1} \cdot \bar{\phi}_{i+1} + \phi_i \cdot \hat{B}_{i+1} + \hat{C}_{i+1} \cdot \bar{\phi}_{i+1} + \hat{D}_{i+1}}. \end{aligned} \quad (5.28)$$

By repeating this step on all the bonds, we find

$$e^H = \int \mathcal{D}[\phi, \bar{\phi}] \left[\cdots e^{-\bar{\phi}_i \phi_i} \hat{U}_{\phi_i, \bar{\phi}_{i+1}} e^{-\bar{\phi}_{i+1}\phi_{i+1}} \hat{U}_{\phi_{i+1}, \bar{\phi}_{i+2}} \cdots \right]. \quad (5.29)$$

This is a matrix product operator in which the auxiliary bonds are labeled by a set of continuous numbers ϕ_i, rather than discrete indices; it is a "coherent state MPO." To bring the result to a discrete form, we note that an integral of the form Eq. (5.29) is a discretized coherent state path integral for N_i bosons, so the integrals can be converted to discrete sums over the *many-body* Hilbert space of N_i bosons. The basic manipulation is the Taylor expansion:

$$Y_\phi \equiv \sum_{n=0}^{\infty} Y_n \frac{\phi^n}{\sqrt{n!}} \quad \text{(and likewise for any tensor)} \quad (5.30)$$

$$\begin{aligned} \frac{1}{\pi} \int d^2\phi\, X_{\bar{\phi}} e^{-\bar{\phi}\phi} Y_\phi &= \frac{1}{\pi} \sum_{\bar{n},n} X_{\bar{n}} Y_n \int d^2\phi\, \frac{\bar{\phi}^{\bar{n}} \phi^n}{\sqrt{\bar{n}!\, n!}} e^{-\bar{\phi}\phi} \\ &= \sum_n X_n Y_n \end{aligned} \quad (5.31)$$

The integer n is the 'occupation.' Note that if a tensor depends on multiple variables (such as the vector ϕ_{i,a_i}), then the above rule extends via a simple product. So if we define a vector of occupations $n_i = (n_{i,1}, \ldots, n_{i,N_i})$, whose values index the Hilbert space of N_i bosons, we can Taylor expand U as

$$\hat{U}_{\phi_i, \bar{\phi}_{i+1}} \equiv \sum_{\{n_i\},\{\bar{n}_i\}} \hat{U}_{n_i, \bar{n}_{i+1}} \frac{\phi_i^{n_i} \bar{\phi}_{i+1}^{\bar{n}_{i+1}}}{\sqrt{|n_i!||\bar{n}_{i+1}!|}} \quad (5.32)$$

with $|n_i!| = \prod_{a_i}(n_{i,a_i})!$. The MPO for the exponential is

$$e^H = \sum_{\{n_i\}} \left[\cdots \hat{U}_{n_i,n_{i+1}} \hat{U}_{n_{i+1},n_{i+2}} \cdots \right] \tag{5.33}$$

Now in principle each sum on the bonds is over the many-body Hilbert space of N_i bosons, which is infinite. But there will be "Boltzmann factors" associated to these states which allows for a sensible truncation.

Furthermore, in certain situations, such as for a nearest-neighbor interaction of Pauli-matrices, $H = \sum_i \hat{X}_i \hat{X}_{i+1}$, $\hat{U}_{n_{i+1},n_{i+2}}$ only has rank 2, resulting in the $\chi = 2$ MPO reported previously [82].

We must slightly modify the procedure if the Hamiltonian is a sum of commuting terms but $\hat{A}, \hat{B}, \hat{C}, \hat{D}$ do not commute (for instance, in the Toric code). Then on each bond we can arbitrarily order the ϕ_a, and when expanding the exponential for $\hat{U}_{\phi_i,\bar{\phi}_{i+1}}$, order the terms accordingly.

5.10 Derivation of $\hat{W}^{II}$

Comparing Eq. (5.23) with Eq. (5.28), we see that $\hat{W}^{II}$ is precisely a truncation of $\hat{U}_{n_i,n_{i+1}}$ to an occupation of at most a single boson on each bond. The occupation number of bosons across a bond encodes the number of terms in the Hamiltonian which cross the bond in the Taylor expansion of $e^{\sum_x H_x}$. Hence by truncating $\hat{U}$ to a maximum occupation of 1, we keep all non bond-overlapping terms. However, in the derivation of the exact MPO e^{tH} we required all terms to commute. Careful inspection shows that the non-commutivity only shows up at 3$^{\text{rd}}$-order in H. Hence in general $\hat{W}^{II}$ is only an approximation to the sum of all non bond-overlapping terms, with errors at $\mathcal{O}(t^3)$. But these errors are subleading in comparison to the terms dropped (by the truncation) at $\mathcal{O}(t^2)$, so are unimportant.

5.11 Taking advantage of different MPO decompositions

There are numerous ways to decompose a Hamiltonian as $H = \sum_x H_x$, and hence many decompositions into an MPO. For instance, a ferromagnetic interaction can be

written as

$$\begin{aligned} H_F &= -\sum_i \hat{Z}_i \hat{Z}_{i+1} \\ &= -\sum_i \left[(\hat{Z}_i - h)(\hat{Z}_{i+1} - h) + 2h\hat{Z}_i - h^2 \right] \end{aligned} \tag{5.34}$$

with MPO

$$\hat{W}^{H_F} = \begin{pmatrix} 1 & -\hat{Z} & 0 \\ 0 & 0 & \hat{Z} \\ 0 & 0 & 1 \end{pmatrix} \text{ or } \begin{pmatrix} 1 & -(\hat{Z}-h) & h^2 - 2h\hat{Z} \\ 0 & 0 & (\hat{Z}-h) \\ 0 & 0 & 1 \end{pmatrix}. \tag{5.35}$$

The MPO $\hat{W}^{II}$ is *not* invariant under such shifts (at 2^{nd}-order). This can be used to improve the effective accuracy of $\hat{W}^{II}$.

In principle one could try to optimize over all the MPO representations of H in order to minimize the error in $\hat{W}^{II}$. It is an open question whether there is a practical method to do this. As a toy model we compute the error $|(U(dt) - W^{II}(dt))|\psi\rangle|$ for the ferromagnet H_F as a function of the shift h given in Eq. (5.35). To leading order,

$$\begin{aligned} &\left| (U(dt) - W^{II}(dt))|\psi\rangle \right|^2 \\ &\quad \propto dt^2 \sum_i \langle\psi|(\hat{Z}_i - h)^2(\hat{Z}_{i+1} - h)^2|\psi\rangle, \end{aligned} \tag{5.36}$$

since W^{II} drops these two-site terms at 2^{nd}-order. So, in principle, the optimal h minimizes this expression.

One possible *heuristic* is to make a mean field approximation and instead minimize $\langle(\hat{Z}_i - h)^2\rangle\langle(\hat{Z}_{i+1} - h)^2\rangle$ by setting $h = \langle\hat{Z}_i\rangle$. With this choice the onsite term of Eq. (5.35) is $\hat{D} = h^2 - 2h\hat{Z}$, the mean field Hamiltonian. Since W^{II} treats $\hat{D}$ exactly, it's not surprising this can reduce the error.

To generalize this heuristic mean field criteria, we can always choose the MPO for H such that the Hamiltonian cut across any bond (cf. Eq. 5.4) satisfies $\langle h_{R_i,a_i}\rangle = \langle h_{L_i,a_i}\rangle = 0$ by shuffling the mean field component into H_{L_i}, H_{R_i}. Then the errors in $\hat{W}^{II}$ at 2^{nd}-order will depend only on the connected part of $\sum_{a_i} h_{L_i,a_i} h_{R_i,a_i}$. For many relevant models, such as a Heisenberg spin model, this heuristic does not help since $\langle h_{R_i,a_i}\rangle = 0$ due to the SU(2) symmetry of $\mathbf{S}$. But for a model with a long-ranged density-density interaction like $\frac{1}{2}\sum_{x,y} n_x V(x-y) n_y$, the mean field approach will treat the 'direct' part of the evolution, $\sum_{x,y} n_x V(x-y)\langle n_y\rangle$, exactly.

5.12 Analytical expressions for dynamical correlation functions of Haldane-Shastry spin chain

We provide here the expression found by Haldane and Zirnbauer [44] for the ground-state dynamical correlations

$$G^{ab}_{mn}(t,t') \equiv \langle 0|S^a_m(t)S^b_n(t')|0\rangle \tag{5.37}$$

of the Haldane-Shastry spin chain [41, 102] with Hamiltonian

$$H_{\rm HS} = J\sum_{m<n,a}\frac{S^a_m S^a_n}{|m-n|^2}. \tag{5.38}$$

(The superscript of S operators denote the spin direction and the subscript denote the lattice site.) The arguments leading to the forms below are somewhat involved and we refer the reader to the original paper for details. In the following $\hbar = 1$. G^{ab}_{mn} is diagonal in spin indices, and translation invariance allows us to define

$$G^{ab}_{mn}(t,t') = \frac{1}{4}\delta^{ab}(-1)^{m-n}C(m-n,t-t'). \tag{5.39}$$

The function $C(x,t)$ is related to the spinon spectrum in the solution for the ground-state wavefunction and can be simplified to two integrals:

$$C(x,t) = \frac{1}{4}\int_{-1}^{1}d\lambda_1\int_{-1}^{1}d\lambda_2\, e^{i\pi\lambda_1\lambda_2 x - \frac{\pi v t}{2}({\lambda_1}^2+{\lambda_2}^2-2{\lambda_1}^2{\lambda_2}^2)}. \tag{5.40}$$

Here v is the spinon velocity, $v = \pi J/2$, and the prefactor of $1/4$ can be understood by noting that $C(0,0) = 1$ as $(S^a)^2 = 1/4$ for each spin direction a. The numerical integrations used to obtain the comparison curves in Fig. 5.4 are straightforward and were carried out using commerical software.

Chapter 6

Conclusion

One of the outstanding problems in the theory of higher dimensional tensor networks is to design an efficient and stable method to variationally minimize the energy of a 2D tensor network given a microscopic Hamiltonian. Since the invention of DMRG [137], optimizing 1D tensor networks has essentially been a solved problem. There are a variety of competing proposals in 2D, but all are made quite complex by the need to work with non-orthogonal bases. In 1D, one can easily guarantee that the boundary map $|\phi\rangle_L$ is an orthogonal basis (the 'canonical form' of an MPS), which drastically simplifies the algorithm. There is currently no equivalent canonical form in 2D, which has proved the essential difficulty. It seems to me that the 'right' algorithm will be found only once the properties of the bulk-boundary map $|\phi\rangle_L$ are fully understood, and in particular what normalization conditions can be imposed during the variational optimization. If the network is non-injective during the intermediate stages of the algorithm, can one efficiently require that $|\phi\rangle_L$ is orthogonal basis about some particular bond? Such a result would drastically simplify the algorithm. Extending the techniques developed here to 2D, particularly the fermionic and bosonic parton ansatz, will prove very useful in understanding the tensor network representations of realistic states and the resolution of these issues.

Bibliography

[1] Ian Affleck et al. "Rigorous results on valence-bond ground states in antiferromagnets". In: *Phys. Rev. Lett.* 59 (7 Aug. 1987), pp. 799–802. DOI: 10.1103/PhysRevLett.59.799. URL: http://link.aps.org/doi/10.1103/PhysRevLett.59.799.

[2] Miguel Aguado and Guifré Vidal. "Entanglement Renormalization and Topological Order". In: *Phys. Rev. Lett.* 100 (7 Feb. 2008), p. 070404. DOI: 10.1103/PhysRevLett.100.070404. URL: http://link.aps.org/doi/10.1103/PhysRevLett.100.070404.

[3] P.W. Anderson. "Resonating valence bonds: A new kind of insulator?" In: *Materials Research Bulletin* 8.2 (1973), pp. 153–160. ISSN: 0025-5408. DOI: http://dx.doi.org/10.1016/0025-5408(73)90167-0. URL: http://www.sciencedirect.com/science/article/pii/0025540873901670.

[4] Daniel P. Arovas, Assa Auerbach, and F. D. M. Haldane. "Extended Heisenberg models of antiferromagnetism: Analogies to the fractional quantum Hall effect". In: *Phys. Rev. Lett.* 60 (6 Feb. 1988), pp. 531–534. DOI: 10.1103/PhysRevLett.60.531. URL: http://link.aps.org/doi/10.1103/PhysRevLett.60.531.

[5] Daniel Arovas, J. R. Schrieffer, and Frank Wilczek. "Fractional Statistics and the Quantum Hall Effect". In: *Phys. Rev. Lett.* 53 (7 Aug. 1984), pp. 722–723. DOI: 10.1103/PhysRevLett.53.722. URL: http://link.aps.org/doi/10.1103/PhysRevLett.53.722.

[6] J. Bardeen, L. N. Cooper, and J. R. Schrieffer. "Microscopic Theory of Superconductivity". In: *Phys. Rev.* 106 (1 Apr. 1957), pp. 162–164. DOI: 10.1103/PhysRev.106.162. URL: http://link.aps.org/doi/10.1103/PhysRev.106.162.

[7] G. Baskaran, Z. Zou, and P.W. Anderson. In: *Solid State Communications* 63.11 (1987), pp. 973–976. ISSN: 0038-1098. DOI: http://dx.doi.org/10.1016/0038-1098(87)90642-9. URL: http://www.sciencedirect.com/science/article/pii/0038109887906429.

[8] E. J. Bergholtz et al. "Pfaffian quantum Hall state made simple: Multiple vacua and domain walls on a thin torus". In: *Phys. Rev. B* 74 (8 Aug. 2006), p. 081308. DOI: 10.1103/PhysRevB.74.081308. URL: http://link.aps.org/doi/10.1103/PhysRevB.74.081308.

[9] B. Béri and N. R. Cooper. "Local Tensor Network for Strongly Correlated Projective States". In: *Phys. Rev. Lett.* 106 (15 Apr. 2011), p. 156401. DOI: 10.1103/PhysRevLett.106.156401. URL: http://link.aps.org/doi/10.1103/PhysRevLett.106.156401.

[10] B. Andrei Bernevig and F. D. M. Haldane. "Model Fractional Quantum Hall States and Jack Polynomials". In: *Phys. Rev. Lett.* 100 (24 June 2008), p. 246802. DOI: 10.1103/PhysRevLett.100.246802. URL: http://link.aps.org/doi/10.1103/PhysRevLett.100.246802.

[11] Parsa Bonderson, Victor Gurarie, and Chetan Nayak. "Plasma analogy and non-Abelian statistics for Ising-type quantum Hall states". In: *Phys. Rev. B* 83 (7 Feb. 2011), p. 075303. DOI: 10.1103/PhysRevB.83.075303. URL: http://link.aps.org/doi/10.1103/PhysRevB.83.075303.

[12] O. Buerschaper. "Twisted Injectivity in PEPS and the Classification of Quantum Phases". In: *ArXiv e-prints* (July 2013). arXiv: 1307.7763 [cond-mat.str-el].

[13] P. Calabrese and J. Cardy. In: *J. Stat. Mech.* P06002 (2004).

[14] F. Calogero. "Solution of the one-dimensional N-body problem with quadratic and/or inversely quadratic pair potentials". In: *J. Math. Phys.* 10 (1969), p. 2191.

[15] John L. Cardy. "Effect of boundary conditions on the operator content of two-dimensional conformally invariant theories". In: *Nuclear Physics B* 275.2 (1986), pp. 200–218. ISSN: 0550-3213. DOI: 10.1016/0550-3213(86)90596-1. URL: http://www.sciencedirect.com/science/article/pii/0550321386905961.

[16] Xie Chen, Zheng-Cheng Gu, and Xiao-Gang Wen. "Classification of gapped symmetric phases in one-dimensional spin systems". In: *Phys. Rev. B* 83 (3 Jan. 2011), p. 035107. DOI: 10.1103/PhysRevB.83.035107. URL: http://link.aps.org/doi/10.1103/PhysRevB.83.035107.

[17] Xie Chen, Zheng-Xin Liu, and Xiao-Gang Wen. "Two-dimensional symmetry-protected topological orders and their protected gapless edge excitations". In: *Phys. Rev. B* 84 (23 Dec. 2011), p. 235141. DOI: 10.1103/PhysRevB.84.235141. URL: http://link.aps.org/doi/10.1103/PhysRevB.84.235141.

[18] Xie Chen et al. "Tensor product representation of a topological ordered phase: Necessary symmetry conditions". In: *Phys. Rev. B* 82 (16 Oct. 2010), p. 165119. DOI: 10.1103/PhysRevB.82.165119. URL: http://link.aps.org/doi/10.1103/PhysRevB.82.165119.

[19] J. Ignacio Cirac and Germán Sierra. "Infinite matrix product states, conformal field theory, and the Haldane-Shastry model". In: *Phys. Rev. B* 81 (10 Mar. 2010), p. 104431. DOI: 10.1103/PhysRevB.81.104431. URL: http://link.aps.org/doi/10.1103/PhysRevB.81.104431.

[20] J. Ignacio Cirac et al. "Entanglement spectrum and boundary theories with projected entangled-pair states". In: *Phys. Rev. B* 83 (24 June 2011), p. 245134. DOI: 10.1103/PhysRevB.83.245134. URL: http://link.aps.org/doi/10.1103/PhysRevB.83.245134.

[21] Philippe Corboz et al. "Stripes in the two-dimensional t-J model with infinite projected entangled-pair states". In: *Phys. Rev. B* 84 (4 July 2011), p. 041108. DOI: 10.1103/PhysRevB.84.041108. URL: http://link.aps.org/doi/10.1103/PhysRevB.84.041108.

[22] Gregory M. Crosswhite and Dave Bacon. "Finite automata for caching in matrix product algorithms". In: *Phys. Rev. A* 78 (1 July 2008), p. 012356. DOI: 10.1103/PhysRevA.78.012356. URL: http://link.aps.org/doi/10.1103/PhysRevA.78.012356.

[23] Gregory M. Crosswhite, A. C. Doherty, and Guifré Vidal. "Applying matrix product operators to model systems with long-range interactions". In: *Phys. Rev. B* 78 (3 July 2008), p. 035116. DOI: 10.1103/PhysRevB.78.035116. URL: http://link.aps.org/doi/10.1103/PhysRevB.78.035116.

[24] A J Daley et al. "Time-dependent density-matrix renormalization-group using adaptive effective Hilbert spaces". In: *Journal of Statistical Mechanics: Theory and Experiment* 2004.04 (2004), P04005. URL: http://stacks.iop.org/1742-5468/2004/i=04/a=P04005.

[25] Stefan Depenbrock, Ian P. McCulloch, and Ulrich Schollwöck. "Nature of the Spin-Liquid Ground State of the S=1/2 Heisenberg Model on the Kagome Lattice". In: *Phys. Rev. Lett.* 109 (6 Aug. 2012), p. 067201. DOI: 10.1103/

PhysRevLett.109.067201. URL: http://link.aps.org/doi/10.1103/PhysRevLett.109.067201.

[26] Jonathan J. Dorando, Johannes Hachmann, and Garnet Kin-Lic Chan. "Analytic response theory for the density matrix renormalization group". In: *The Journal of Chemical Physics* 130.18, 184111 (2009), pages. DOI: http://dx.doi.org/10.1063/1.3121422. URL: http://scitation.aip.org/content/aip/journal/jcp/130/18/10.1063/1.3121422.

[27] J. Dubail and N. Read. "Entanglement Spectra of Complex Paired Superfluids". In: *Phys. Rev. Lett.* 107 (15 Oct. 2011), p. 157001. DOI: 10.1103/PhysRevLett.107.157001. URL: http://link.aps.org/doi/10.1103/PhysRevLett.107.157001.

[28] J. Dubail, N. Read, and E. H. Rezayi. "Edge state inner products and real-space entanglement spectrum of trial quantum Hall states". unpublished. 2012.

[29] J. Dubail, N. Read, and E. H. Rezayi. "Real-space entanglement spectrum of quantum Hall systems". In: *Phys. Rev. B* 85 (11 Mar. 2012), p. 115321. DOI: 10.1103/PhysRevB.85.115321. URL: http://link.aps.org/doi/10.1103/PhysRevB.85.115321.

[30] G. Evenbly and G. Vidal. In: *ArXiv e-prints* (Sept. 2011). arXiv: 1109.5334 [quant-ph].

[31] M. Fannes, B. Nachtergaele, and R. Werner. "Finitely correlated states on quantum spin chains". In: *Communications in Mathematical Physics* 144 (3 1992), pp. 443–490. ISSN: 0010-3616. URL: http://dx.doi.org/10.1007/BF02099178.

[32] Adrian E. Feiguin and Steven R. White. "Time-step targeting methods for real-time dynamics using the density matrix renormalization group". In: *Phys. Rev. B* 72 (2 July 2005), p. 020404. DOI: 10.1103/PhysRevB.72.020404. URL: http://link.aps.org/doi/10.1103/PhysRevB.72.020404.

[33] Paul Fendley, Matthew Fisher, and Chetan Nayak. "Topological Entanglement Entropy from the Holographic Partition Function". In: *Journal of Statistical Physics* 126 (6 2007), pp. 1111–1144. ISSN: 0022-4715. URL: http://dx.doi.org/10.1007/s10955-006-9275-8.

[34] Lukasz Fidkowski and Alexei Kitaev. "Topological phases of fermions in one dimension". In: *Phys. Rev. B* 83 (7 Feb. 2011), p. 075103. DOI: 10.1103/PhysRevB.83.075103. URL: http://link.aps.org/doi/10.1103/PhysRevB.83.075103.

[35] M. Ganahl, M. Haque, and H. G. Evertz. unpublished. 2013.

[36] T. Giamarchi. *Quantum Physics in one Dimension*. Oxford University Press, 2003. DOI: 10.1093/acprof:oso/9780198525004.001.0001.

[37] Paul H. Ginsparg. "Applied Conformal Field Theory". 1988.

[38] Daniel Gottesman and M B Hastings. "Entanglement versus gap for one-dimensional spin systems". In: *New J. Phys.* 12.2 (2010), p. 025002. URL: http://stacks.iop.org/1367-2630/12/i=2/a=025002.

[39] Z.-C. Gu, F. Verstraete, and X.-G. Wen. "Grassmann tensor network states and its renormalization for strongly correlated fermionic and bosonic states". In: *ArXiv e-prints* (Apr. 2010). arXiv: 1004.2563 [cond-mat.str-el].

[40] Jutho Haegeman et al. "Time-Dependent Variational Principle for Quantum Lattices". In: *Phys. Rev. Lett.* 107 (7 Aug. 2011), p. 070601. DOI: 10.1103/PhysRevLett.107.070601. URL: http://link.aps.org/doi/10.1103/PhysRevLett.107.070601.

[41] F. D. M. Haldane. "Exact Jastrow-Gutzwiller resonating-valence-bond ground state of the spin-1/2 antiferromagnetic Heisenberg chain with 1/r2 exchange". In: *Phys. Rev. Lett.* 60 (7 Feb. 1988), pp. 635–638. DOI: 10.1103/PhysRevLett.60.635.

[42] F. D. M. Haldane. "Fractional Quantization of the Hall Effect: A Hierarchy of Incompressible Quantum Fluid States". In: *Phys. Rev. Lett.* 51 (7 Aug. 1983), pp. 605–608. DOI: 10.1103/PhysRevLett.51.605.

[43] F. D. M. Haldane. "Nonlinear Field Theory of Large-Spin Heisenberg Antiferromagnets: Semiclassically Quantized Solitons of the One-Dimensional Easy-Axis Néel State". In: *Phys. Rev. Lett.* 50 (15 Apr. 1983), pp. 1153–1156. DOI: 10.1103/PhysRevLett.50.1153. URL: http://link.aps.org/doi/10.1103/PhysRevLett.50.1153.

[44] F. D. M. Haldane and M. R. Zirnbauer. "Exact calculation of the ground-state dynamical spin correlation function of a S=1/2 antiferromagnetic Heisenberg chain with free spinons". In: *Phys. Rev. Lett.* 71 (24 Dec. 1993), pp. 4055–4058. DOI: 10.1103/PhysRevLett.71.4055. URL: http://link.aps.org/doi/10.1103/PhysRevLett.71.4055.

[45] B. I. Halperin. "Theory of quantized Hall conductance". In: *Helv. Phys. Acta.* 56 (1–3 Mar. 1983), pp. 75–102. DOI: 10.5169/seals-115362.

[46] T. H. Hansson, M. Hermanns, and S. Viefers. "Quantum Hall quasielectron operators in conformal field theory". In: *Phys. Rev. B* 80 (16 Oct. 2009), p. 165330. DOI: 10.1103/PhysRevB.80.165330. URL: http://link.aps.org/doi/10.1103/PhysRevB.80.165330.

[47] Masudul Haque, Oleksandr Zozulya, and Kareljan Schoutens. "Entanglement Entropy in Fermionic Laughlin States". In: *Phys. Rev. Lett.* 98 (6 Feb. 2007), p. 060401. DOI: 10.1103/PhysRevLett.98.060401. URL: http://link.aps.org/doi/10.1103/PhysRevLett.98.060401.

[48] M. B. Hastings. "An area law for one-dimensional quantum systems". In: *J. Stat. Mech.* P08024.08 (2007). URL: http://stacks.iop.org/1742-5468/2007/P08024.

[49] M. B. Hastings. "Light-cone matrix product". In: *J. Math. Phys.* 50.9, 095207 (2009), p. 095207. DOI: 10.1063/1.3149556. URL: http://link.aip.org/link/?JMP/50/095207/1.

[50] P. Hauke and L. Tagliacozzo. "Spread of Correlations in Long-Range Interacting Quantum Systems". In: *Phys. Rev. Lett.* 111 (20 Nov. 2013), p. 207202. DOI: 10.1103/PhysRevLett.111.207202. URL: http://link.aps.org/doi/10.1103/PhysRevLett.111.207202.

[51] Christoph Holzhey, Finn Larsen, and Frank Wilczek. "Geometric and renormalized entropy in conformal field theory". In: *Nuclear Physics B* 424.3 (1994), pp. 443–467. ISSN: 0550-3213. DOI: http://dx.doi.org/10.1016/0550-3213(94)90402-2. URL: http://www.sciencedirect.com/science/article/pii/0550321394904022.

[52] S. Iblisdir, J. I. Latorre, and R. Orús. "Entropy and Exact Matrix-Product Representation of the Laughlin Wave Function". In: *Phys. Rev. Lett.* 98 (6 Feb. 2007), p. 060402. DOI: 10.1103/PhysRevLett.98.060402. URL: http://link.aps.org/doi/10.1103/PhysRevLett.98.060402.

[53] Eric Jeckelmann. "Density-Matrix Renormalization Group Methods for Momentum- and Frequency-Resolved Dynamical Correlation Functions". In: *Progress of Theoretical Physics Supplement* 176 (2008), pp. 143–164. DOI: 10.1143/PTPS.176.143.

[54] J. Jordan et al. "Classical Simulation of Infinite-Size Quantum Lattice Systems in Two Spatial Dimensions". In: *Phys. Rev. Lett.* 101 (25 Dec. 2008), p. 250602. DOI: 10.1103/PhysRevLett.101.250602. URL: http://link.aps.org/doi/10.1103/PhysRevLett.101.250602.

[55] Juan José and García-Ripoll. "Time evolution of Matrix Product States". In: *New Journal of Physics* 8.12 (2006), p. 305. DOI: 10.1088/1367-2630/8/12/305. URL: http://stacks.iop.org/1367-2630/8/i=12/a=305.

[56] Alexei Kitaev. "Anyons in an exactly solved model and beyond". In: *Ann. Phys. (NY)* 321.1 (Jan. 2006), pp. 2–111. ISSN: 0003-4916. DOI: 10.1016/j.aop.2005.10.005.

[57] Alexei Yu Kitaev. "Fault-tolerant quantum computation by anyons". In: *Ann. Phys. (NY)* 303.1 (Jan. 2003), pp. 2–30. DOI: 10.1016/S0003-4916(02)00018-0.

[58] Alexei Kitaev and John Preskill. "Topological Entanglement Entropy". In: *Phys. Rev. Lett.* 96 (11 Mar. 2006), p. 110404. DOI: 10.1103/PhysRevLett.96.110404.

[59] Jonas A. Kjäll et al. "Phase diagram of the anisotropic spin-2 XXZ model: Infinite-system density matrix renormalization group study". In: *Phys. Rev. B* 87 (23 June 2013), p. 235106. DOI: 10.1103/PhysRevB.87.235106. URL: http://link.aps.org/doi/10.1103/PhysRevB.87.235106.

[60] Christina V. Kraus et al. "Fermionic projected entangled pair states". In: *Phys. Rev. A* 81 (5 May 2010), p. 052338. DOI: 10.1103/PhysRevA.81.052338. URL: http://link.aps.org/doi/10.1103/PhysRevA.81.052338.

[61] S. Kung and D.W. Lin. "Optimal Hankel-norm model reductions: Multivariable systems". In: *Automatic Control, IEEE Transactions on* 26.4 (Aug. 1981), pp. 832–852. ISSN: 0018-9286. DOI: 10.1109/TAC.1981.1102736.

[62] Andreas M Läuchli, Emil J Bergholtz, and Masudul Haque. "Entanglement scaling of fractional quantum Hall states through geometric deformations". In: *New Journal of Physics* 12.7 (2010), p. 075004. URL: http://stacks.iop.org/1367-2630/12/i=7/a=075004.

[63] Andreas M. Läuchli et al. "Disentangling Entanglement Spectra of Fractional Quantum Hall States on Torus Geometries". In: *Phys. Rev. Lett.* 104 (15 Apr. 2010), p. 156404. DOI: 10.1103/PhysRevLett.104.156404. URL: http://link.aps.org/doi/10.1103/PhysRevLett.104.156404.

[64] R. B. Laughlin. "Anomalous Quantum Hall Effect: An Incompressible Quantum Fluid with Fractionally Charged Excitations". In: *Phys. Rev. Lett.* 50 (18 May 1983), pp. 1395–1398. DOI: 10.1103/PhysRevLett.50.1395. URL: http://link.aps.org/doi/10.1103/PhysRevLett.50.1395.

[65] Michael Levin and Xiao-Gang Wen. "Detecting Topological Order in a Ground State Wave Function". In: *Phys. Rev. Lett.* 96 (11 Mar. 2006), p. 110405. DOI: 10.1103/PhysRevLett.96.110405.

[66] H. Li and F. D. M. Haldane. "Entanglement Spectrum as a Generalization of Entanglement Entropy: Identification of Topological Order in Non-Abelian Fractional Quantum Hall Effect States". In: *Phys. Rev. Lett.* 101 (2008), p. 010504.

[67] Zhao Liu et al. "Edge-mode combinations in the entanglement spectra of non-Abelian fractional quantum Hall states on the torus". In: *Phys. Rev. B* 85 (4 Jan. 2012), p. 045119. DOI: 10.1103/PhysRevB.85.045119. URL: http://link.aps.org/doi/10.1103/PhysRevB.85.045119.

[68] I. P. McCulloch. "Infinite size density matrix renormalization group, revisited". 2008.

[69] Ian P McCulloch. "From density-matrix renormalization group to matrix product states". In: *J. Stat. Mech.* P10014.10 (2007). URL: http://stacks.iop.org/1742-5468/2007/i=10/a=P10014.

[70] Gregory Moore and Nicholas Read. "Nonabelions in the fractional quantum hall effect". In: *Nuclear Physics B* 360.23 (1991), pp. 362–396. ISSN: 0550-3213. DOI: 10.1016/0550-3213(91)90407-O. URL: http://www.sciencedirect.com/science/article/pii/055032139190407O.

[71] Masaaki Nakamura, Zheng-Yuan Wang, and Emil J. Bergholtz. In: *Phys. Rev. Lett.* 109 (1 July 2012), p. 016401. DOI: 10.1103/PhysRevLett.109.016401. URL: http://link.aps.org/doi/10.1103/PhysRevLett.109.016401.

[72] Anne E. B. Nielsen, Germán Sierra, and J. Ignacio Cirac. "Violation of the area law and long-range correlations in infinite-dimensional-matrix product states". In: *Phys. Rev. A* 83 (5 May 2011), p. 053807. DOI: 10.1103/PhysRevA.83.053807. URL: http://link.aps.org/doi/10.1103/PhysRevA.83.053807.

[73] R. Orús and G. Vidal. "Infinite time-evolving block decimation algorithm beyond unitary evolution". In: *Phys. Rev. B* 78.15, 155117 (2008), p. 155117. DOI: 10.1103/PhysRevB.78.155117. URL: http://link.aps.org/abstract/PRB/v78/e155117.

[74] Roman Orus. "A practical introduction to tensor networks: Matrix product states and projected entangled pair states". In: *Annals of Physics* 349 (2014), pp. 117–158. ISSN: 0003-4916. DOI: http://dx.doi.org/10.1016/j.aop.2014.06.013. URL: http://www.sciencedirect.com/science/article/pii/S0003491614001596.

[75] Stellan Östlund and Stefan Rommer. "Thermodynamic Limit of Density Matrix Renormalization". In: *Phys. Rev. Lett.* 75 (19 Nov. 1995), pp. 3537–3540. DOI: 10.1103/PhysRevLett.75.3537. URL: http://link.aps.org/doi/10.1103/PhysRevLett.75.3537.

[76] Z. Papi ć, B. A. Bernevig, and N. Regnault. "Topological Entanglement in Abelian and Non-Abelian Excitation Eigenstates". In: *Phys. Rev. Lett.* 106 (5 Feb. 2011), p. 056801. DOI: 10.1103/PhysRevLett.106.056801. URL: http://link.aps.org/doi/10.1103/PhysRevLett.106.056801.

[77] D Perez-Garcia et al. "Characterizing symmetries in a projected entangled pair state". In: *New Journal of Physics* 12.2 (2010), p. 025010. URL: http://stacks.iop.org/1367-2630/12/i=2/a=025010.

[78] D. Perez-Garcia et al. "Matrix Product State Representations". In: *Quantum Inf. Comput.* 7 (2007), p. 401.

[79] D. Perez-Garcia et al. "Peps As Unique Ground States of Local Hamiltonians". In: *Quantum Info. Comput.* 8.6 (July 2008), pp. 650–663. ISSN: 1533-7146. URL: http://dl.acm.org/citation.cfm?id=2016976.2016982.

[80] D. Perez-Garcia et al. "String Order and Symmetries in Quantum Spin Lattices". In: *Phys. Rev. Lett.* 100 (2008), p. 167202.

[81] Ingo Peschel. "Calculation of reduced density matrices from correlation functions". In: *Journal of Physics A: Mathematical and General* 36.14 (2003), p. L205. URL: http://stacks.iop.org/0305-4470/36/i=14/a=101.

[82] B Pirvu et al. "Matrix product operator representations". In: *New Journal of Physics* 12.2 (2010), p. 025012. URL: http://stacks.iop.org/1367-2630/12/i=2/a=025012.

[83] B. Pirvu et al. "Matrix product states for critical spin chains: Finite-size versus finite-entanglement scaling". In: *Phys. Rev. B* 86 (7 Aug. 2012), p. 075117. DOI: 10.1103/PhysRevB.86.075117. URL: http://link.aps.org/doi/10.1103/PhysRevB.86.075117.

[84] F. Pollmann et al. In: *Phys. Rev. Lett.* 102 (2009), p. 255701.

[85] David Poulin et al. "Quantum Simulation of Time-Dependent Hamiltonians and the Convenient Illusion of Hilbert Space". In: *Phys. Rev. Lett.* 106 (17 Apr. 2011), p. 170501. DOI: 10.1103/PhysRevLett.106.170501. URL: http://link.aps.org/doi/10.1103/PhysRevLett.106.170501.

[86] Xiao-Liang Qi, Hosho Katsura, and Andreas W. W. Ludwig. "General Relationship between the Entanglement Spectrum and the Edge State Spectrum of Topological Quantum States". In: *Phys. Rev. Lett.* 108 (19 May 2012), p. 196402. DOI: 10.1103/PhysRevLett.108.196402. URL: http://link.aps.org/doi/10.1103/PhysRevLett.108.196402.

[87] N. Read. "Non-Abelian adiabatic statistics and Hall viscosity in quantum Hall states and $p_x + ip_y$ paired superfluids". In: *Phys. Rev. B* 79 (4 Jan. 2009), p. 045308. DOI: 10.1103/PhysRevB.79.045308. URL: http://link.aps.org/doi/10.1103/PhysRevB.79.045308.

[88] N. Read and Dmitry Green. "Paired states of fermions in two dimensions with breaking of parity and time-reversal symmetries and the fractional quantum Hall effect". In: *Phys. Rev. B* 61.15 (Apr. 2000), pp. 10267–10297. DOI: 10.1103/PhysRevB.61.10267.

[89] N. Read and E. Rezayi. "Beyond paired quantum Hall states: Parafermions and incompressible states in the first excited Landau level". In: *Phys. Rev. B* 59 (12 Mar. 1999), pp. 8084–8092. DOI: 10.1103/PhysRevB.59.8084. URL: http://link.aps.org/doi/10.1103/PhysRevB.59.8084.

[90] Aaron Reinhard et al. "Self-Trapping in an Array of Coupled 1D Bose Gases". In: *Phys. Rev. Lett.* 110 (3 Jan. 2013), p. 033001. DOI: 10.1103/PhysRevLett.110.033001. URL: http://link.aps.org/doi/10.1103/PhysRevLett.110.033001.

[91] A. Rényi. "On measures of entropy and information". In: Proc. 4$^{\text{th}}$ Berkeley Symp. Math. Stat. Prob. 1961, pp. 547–561.

[92] Iván D. Rodríguez and Germán Sierra. "Entanglement entropy of integer quantum Hall states". In: *Phys. Rev. B* 80 (15 Oct. 2009), p. 153303. DOI: 10.1103/PhysRevB.80.153303.

[93] Iván D. Rodríguez, Steven H. Simon, and J. K. Slingerland. "Evaluation of Ranks of Real Space and Particle Entanglement Spectra for Large Systems". In: *Phys. Rev. Lett.* 108 (25 June 2012), p. 256806. DOI: 10.1103/PhysRevLett.108.256806. URL: http://link.aps.org/doi/10.1103/PhysRevLett.108.256806.

[94] Stefan Rommer and Stellan Östlund. "Class of ansatz wave functions for one-dimensional spin systems and their relation to the density matrix renormalization group". In: *Phys. Rev. B* 55 (4 Jan. 1997), pp. 2164–2181. DOI: 10.1103/PhysRevB.55.2164. URL: http://link.aps.org/doi/10.1103/PhysRevB.55.2164.

[95] J. P. Ronzheimer et al. "Expansion Dynamics of Interacting Bosons in Homogeneous Lattices in One and Two Dimensions". In: *Physical Review Letters* 110.20, 205301 (May 2013), p. 205301. DOI: 10.1103/PhysRevLett.110.205301.

[96] Peter Schmitteckert. "Nonequilibrium electron transport using the density matrix renormalization group method". In: *Phys. Rev. B* 70 (12 Sept. 2004), p. 121302. DOI: 10.1103/PhysRevB.70.121302. URL: http://link.aps.org/doi/10.1103/PhysRevB.70.121302.

[97] Ulrich Schollwöck. "The density-matrix renormalization group in the age of matrix product states". In: *Annals of Physics* 326.1 (2011), pp. 96–192. ISSN: 0003-4916. DOI: 10.1016/j.aop.2010.09.012.

[98] Norbert Schuch, Ignacio Cirac, and David Perez-Garcia. "{PEPS} as ground states: Degeneracy and topology". In: *Annals of Physics* 325.10 (2010), pp. 2153–2192. ISSN: 0003-4916. DOI: http://dx.doi.org/10.1016/j.aop.2010.05.008. URL: http://www.sciencedirect.com/science/article/pii/S0003491610000990.

[99] Norbert Schuch, David Perez-Garcia, and Ignacio Cirac. "Classifying quantum phases using matrix product states and projected entangled pair states". In: *Phys. Rev. B* 84 (16 Oct. 2011), p. 165139. DOI: 10.1103/PhysRevB.84.165139. URL: http://link.aps.org/doi/10.1103/PhysRevB.84.165139.

[100] N. Schuch et al. "Entropy Scaling and Simulability by Matrix Product States". In: *Phys. Rev. Lett.* 100.3, 030504 (2008), p. 030504. DOI: 10.1103/PhysRevLett.100.030504. URL: http://link.aps.org/abstract/PRL/v100/e030504.

[101] R. Shankar and Ashvin Vishwanath. "Equality of Bulk Wave Functions and Edge Correlations in Some Topological Superconductors: A Spacetime Derivation". In: *Phys. Rev. Lett.* 107 (10 Sept. 2011), p. 106803. DOI: 10.1103/PhysRevLett.107.106803. URL: http://link.aps.org/doi/10.1103/PhysRevLett.107.106803.

[102] B. Sriram Shastry. "Exact solution of an S=1/2 Heisenberg antiferromagnetic chain with long-ranged interactions". In: *Phys. Rev. Lett.* 60 (7 Feb. 1988), pp. 639–642. DOI: 10.1103/PhysRevLett.60.639.

[103] Y.-Y. Shi, L.-M. Duan, and G. Vidal. "Classical simulation of quantum many-body systems with a tree tensor network". In: *Phys. Rev. A* 74 (2 Aug. 2006), p. 022320. DOI: 10.1103/PhysRevA.74.022320.

[104] S. Singh and G. Vidal.

[105] Sukhwinder Singh, Robert N. C. Pfeifer, and Guifre Vidal. "Tensor network states and algorithms in the presence of a global U(1) symmetry". In: *Phys. Rev. B* 83 (11 Mar. 2011), p. 115125. DOI: 10.1103/PhysRevB.83.115125. URL: http://link.aps.org/doi/10.1103/PhysRevB.83.115125.

[106] Sukhwinder Singh, Robert N. C. Pfeifer, and Guifré Vidal. "Tensor network decompositions in the presence of a global symmetry". In: *Phys. Rev. A* 82 (5 Nov. 2010), p. 050301. DOI: 10.1103/PhysRevA.82.050301. URL: http://link.aps.org/doi/10.1103/PhysRevA.82.050301.

[107] H. Francis Song, Stephan Rachel, and Karyn Le Hur. "General relation between entanglement and fluctuations in one dimension". In: *Phys. Rev. B* 82 (1 July 2010), p. 012405. DOI: 10.1103/PhysRevB.82.012405. URL: http://link.aps.org/doi/10.1103/PhysRevB.82.012405.

[108] H. Francis Song et al. "Bipartite fluctuations as a probe of many-body entanglement". In: *Phys. Rev. B* 85 (3 Jan. 2012), p. 035409. DOI: 10.1103/PhysRevB.85.035409. URL: http://link.aps.org/doi/10.1103/PhysRevB.85.035409.

[109] Mark Srednicki. "Entropy and area". In: *Phys. Rev. Lett.* 71 (5 Aug. 1993), pp. 666–669. DOI: 10.1103/PhysRevLett.71.666. URL: http://link.aps.org/doi/10.1103/PhysRevLett.71.666.

[110] A. Sterdyniak et al. "Real-space entanglement spectrum of quantum Hall states". In: *Phys. Rev. B* 85 (12 Mar. 2012), p. 125308. DOI: 10.1103/PhysRevB.85.125308. URL: http://link.aps.org/doi/10.1103/PhysRevB.85.125308.

[111] E M Stoudenmire and Steven R White. "Minimally entangled typical thermal state algorithms". In: *New Journal of Physics* 12.5 (2010), p. 055026. URL: http://stacks.iop.org/1367-2630/12/i=5/a=055026.

[112] E.M. Stoudenmire and Steven R. White. "Studying Two-Dimensional Systems with the Density Matrix Renormalization Group". In: *Annual Review of Condensed Matter Physics* 3.1 (2012), pp. 111–128. DOI: 10.1146/annurev-conmatphys-020911-125018. URL: http://dx.doi.org/10.1146/annurev-conmatphys-020911-125018.

[113] B. Sutherland. "Exact results for a quantum many-body problem in one dimension. I". In: *Phys. Rev. A* 4 (1971), p. 2019.

[114] B. Swingle and X.-G. Wen. "Topological Properties of Tensor Network States From Their Local Gauge and Local Symmetry Structures". In: (Jan. 2010). arXiv: 1001.4517 [cond-mat.str-el].

[115] L. Tagliacozzo et al. In: *Phys. Rev. B* 78 (2008), p. 024410.

[116] R. Tao and D. J. Thouless. In: *Phys. Rev. B* 28 (2 July 1983), pp. 1142–1144. DOI: 10.1103/PhysRevB.28.1142. URL: http://link.aps.org/doi/10.1103/PhysRevB.28.1142.

[117] R. Thomale et al. "Entanglement Gap and a New Principle of Adiabatic Continuity". In: *Phys. Rev. Lett.* 104 (18 May 2010), p. 180502. DOI: 10.1103/PhysRevLett.104.180502. URL: http://link.aps.org/doi/10.1103/PhysRevLett.104.180502.

[118] D. C. Tsui, H. L. Stormer, and A. C. Gossard. "Two-dimensional magnetotransport in the extreme quantum limit". In: *Phys. Rev. Lett.* 48 (1982), pp. 1559–62. DOI: 10.1103/PhysRevLett.48.1559.

[119] Ari M. Turner, Frank Pollmann, and Erez Berg. "Topological phases of one-dimensional fermions: An entanglement point of view". In: *Phys. Rev. B* 83 (7 Feb. 2011), p. 075102. DOI: 10.1103/PhysRevB.83.075102. URL: http://link.aps.org/doi/10.1103/PhysRevB.83.075102.

[120] Ari M. Turner, Yi Zhang, and Ashvin Vishwanath. "Entanglement and inversion symmetry in topological insulators". In: *Phys. Rev. B* 82 (24 Dec. 2010), p. 241102. DOI: 10.1103/PhysRevB.82.241102. URL: http://link.aps.org/doi/10.1103/PhysRevB.82.241102.

[121] F. Verstraete and J. I. Cirac. "Continuous Matrix Product States for Quantum Fields". In: *Phys. Rev. Lett.* 104 (19 May 2010), p. 190405. DOI: 10.1103/PhysRevLett.104.190405. URL: http://link.aps.org/doi/10.1103/PhysRevLett.104.190405.

[122] F. Verstraete and J. I. Cirac. "Matrix product states represent ground states faithfully". In: *Phys. Rev. B* 73 (9 Mar. 2006), p. 094423. DOI: 10.1103/PhysRevB.73.094423. URL: http://link.aps.org/doi/10.1103/PhysRevB.73.094423.

[123] F. Verstraete and J.I. Cirac. "Renormalization algorithms for Quantum-Many Body Systems in two and higher dimensions". 2004.

[124] F. Verstraete, D. Porras, and J. I. Cirac. "Density Matrix Renormalization Group and Periodic Boundary Conditions: A Quantum Information Perspective". In: *Phys. Rev. Lett.* 93 (22 Nov. 2004), p. 227205. DOI: 10.1103/PhysRevLett.93.227205. URL: http://link.aps.org/doi/10.1103/PhysRevLett.93.227205.

[125] F. Verstraete et al. "Renormalization-Group Transformations on Quantum States". In: *Phys. Rev. Lett.* 94 (14 Apr. 2005), p. 140601. DOI: 10.1103/PhysRevLett.94.140601. URL: http://link.aps.org/doi/10.1103/PhysRevLett.94.140601.

[126] G. Vidal. "Classical Simulation of Infinite-Size Quantum Lattice Systems in One Spatial Dimension". In: *Phys. Rev. Lett.* 98 (7 Feb. 2007), p. 070201. DOI: 10.1103/PhysRevLett.98.070201. URL: http://link.aps.org/doi/10.1103/PhysRevLett.98.070201.

[127] Guifré Vidal. "Efficient Classical Simulation of Slightly Entangled Quantum Computations". In: *Phys. Rev. Lett.* 91 (14 Oct. 2003), p. 147902. DOI: 10.1103/PhysRevLett.91.147902. URL: http://link.aps.org/doi/10.1103/PhysRevLett.91.147902.

[128] G. Vidal et al. "Entanglement in Quantum Critical Phenomena". In: *Phys. Rev. Lett.* 90 (22 June 2003), p. 227902. DOI: 10.1103/PhysRevLett.90.227902. URL: http://link.aps.org/doi/10.1103/PhysRevLett.90.227902.

[129] L. Vidmar et al. "Sudden expansion of Mott insulators in one dimension". In: *Phys. Rev. B* 88 (23 Dec. 2013), p. 235117. DOI: 10.1103/PhysRevB.88.235117. URL: http://link.aps.org/doi/10.1103/PhysRevB.88.235117.

[130] Grigory E. Volovik. *The Universe in a Helium Droplet*. Oxford University Press, May 2003. ISBN: 978-0198507826.

[131] M L Wall and Lincoln D Carr. "Out-of-equilibrium dynamics with matrix product states". In: *New Journal of Physics* 14.12 (2012), p. 125015. URL: http://stacks.iop.org/1367-2630/14/i=12/a=125015.

[132] X. G. Wen. *Quantum Field Theory of Many-Body Systems*. Oxford: Oxford Graduate Texts, 2004.

[133] Xiao-Gang Wen. "Theory of the Edge States in Fractional Quantum Hall Effects". In: *International Journal of Modern Physics B* 06.10 (1992), pp. 1711–1762. DOI: 10.1142/S0217979292000840. URL: http://www.worldscientific.com/doi/pdf/10.1142/S0217979292000840.

[134] Xiao-Gang Wen. "Topological order and edge structure of ν=1/2 quantum Hall state". In: *Phys. Rev. Lett.* 70 (3 Jan. 1993), pp. 355–358. DOI: 10.1103/PhysRevLett.70.355. URL: http://link.aps.org/doi/10.1103/PhysRevLett.70.355.

[135] Xiao-Gang Wen. "Topological orders and edge excitations in fractional quantum Hall states". In: *Adv. Phys.* 44 (Oct. 1995), pp. 405–473. DOI: 10.1080/00018739500101566.

[136] Xiao-Gang Wen and Zhenghan Wang. "Topological properties of Abelian and non-Abelian quantum Hall states classified using patterns of zeros". In: *Phys. Rev. B* 78 (15 Oct. 2008), p. 155109. DOI: 10.1103/PhysRevB.78.155109.

[137] Steven R. White. "Density matrix formulation for quantum renormalization groups". In: *Phys. Rev. Lett.* 69 (19 Nov. 1992), pp. 2863–2866. DOI: 10.1103/PhysRevLett.69.2863. URL: http://link.aps.org/doi/10.1103/PhysRevLett.69.2863.

[138] Steven R. White and Adrian E. Feiguin. "Real-Time Evolution Using the Density Matrix Renormalization Group". In: *Phys. Rev. Lett.* 93 (7 Aug. 2004), p. 076401. DOI: 10.1103/PhysRevLett.93.076401. URL: http://link.aps.org/doi/10.1103/PhysRevLett.93.076401.

[139] K. Winkler et al. "Repulsively bound atom pairs in an optical lattice". In: 441 (June 2006), pp. 853–856. DOI: 10.1038/nature04918.

[140] S. Yan, D. A. Huse, and S. R. White. "Spin-Liquid Ground State of the S = 1/2 Kagome Heisenberg Antiferromagnet". In: *Science* 332 (June 2011), pp. 1173–. DOI: 10.1126/science.1201080.

[141] V. P. Yurov and AL. B. Zamolodchikov. "Truncated conformal space approach to scaling Lee-Yang model". In: *International Journal of Modern Physics A* 05.16 (1990), pp. 3221–3245. DOI: 10.1142/S0217751X9000218X. URL: http://www.worldscientific.com/doi/abs/10.1142/S0217751X9000218X.

[142] V. P. Yurov and AL. B. Zamolodchikov. "Truncated-fermionic-space approach to the critical 2D Ising model with magnetic field". In: *International Journal of Modern Physics A* 06.25 (1991), pp. 4557–4578. DOI: 10.1142/S0217751X91002161. URL: http://www.worldscientific.com/doi/abs/10.1142/S0217751X91002161.

[143] Yi Zhang et al. "Quasiparticle statistics and braiding from ground-state entanglement". In: *Phys. Rev. B* 85 (23 June 2012), p. 235151. DOI: 10.1103/PhysRevB.85.235151. URL: http://link.aps.org/doi/10.1103/PhysRevB.85.235151.

[144] O. S. Zozulya et al. "Bipartite entanglement entropy in fractional quantum Hall states". In: *Phys. Rev. B* 76 (12 Sept. 2007), p. 125310. DOI: 10.1103/PhysRevB.76.125310. URL: http://link.aps.org/doi/10.1103/PhysRevB.76.125310.